ISBN 978-82-575-1000-8
ISSN 1503-1667

Norwegian University of Life Sciences
NO–1432 Ås, Norway
Phone +47 64 96 50 00
www.umb.no, e-mail: postmottak@umb.no

Anna Oleynik

Norwegian University of Life Sciences • Universitetet for miljø- og biovitenskap
Department of Mathematical Sciences and Technology
Philosophiae Doctor (PhD) Thesis 2011:37

Mathematical aspects of localized activity in neural field models

Matematiske aspekter ved lokalisert aktivitet i nevrofeltmodeller

Anna Oleynik

Philosophiae Doctor (PhD) Thesis 2011:37

Mathematical aspects of localized activity in neural field models

Matematiske aspekter ved lokalisert aktivitet i nevrofeltmodeller

Philosophiae Doctor (PhD) Thesis

Anna Oleynik

Department of Mathematical Sciences and Technology
Norwegian University of Life Sciences

Ås 2011

Thesis number 2011: 37

ISSN 1503-1667

ISBN 978-82-575-1000-8

Acknowlegment

This work was carried out at the Department of Mathematical Sciences and Technology (IMT), Norwegian University of Life Sciences (UMB) in the period of 2007-2011. The research was supported by the Norwegian State Educational Loan Fund and the Norwegian University of Life Sciences. The work has also been supported by The Research Council of Norway under the grant No. 178892 (eNEURO-multilevel modeling and simulation of the nervous system) and the grant No. 178901 (Bridging the gap: disclosure, understanding and exploitation of the genotype-phenotype map).

Here I would like to mention a number of people who made this thesis possible. First of all I am cordially grateful to my main supervisor John Wyller for his patient guidance, support, and enthusiasm. Your encouragement and care have been a great value for me over these years. I also would like to thank my co-supervisor Arkadi Ponossov not only for his capable research guidance but for the help with many practical questions. I can not imagine to have had a better supervising team than John and Arkadi. It has been a great pleasure to work with you both.

I sincerely want to thank Gaute T. Einevoll for always being accessible and willing to help, for his support and encouragement. Thanks to Stephen Coombes for his kind hospitality during my stay in Nottingham, to Vadim Kostrykin for interesting and stimulating discussions, to Tom Tetzlaff and to my co-supervisor in Russia Igor Wertgeim for their collaboration. I also extend my gratitude to my colleagues at IMT for a friendly and warm working atmosphere.

I have been fortunate to be surrounded by great friends. Thanks to all of you for making the time of my study so memorably splendid. I wish to thank "my Russians" and especially Anya, Irina, Julia, and Lera for being like a family to me here in Norway.

I thank Mårten for his love and support that followed me through distances and countries.

Finally I would like to thank my family for supporting me and the choices I make, and for being so close despite of being so far.

Ås, August 2011
Anna Oleynik

Abstract

Neural field models assume the form of integral and integro-differential equations, and describe non-linear interactions between neuron populations. Such models reduce the dimensionality and complexity of the microscopic neural-network dynamics and allow for mathematical treatment, efficient simulation and intuitive understanding. Since the seminal studies by Wilson and Cowan (1973) and Amari (1977) neural field models have been used to describe phenomena like persistent neuronal activity, waves and pattern formation in the cortex. In the present thesis we focus on mathematical aspects of localized activity which is described by stationary solutions of a neural field model, so called bumps.

While neural field models represent a considerable simplification of the neural dynamics in a large network, they are often studied under further simplifying assumptions, e.g., approximating the firing-rate function with a unit step function.

In some cases these assumptions may not change essential features of the model, but in other cases they may cause some properties of the model to vary significantly or even break down. The work presented in the thesis aims at studying properties of bump solutions in one- and two-population models relaxing on the common simplifications.

Numerical approaches used in mathematical neuroscience sometimes lack mathematical justification. This may lead to numerical instabilities, ill-conditioning or even divergence. Moreover, there are some methods which have not been used in neuroscience community but might be beneficial. We have initiated a work in this direction by studying advantages and disadvantages of a wavelet-Galerkin algorithm applied to a simplified framework of a one-population neural field model. We also focus on rigorous justification of iteration methods for constructing bumps.

We use the theory of monotone operators in ordered Banach spaces, the theory of Sobolev spaces in unbounded domains, degree theory, and other functional analytical methods, which are still not very well developed in neuroscience, for analysis of the models.

Sammendrag

Nevrofeltmodeller formuleres som integral og integro-differensiallikninger. De beskriver ikke-lineære vekselvirkninger mellom populasjoner av nevroner. Slike modeller reduserer dimensjonalitet og kompleksitet til den mikroskopiske nevrale nettverksdynamikken og tillater matematisk behandling, effektiv simulering og intuitiv forståelse. Siden pionerarbeidene til Wilson og Cowan (1973) og Amari (1977), har nevrofeltmodeller blitt brukt til å beskrive fenomener som vedvarende nevroaktivitet, bølger og mønsterdannelse i hjernebarken. I denne avhandlingen vil vi fokusere på matematiske aspekter ved lokalisert aktivitet som beskrives ved stasjonære løsninger til nevrofeltmodeller, såkalte bumps.

Mens nevrofeltmodeller innebærer en betydelig forenkling av den nevrale dynamikken i et større nettverk, så blir de ofte studert ved å gjøre forenklende tilleggsantakelser, som for eksempel å approksimere fyringratefunksjonen med en Heaviside-funksjon.

I noen tilfeller vil disse forenklingene ikke endre vesentlige trekk ved modellen, mens i andre tilfeller kan de forårsake at modellegenskapene endres betydelig eller at de bryter sammen. Arbeidene presentert i denne avhandlingen har som mål å studere egenskapene til bump-løsninger i en- og to-populasjonsmodeller når en lemper på de vanlige antakelsene.

Numeriske teknikker som brukes i matematisk nevrovitenskap mangler i noen tilfeller matematisk begrunnelse. Dette kan lede til numeriske instabiliteter, dårlig kondisjonering, og til og med divergens. I tillegg finnes det metoder som ikke er blitt brukt i nevrovitenskap, men som kunne være fordelaktige å bruke. Vi har startet et arbeid i denne retningen ved å studere fordeler og ulemper ved en wavelet-Galerkin algoritme anvendt på et forenklet rammeverk for en en-populasjons nevrofelt modell. Vi fokuserer også på rigorøs begrunnelse for iterasjonsmetoder for konstruksjon av bumps.

Vi bruker teorien for monotone operatorer i ordnede Banachrom, teorien for Sobolevrom for ubegrensede domener, gradteori, og andre funksjonalanalytiske metoder, som for tiden ikke er vel utviklet i nevrovitenskap, for analyse av modellene.

List of papers

I. A. Oleynik, A. Ponosov, and J. Wyller, Iterative schemes for bump solutions in a neural field model, Submitted to SIAM Journal on Applied Mathematics, April 2011.

II. A. Oleynik, J. Wyller, and I. Wertgeim, The weakly nonlocal limit of a one-population Wilson-Cowan model, Physica D 239 (2010) pp. 1766-1780.

III. A. Oleynik, J. Wyller, T. Tetzlaff, and G.T. Einevoll, Stability of bumps in a two-population neural-field model with quasi-power temporal kernels, Nonlinear Analysis: Real World Applications 12 (2011) pp. 3073-3094.

IV. A. Oleynik, A. Ponosov, and J. Wyller, On the properties of nonlinear nonlocal operators arising in neural field models, Submitted to Journal of Mathematical Analysis and Applications, August 2011.

Contents

Acknowlegment . . . . . **iii**

Abstract . . . . . **v**

Sammendrag . . . . . **vii**

List of papers . . . . . **ix**

1 Introduction **1**

1.1 Background 1

1.2 Firing-rate neural field models 1

1.3 One-population neural field model 3

1.4 Two-population neural field model 6

2 Paper summaries **8**

2.1 Paper I 8

2.2 Paper II 8

2.3 Paper III 8

2.4 Paper IV 9

3 Conclusions and Outlook **9**

3.1 Contribution 9

3.2 Future perspectives 10

4 References **11**

Paper I **13**

Paper II **33**

Paper III **51**

Paper IV **75**

1 Introduction

1.1 Background

The human neocortex is a convoluted thin layer (2-4 mm) located just below the brain surface. It is a large complex biological system which consists of about 10 billion (10×10^9) neurons and 60 trillion (60×10^{12}) connections, [1]. The interaction between neurons of this large network enable us to think, behave, and understand.

The fundamental processing unit of the brain is the neuron. It consists of *dendrites*, *cell body* (or *soma*), and *axon*. These parts carry out input, processing, and output functions, respectively: The dendrites receive electrical signals from surrounding neurons and propagate them to the soma. If the summed electrical potential accumulated in the soma exceeds a certain threshold value, the neuron *fires*, i.e., produces a short electrical spike, or *action potential*, which then propagates along the axon to thousands of target neurons.

The macroscopic dynamics of neuronal tissue is often studied by means of *population* or *firing-rate* models. Rather than describing the activity of each individual neuron, they focus on the average activity, the *firing rate*, of populations of cells. The main purpose of such models is to reduce the dimensionality and complexity of the microscopic neural-network dynamics to obtain tools which allow mathematical treatment, efficient simulation and intuitive understanding. *Neural field models* constitute a special class of population models where the neuronal tissue is treated as a continuous structure. This approach is based on the assumption that the spatial length scale of a macroscopic state variable is much larger than the typical size of and distance between single neurons.

The continuum approximation of neural activity in its modern formulation can be attributed to Wilson and Cowan [2, 3] and Amari [4, 5]. Since these seminal studies the neural field models have been the subject of constant mathematical attention.

1.2 Firing-rate neural field models

Firing-rate models describe the temporal evolution of the firing rate r_m of a neuron population m. Each point $x \in \mathbb{R}^s$, $s = 1, 2$, represents a subpopulation $m(x)$ of neurons. The spatial coupling between subpopulations $m(x)$, $n(y)$ is described by a *connectivity kernel* $\omega_{mn}(x, y)$ which is typically assumed to be distance dependent and homogeneous, i.e., $\omega_{mn}(x, y) = \omega_{mn}(|x - y|)$, see for example [2, 3, 4, 5].

The time dependence of the interaction is frequently modeled by a *temporal kernel* $\alpha_{mn}(t)$. Given these ingredients, the dynamics of firing rates $r_n(x,t)$ of N interconnected populations is often described in terms of a Volterra equation system

$$\begin{aligned} u_n(x,t) &= \sum_{m\in\mathcal{N}} \left(\alpha_{mn} * \omega_{mn} \otimes r_m\right)(x,t) \\ r_n(x,t) &= P(u_n(x,t),\theta_n) \qquad \forall n \in \mathcal{N} \end{aligned} \tag{1}$$

where $\mathcal{N}$ is a set of subindexes with the cardinality N. Here, $u_n(x,t)$ denotes an (auxiliary) variable representing the *activity* of population n, $P_n(\cdot,\theta_n)$ the (typically sigmoidal) *firing-rate function*, and θ_n the firing threshold. The index m represents the presynaptic (sender) and n the postsynaptic (target) population. The operators $*$ and $\otimes$ denote the temporal and spatial convolution integrals, respectively, i.e.,

$$\begin{aligned} (\alpha * \beta)(t) &= \int_{-\infty}^{t} \alpha(t-s)\beta(s)ds \\ (f \otimes g)(x) &= \int_{\mathbb{R}^s} f(y-x)g(y)dy \end{aligned} \tag{2}$$

It is commonly assumed that the neurons of each population are homogeneous with respect to some properties, e.g., spatial coupling, temporal kernel, and/or probability of firing (firing-rate function). In general, all neurons can be divided into two main categories: *excitatory* and *inhibitory* neurons. The input from excitatory neurons increases the probability of the receiving neurons to fire, while inputs from the inhibitory neurons have the opposite effect. Thus, the connectivity function ω corresponding to the excitatory population as a sender-population is modeled by a positive function, and ω corresponding to the inhibitory population, as a sender-population, is modeled by a negative function.

The dynamical behavior observed in neural field models includes spatially and temporally periodic patterns, traveling waves, and localized regions of activity (*bumps*), [6]. The spatially and temporally periodic patterns are obtained beyond a Turing instability and have been related to visual hallucinations, [7, 8, 9]. Neurological disorders in humans such as epileptic seizure [10] and migraines [11] are characterized by traveling waves. Traveling waves also have been observed at the onset of sleep [12] and been related to sensory processing within cortex [13]. Bumps have been linked to the mechanism of working memory in the prefrontal cortex [14], representation in the head-direction system [15], and feature selectivity in the visual cortex [16].

Most studies are related to one- and two-population neural field models, and only a few

models to a larger number of neural populations, e.g., [17]. In the present thesis we will focus on the stationary localized solutions (bumps) of (1) in the case of one and two populations. We study existence, stability, and continuous dependence of bumps on the steepness of the firing-rate function. We also develop numerical algorithms to construct bump solutions and work on development of a wavelet-Galerkin algorithm to analyze a one-population model.

1.3 One-population neural field model

A one-population neural field model in one spatial dimension, $x \in \mathbb{R}$, in accordance with (1) assumes the form of a Volterra equation

$$u(x,t) = \int_{-\infty}^{t} \alpha(s-t) \int_{-\infty}^{+\infty} \omega(x-y) P(u(y,s),\theta) dy ds. \tag{3}$$

Under the assumption that the temporal kernel α is modeled by the exponentially decaying function

$$\alpha(t) = e^{-t}, \quad t > 0, \tag{4}$$

i.e., the present time carries more weight than the past, the equation (3) can be transformed to the integro-differential equation, [6]

$$\partial_t u(x,t) = -u(x,t) + \int_{-\infty}^{+\infty} \omega(x,y) P(u(y,s),\theta) dy. \tag{5}$$

The one-population model usually combines properties of both excitatory and inhibitory neurons. Commonly, these models assume a lateral-inhibition type of connection (a local excitation and distal inhibition) which corresponds to a function of a "Mexican hat" type, e.g.,

$$\omega(x) = Ke^{-A|x|} - ke^{-a|x|}, \quad K > k > 0, \quad A > a > 0. \tag{6}$$

However, some brain regions, and in particular the prefrontal cortex, possess a periodic modulation of anatomical connection strength [18]. One example of this type of connection is, [19]

$$\omega(x) = e^{-b|x|}(b \sin|x| + \cos(x)), \quad b > 0. \tag{7}$$

See graphics of the functions (6) and (7) in Fig. 1.

Furthermore, the brain is not a homogeneous media and it is natural to assume that the neuronal microstructure has an impact on processes at the mesoscale level. Thus, one

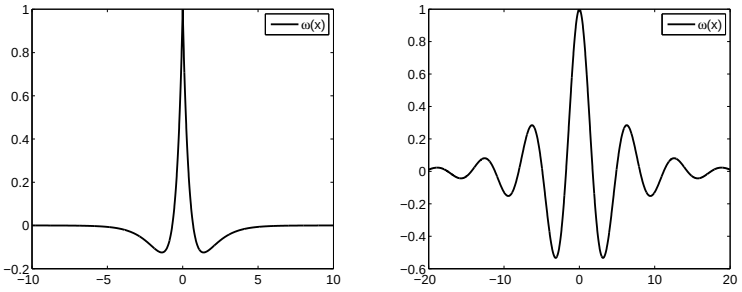

Figure 1: Examples of the connectivity function ω: (left) The "Mexican-hat" function (6) with K=A=2, k=a=1, and (right) the function (7) with b=0.2.

should not exclude inhomogeneous types of connectivity from mathematical consideration. Bressloff [20] was the first to study traveling fronts in a neural model with a periodically modulated micro-structure. Coupling between the periodic micro-level structure of the cortex and nonlocal mean-field description has been addressed in some other papers as well, see for example [21, 22, 23, 24, 25, 26]. It turns out that the detailed microstructure has an impact on pattern forming mechanisms as well as existence and stability of traveling fronts and pulses.

In [5] a one-population model of the lateral-inhibition type in one spatial dimension is considered. There the firing-rate function was modeled by the unit step function, i.e.,

$$P(u,\theta) = l(u-\theta),\ l(u) = \begin{cases} 0, & u < \theta \\ 1, & u \geq \theta \end{cases}. \tag{8}$$

We will make use of the following definitions which were introduced in [5]:

Definition 1.1. *Let θ be fixed, and $U(x)$ a stationary solution of* (5)*. Then a set $R[U] = \{x : U(x) \geq \theta\}$ is called an excited region of $U(x)$.*

Definition 1.2. *Let θ be fixed, and $U(x)$ be a stationary solution of* (5) *with the unit step firing-rate function* (8)*. If the excited region of U is such that $R[U] = [a_1, a_2]$ then $U(x)$ is called a local excitation solution, or simply, a bump.*

Amari [5] made an observation that one can find analytical expressions for bump solutions. Moreover, it was shown that there exist stable and unstable bumps in the framework of the model, [5].

Later, Kishimoto and Amari [27] proved the existence of stable bumps for the same type

of model but with a firing-rate function given as

$$P(u,\theta) = f(u-\theta),\ f(u) = \begin{cases} 0, & u \le 0 \\ \phi(u), & 0 < u < \varepsilon \\ 1, & u \ge \varepsilon \end{cases}, \tag{9}$$

where $\varepsilon > 0$, and ϕ is an arbitrary differentiable, monotonically increasing, and normalized function such that $\phi(0) = 0$, $\phi(\varepsilon) = 1$.

Coombes and Schmidt [28] observed that this type of function possesses the representation

$$f(u) = \int_{\mathbb{R}} \rho(\xi) l(u-\xi) d\xi, \quad \rho(\xi) = f'(\xi).$$

They call this function a smoothed Heaviside function, [28].

Remark 1.3. *We notice here that the definition of a bump (Definition 1.2) is given for the case when the firing-rate function is as in* (8)*. Therefore it is necessary to specify what is meant by a bump when P differs from* (8)*. Kishimoto and Amari [27] gave a definition of bumps in the framework of the model* (5) *with* (9) *which however is not introduced here.*

Bump solutions of the model (5) with the firing-rate function (9) have no closed form analytical representation, [27]. Coombes and Schmidt in [28] suggested an iterative scheme for construction of these bumps. They, however, did not give a mathematical verification of their approach. In Paper I two iterative schemes for construction of such bumps are introduced and the convergence of the schemes is proved.

In a modern terminology, bumps (Definition 1.2) are often referred to as 1-bumps. This is due to the following extended definition of the localized activities:

Definition 1.4. *Let θ be fixed, and $U(x)$ be a stationary solution of* (5)*. If the excited region of U is such that $R[U] = \bigcup_{k=1}^{N} [a_{2k-1}, a_{2k}]$ then $U(x)$ is called a bump solution or an N-bump.*

In [29] existence and stability of 2-bumps was studied in the framework of a lateral-inhibition type of connectivity. For studies on multibumps we refer to [30].

In principle, bumps can be constructed provided the Fourier transform of ω is a real rational function [19, 31]. In this case the model can be converted to a higher order nonlinear differential equations which can be represented as a Hamiltonian system. The bumps then are given by homoclinic orbits within the framework of these systems, see [19, 30, 31].

In Paper IV we show existence of 1-bumps for quite general ω when the firing-rate function is in a steep firing-rate regime and $P(u,\theta) = 0, \forall u < \theta$. We also prove the continuous dependence of bumps on the steepness of the firing rate.

There are studies on existence and stability of bumps in two spatial dimension, $x \in \mathbb{R}^2$, for one-population models, see for example [29, 30, 32]. Evolution of bumps in two dimensions demonstrates emergence of multibumps and labyrinthine patterns beyond the instabilities, [32]. However, the mathematical treatment of the model in two spatial dimensions gets more complicated. Hence most studies of these problems are carried out by numerical simulations.

Amari [5] studied existence of spatially periodic patterns in a one-population neural field model (5) with a unit step firing-rate function. In Paper II we study existence of stationary periodic solutions in the simplified one-population model, so called weakly nonlocal limit, where the firing-rate function is modeled by a sigmoid function, and the functions of a smoothed Heaviside type. For other studies on traveling waves and spatial patterns in one-population models (3) we refer to [33] and [5], respectively. For a more general overview see [6].

1.4 Two-population neural field model

A two-population model for the excitatory activity level u_e and the inhibitory activity level u_i reads

$$\begin{aligned} u_e &= \alpha_{ee} * \omega_{ee} \otimes P_e(u_e,\theta_e) - \alpha_{ie} * \omega_{ie} \otimes P_i(u_i,\theta_i), \\ u_i &= \alpha_{ei} * \omega_{ei} \otimes P_e(u_e,\theta_e) - \alpha_{ii} * \omega_{ii} \otimes P_i(u_i,\theta_i). \end{aligned} \tag{10}$$

Here the convolutions are defined as in (2). The dynamics of the excitatory and inhibitory interactions is modeled in a symmetric way: Each neural population receives impulses from, in principle, all neurons from another neural population as well as neurons from the same population, see Fig. 2.

Notice that we have modified the original definition of ω_{mn} given in Section 1.2. For simplicity we assume ω_{mn}, $m,n \in \{e,i\}$ to be positive functions. This explains the minus sign that appears in the model (10) as compared to (1).

When the temporal kernels are given as

$$\alpha_{ee}(t) = \alpha_{ie}(t) = e^{-t}, \quad \alpha_{ei}(t) = \alpha_{ii}(t) = \frac{1}{\tau} e^{-t/\tau} \tag{11}$$

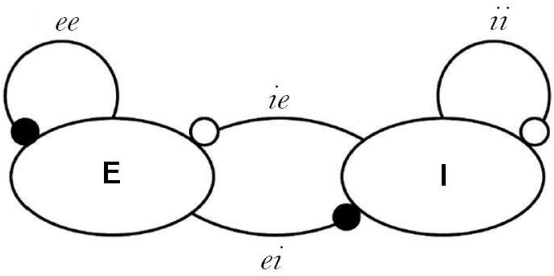

Figure 2: A schematic illustration of the connections within a generic neural field model consisting of an excitatory (E) and an inhibitory (I) population. The model possesses connections between two different populations (ei and ie), as well as recurrent connections within each population (ee and ii).

the model (10) can be converted to a system of rate equations, [34]

$$\begin{aligned} \partial_t u_e &= -u_e + \omega_{ee} \otimes P_e(u_e, \theta_e) - \omega_{ie} \otimes P_i(u_i, \theta_i) \\ \tau \partial_t u_e &= -u_i + \omega_{ei} \otimes P_e(u_e, \theta_e) - \omega_{ii} \otimes P_i(u_i, \theta_i). \end{aligned} \tag{12}$$

Here the parameter τ represents a ratio between the inhibitory and excitatory time constant and is called the *relative inhibition time*.

Next, we make a short review of works on two-population models in one spatial dimension. To the best of our knowledge there are no studies of these models in two spatial dimensions.

In [35] a simplified version of (12) has been considered: The recurrent inhibition is neglected (i.e., $\omega_{ii} \equiv 0$) and, in addition, the inhibitory term in the excitatory equation was linearized, i.e., $P_i(u_i, \theta_i) \equiv u_i$. It is shown that this model can be reduced to a one-population model (5) of a lateral-inhibition type as $\tau \to 0$.

The existence and stability of stationary localized solutions (a pair of 1-bumps U_e and U_i) in a two-population model (12) with the firing-rate functions P_e, P_i modeled by the unit step function (8) have been studied in [36]. In this case bumps possess an analytical representation and it has been shown that there is always a set of threshold values (θ_e, θ_i) for which bumps exist. In Paper III the existence and stability of bumps have been studied in the framework of the model (10) with more general choices of temporal kernels. The paper [9] is devoted to the study of a pattern formation within the framework of the model (12).

2 Paper summaries

2.1 Paper I

In Paper I we study a one-population neural field model given by (5) often referred to as the Wilson-Cowan model. In the framework of this model we study time-independent spatially localized solutions (bumps). We develop two iteration schemes for constructing such bumps when the firing-rate function is a continuous function of a special type (smoothed Heaviside function). The first scheme is based on the fixed point problem introduced in [27] while the second one is an iteration scheme for the excitation width (the length of the excited region) of the bumps. Using the theory of monotone operators in ordered Banach spaces we prove convergence of both iteration schemes. We demonstrate the applicability of the schemes with a numerical example.

2.2 Paper II

Wavelets are an effective tool in signal and image processing, [37]. While the utility of wavelets in solving differential and integro-differential equations is still quite questionable, there are some examples of successful usage of wavelet bases. In Paper II we implement a numerical algorithm based on the wavelet-Galerkin approach to study solutions of the weakly nonlocal limit of a one population neural field model. Roughly speaking, a weakly nonlocal limit is a one-population Wilson-Cowan model with almost local connectivity: It is assumed that the characteristic spatial scale length of the activity level is much greater than the synaptic footprint. First, we study the stability of homogeneous solutions and existence of periodical solutions of the model, using a pseudo-potential analysis. Next, we show that the numerical solutions agree with the theoretical prediction.

2.3 Paper III

In Paper III we consider a two-population model (12) when the firing-rate functions P_e, P_i are unit step functions. Just as for the one-population model, the Wilson-Cowan type of model (12) can be obtained from (10) when the temporal kernels are exponentially decaying functions (11). We study stability of symmetric bumps when the temporal kernels belong to a more general class of functions than exponentially decaying, namely the set of quasi-power functions. We compare two stability approaches known in literature as the Amari approach and the Evans function technique. We show that in the framework of the quasi-power temporal kernels these two approaches give the same predictions. We illuminate our results by numerical simulations.

2.4 Paper IV

In Paper IV we study properties of the one-parameter family of Hammerstein operators

$$(\mathcal{H}_\beta u)(x) = \int_{\mathbb{R}} k(x,y)S(\beta,u(y))d\mu(x),\ 0<\beta\leq\infty$$

in Sobolev spaces. The motivation for this study stems from the fact that bump solutions of a one-population neural field model appear as fixed points of these operators. We study continuity, compactness, and convergence $\mathcal{H}_\beta u \to \mathcal{H}_\infty u$ when $\beta \to \infty$, in the vicinity of a bump. We prove continuous dependence of bumps on the parameter β as well as existence of 1-bumps for large $\beta > 0$ under some restrictions on ω and $S(\beta, u)$.

3 Conclusions and Outlook

3.1 Contribution

In this thesis one- and two-population neural field models have been studied. While neural field models represent a considerable simplification of the neural dynamics in a large network, they are often studied under further simplifying assumptions on the connectivity functions, firing-rate functions, and/or temporal kernels. In some cases these assumptions may not change essential features of the model, but in other cases they may cause some properties of the model to break down.

We have considered generalizations of existing models by relaxing the common assumption on temporal kernels to be exponentially decaying functions (Paper III), the assumption on the connectivity function to describe a lateral-inhibition type of connection (Paper I, Paper IV), the assumption on the firing-rate function to be a unit step function (Paper I, Paper II, Paper IV). We also have focused on finding numerical schemes for solving such models (Paper I and Paper II to some extent), and worked on specific limit of an existing model (Paper II). We used the theory of monotone operators in ordered Banach spaces, the theory of Sobolev spaces in unbounded domains, degree theory, and other functional analytical methods for analysis of the models.

We also believe it is necessary to justify rigorously numerical approaches used in mathematical neuroscience. A lack of such justification may lead to numerical instabilities, ill-conditioning or even divergence. On the other hand, some of the previously used techniques might turn out to be very efficient, simple in realization, and allow further generalization. They just need to be properly analyzed. Moreover, there are some methods which

have not been used in neuroscience community but might be beneficial. In this thesis we have initiated a work in that direction: In Paper I we have developed and proved convergence of two iteration schemes for constructing 1-bump solutions of (5) in the framework of a smoothed Heaviside firing-rate function. In Paper II we develop a wavelet-Galerkin method to solve the weekly nonlocal limit of a one-population model. We use this simplified framework as a test example and to investigate advantages and disadvantages of the method for future use.

3.2 Future perspectives

While there is a growing number of publications devoted to the study of existence and stability of bumps, traveling waves, and emergence of spatial and spatio-temporal patterns in neural field models under simplifying assumptions, there are not so many publications that mathematically justify these simplifications. The relation between simplified and "full" models is often investigated in a way developed within the continuum mechanics tradition. However, in order to justify common simplifications and find true relations between simplified and "full" models one has to use methods which are not so well established in the mathematical neuroscience community, such as tools offered by functional analysis.

The future development of the neural field should also focus on developing new and more realistic models which account for micro- and stochastic effects, [21].

4 References

[1] The synaptic organization of the brain, Edt. Gordon M.Shepherd, Oxford university press, 2004.

[2] H.R. Wilson and J.D. Cowan, Excitatory and inhibitory interactions in localized populations of model neurons, Biophysical journal 12 (1972) pp.1-24.

[3] H.R. Wilson and J.D. Cowan, A mathematical theory of the functional dynamics of cortical and thalamic nervous tissue, Kybernetic 12 (1973) pp.55-80.

[4] S.Amari, Homogeneous nets of neuron-like elements, Biological Cybernetics 17 (1975) pp.211-220.

[5] S.Amari, Dynamics of pattern formation in lateral-inhibition type neural fields, Biological Cybernetics, 27 (1977) pp.77-87.

[6] S.Coombes, Waves, bumps, and patterns in neural field theories, Biol.Cybernet. 93 (2005) pp. 91-108.

[7] G.B. Ermentrout and J.D. Cowan, A mathematical theory of visual hallucination patterns, Biological Cybernetics 34 (1979) pp. 137-150.

[8] P.Tass, Cortical pattern formation for Motion Perception, Kluwer Academic Publishers, 1999.

[9] J. Wyller, P. Blomquist, and G.T. Einevoll, Turing instability and pattern formation in a two-population neural network model, Physica D 225 (2007) pp. 75-93.

[10] B.W. Connors and Y. Amitai, Generation of epileptiform discharge in the propagation of excitation in neural network model, J. Neurophysiol. 60 (1988) pp. 1695-1713.

[11] J.W. Lance, Current concept of migraine parthenogenesis, Neurology 43 (1993) pp.11-15.

[12] M.Steriade, E.G. Jones, and R.R. Linas, Thalamica Oscillations and Signalling, Wiley, New York, 1990.

[13] G.B. Ermentrout and D. Kleinfeld, Traveling electrical waves in cortex: Insights from phase dynamics and speculation on a computational role, Neuron 29 (2001) pp. 33-44.

[14] P.S. Goldman-Rakic, Cellular basis of working memory, Neuron 14 (1995) pp. 477-485.

[15] K. Zhang, Representation of spatial orientation by the intrinsic dynamics of the head-direction cell ensemble: a theory, Journal of Neuroscience 16 (1996) pp. 2112-2126.

[16] R. Ben-Yishai, L. Bar-Or, and H. Sompolinsky, Theory of orientation tuning in visual cortex, Proceedings of the National Academy of Sciences USA 92 (1995) pp. 3844-3848.

[17] O. Faugeras, F. Grimbert, and J.-J. Slotine, Absolute stability and complete synchronization in a class of neural fields models, SIAM J. Appl. Math. 69 (2008) pp. 205-250.

[18] J.B. Levitt, D.A. Lewis,T. Yoshioka, and J.S. Lund, Topography of pyramidal neuron intrinsic connections in macaque prefrontal cortex (areas 9 and 46), Journal of Comparative Neurology 338 (1993) pp. 360-376.

[19] A.J. Elvin, C.R. Laing, R.I. McLachlan, and M.G. Roberts, Exploiting the Hamiltonian structure of a neural field model, Physica D 239(2010) pp. 537-546.

[20] P. C. Bressloff, Traveling fronts and wave propagation failure in an inhomogeneous neural network, Physica D 155 (2001) pp. 83-100.

[21] S. Coombes, C. Laing, H. Schmidt, N. Svanstedt and J. Wyller, Waves in random neural media, Discrete and Continuous Dynamical Systems:Series A (2011).

[22] Z. P. Kilpatrick, S. E. Folias and P. C. Bressloff, Traveling pulses and wave propagation failure in an inhomogeneous neural network, SIAM J. Appl. Dyn. Syst. 7 (2008) pp.161 - 185.

[23] S. Coombes and C. R. Laing, Pulsating fronts in periodically modulated neural field models, Submitted to Phys. Rev. E. (2010).

[24] P. C. Bressloff, Spatially periodic modulation of cortical patterns by long-range horizontal connections, Physica D 185 (2003) pp. 131 - 157.

[25] P. C. Bressloff, S. E. Folias, A. Pratt and Y-X Li, Oscillatory waves in inhomogeneous neural media, Phys. Rev. Lett. 91:178101 (2003).

[26] X. Huang, W.C. Troy, Q. Yang, H. Ma, C.R. Laing, S.J. Schiff, J.-Y. Wu, Spiral waves in disinhibited mammalian neocortex, J. Neurosci. 24:44 (2004) pp. 9897 - 9902.

[27] K. Kishimoto and S. Amari, Existence and stability of local excitations in homogeneous neural fields, J.Math. Biology 7 (1979) pp.303-31.

[28] S.Coombes and H.Schmidt, Neural fields with sigmoidal firing rates: Approximate Solutions, Discrete and Continuous Dynamical Systems 28 (2010) pp.1369-1379.

[29] C.R. Laing and W.C. Troy, Two-bump solutions of Amari-type models of neuronal patter formation, Physica D 178(2003) pp. 190-218.

[30] C.R. Laing, W.C. Troy, B. Gutkin, and G.B. Ermentrout, Multiple bumps in a neural model of working memory, SIAM J. Appl. Math. 63:1 (2002) pp.62-97.

[31] C.R. Laing and W.C. Troy, PDE methods for nonlocal models, SIAM J. Applied Dynamical Systems 2:3 (2003) pp.487-516.

[32] M.R. Owen, C.R. Laing, and S.Coombes, Bumps and ringes in a two-dimensional neural fields: Splitting and rotational instabilities, New J. Phys. 9 (2007) 379.

[33] G.B. Ermentrout and J.B. McLeod, Existence and uniquiness of travelling waves in neural network, Proceedings of the Roal Society of Edinburg, 123A (1993) pp.461-478.

[34] J. Wyller, P. Blomquist, G.T. Einevoll, On the origin and properties of twopopulation neural field models-a tutorial introduction, Biophys. Rev. Lett. 2 (2007) pp. 79-98.

[35] D.J. Pinto, G.B. Ermentrout, Spatially structured activity in synaptically coupled neuronal networks: II. Lateral inhibition and standing pulses, SIAM J. Appl.Math. 62 (2001) pp. 226-243.

[36] P. Blomquist, J. Wyller, and G.T. Einevoll, Localized activity patterns in two population neuronal network, Physica D 206 (2005) pp. 180-212.

[37] I. Daubechies, Ten lectures on wavelets, CBMS-NSF Regional Conference Series in Applied Mathematics 61 (1993) p.357.

Paper I

ITERATIVE SCHEMES FOR BUMP SOLUTIONS IN A NEURAL FIELD MODEL

ANNA OLEYNIK, ARCADY PONOSOV, AND JOHN WYLLER

ABSTRACT. We develop two iteration schemes for construction of localized stationary solutions (bumps) of a one-population Wilson-Cowan model with a smoothed Heaviside firing rate function. The first scheme is based on the fixed point formulation of the stationary Wilson-Cowan model. The second one is formulated in terms of the excitation width of a bump. Using the theory of monotone operators in ordered Banach spaces we justify convergence of both iteration schemes.

1. INTRODUCTION

Neural field models have been the subject of mathematical attention since the publications [1, 2, 3, 4]. These models typically take the form of integro-differential equations. We consider a one-population neural field model of the Wilson-Cowan type [1, 2, 3, 4, 5]

$$u_t = -u + \psi, \quad \psi(x,t) = \int_{-\infty}^{+\infty} \omega(y-x) f(u(y,t) - h) dy. \tag{1.1}$$

Here $u(x,t)$ denotes an variable representing the activity of population, f the firing-rate function, ω the connectivity function, and h the firing threshold. For review on the model (1.1) see [5]. Existence and stability of spatially localized solutions and traveling waves are commonly studied for the case when the firing rate function is given by the unit step function [4, 5, 6]. However, the results for the case when the firing rate function is smooth are few and far between [7, 8, 9].

In the mathematical neuroscience community time-independent spatially localized solutions of (1.1) are referred to as *bumps*. The motivation for studying bumps stems from the fact that they are believed to be linked to the mechanisms of a short memory [10]. In the case when f is given as a unit step function, one can find analytical expressions for the bump solutions [4]. In principle, bumps solutions can also be constructed when the firing rate function is smooth provided the Fourier-transform of the connectivity function is a real, rational function. In that case the model can be converted to a higher order nonlinear differential equation which can be represented as a Hamiltonian system. The bumps are represented then by homoclinic orbits within the framework of these systems. See [11, 12].

Kishimoto and Amari [7] have proved the existence of bump solutions of (1.1) when f is a smooth function of a special type (smoothed Heaviside function), using the Schauder fixed point theorem. The Schauder fixed point theorem, however, does not give a method for construction of the bumps. Coombes and Schmidt in [8] developed an iteration scheme for constructing bumps of the model (1.1) with a smoothed Heaviside function. They, however, did not give a mathematical verification of their approach. Apart from the work of Coombes and Schmidt [8], the authors of the present paper do not know about other attempts to develop iterative algorithms for the construction of bumps. Thus there is a need for a more rigorous analysis of iteration

Key words and phrases. Neural field models, iteration schemes for bumps, monotone operators in ordered Banach spaces.

schemes for bumps. This serves as a motivation for the present work.

We present two different iteration schemes for constructing bumps. The first one is based on the fixed point problem introduced in [7]. The second scheme, which is modification of the procedure introduced in [8], is an iteration scheme for the excitation width of the bumps. We prove that both schemes converge using the theory of monotone operators in Banach spaces.

The present paper is organized in the following way: In Section 2 the properties of the one-population Wilson-Cowan model are reviewed with emphasis on the results of Kishimoto and Amari [7]. In Section 3 some necessary mathematical preliminaries are introduced. Section 4 is devoted to the study of a direct iteration scheme based on the fixed point problem proposed by of Kishimoto and Amari [7]. We illustrate the results with a numerical example. In Section 5 we introduce a fixed problem based on the specific representation of the firing rate function studied in [8]. The fixed problem is formulated for the crossing between bumps and a shifted parameterized threshold value $h+t$, $t \geq 0$. The bump solution can be restored from these crossings. We prove that there is a fixed point which can be obtained by iterations. We illustrate the results with a numerical example. In Section 6 we summarize our findings and describe open problems.

2. MODEL

We consider the *connectivity function* ω with the following properties:

(i) ω is symmetric , i.e. $\omega(-x) = \omega(x)$,
(ii) $\omega \in L_1(\mathbb{R})$,
(iii) ω is continuous and bounded, i.e., $\omega \in BC(\mathbb{R})$,
(iv) ω is differentiable a.e. with bounded derivatives, i.e., $\omega \in W^{1,\infty}(\mathbb{R})$.

A well known example of the connectivity function is the 'Mexican-hat' function modeling 'lateral inhibition' coupling, [4, 12]

$$\omega(x) = Ke^{-k|x|} - Me^{-m|x|}, \quad 0 < M < K,\ 0 < m < k. \tag{2.1}$$

In this paper we, however, use the following example of ω, [13]

$$\omega(x) = e^{-b|x|}(b \sin|x| + \cos x), \quad b > 0. \tag{2.2}$$

We have plotted the 'Mexican-hat' function (2.1) with parameters $K = k = 2$, $M = m = 1$, in Fig.1(a). In Fig.1(b) we have plotted the connectivity function (2.2) when $b = 0.3$.

If the model (1.1) possesses steady states they have to satisfy the integral equation

$$u(x) = \int_{-\infty}^{+\infty} w(y-x) f(u(y) - h) dy. \tag{2.3}$$

Notice that, when $u(x)$ is an equilibrium solution, so is $u(x-c)$ for arbitrary constant c. If an equilibrium solution (2.3) is symmetric, it can be expressed as

$$u(x) = \int_{0}^{+\infty} r(x,y) f(u(y) - h) dy \tag{2.4}$$

where

$$r(x,y) = w(y-x) + w(y+x).$$

The firing rate function, f, is a non-decreasing function mapping $\mathbb{R}$ to the unit interval $[0, 1]$. In [4] the firing-rate function f has been assumed to be a step function, i.e.,

$$f = \theta, \quad \theta(u) = \begin{cases} 0, & u < 0 \\ 1, & u \geq 0. \end{cases} \tag{2.5}$$

In this case the spatially localized solutions can be explicitly constructed. Following [4] we introduce the following definitions:

Definition 2.1. *The set $R[u] = \{x|\ u(x) > h\}$ is called the excited region of $u(x)$,* [4].

Definition 2.2. *An equilibrium solution $u(x)$ of* (1.1) *with $f = \theta$ is called an $a-$solution or a 1-bump with the width a if the excited region $R[u] = (a_1, a_2)$, $a = a_2 - a_1$ is the length of the excited region.*

Then a $1-$bump solution is given as

$$u(x) = \int_{a_1}^{a_2} \omega(y - x)dy.$$

In this paper we do not consider multiple bump solutions ($n-$bumps) or any other steady states of (1.1). We restrict ourselves to $1-$bumps. Therefore, we refer to 1-bumps as bumps in the rest of the paper. Without loss of generality we from now on consider only symmetric bumps, which can be represented as

$$u(x) = \int_0^{a/2} r(x, y)dy.$$

Here $a_2 = -a_1 = a/2$.

Let

$$\Phi(x, y) = \int_0^y r(x, z)dz,\ x, y \in \mathbb{R}, y > 0,$$

with

$$\frac{\partial \Phi}{\partial x}(x, y) = w(y + x) - w(y - x). \tag{2.6}$$

We conveniently express the bumps by means of the function Φ:

Theorem 2.3. *The model* (1.1) *with the firing-rate function $f = \theta$ possesses a bump solution if and only if there exist a width, a, such that*

$$\Phi(a/2, a/2) \equiv \int_0^a w(y)dy = h$$

and

(i) $\Phi(x, a/2) \leq h,\ \forall x > a/2,$
(ii) $\Phi(x, a/2) \geq h,\ \forall x \in [0, a/2).$

The bump solution is given by $u(x) = \Phi(x, a/2)$.

The stability of bumps can be studied by the Amari approach [4], or using the Evans function technique, [5]. We get the following stability result:

Theorem 2.4. *Let $f = \theta$, and there exist a bump with the width a. The bump is stable if $\omega(a) < 0$ and unstable if $\omega(a) > 0$.*

The firing-rate function treated here is of the following type, [7]

$$f(u) = \begin{cases} 0, & u \le 0 \\ \phi(u), & 0 < u < \tau \\ 1, & u \ge \tau \end{cases}, \tag{2.7}$$

where $\tau > 0$, ϕ is an arbitrary continuous, monotonically increasing, and normalized function such that

$$\phi(0) = 0, \quad \phi(\tau) = 1.$$

When $\tau \to 0$, the firing rate function approaches a unit step function. As an example of such a function we have

$$f(u) = \Sigma\left(u/\tau, p\right), \quad \Sigma(u,p) = \begin{cases} 0, & u \le 0 \\ \dfrac{u^p}{u^p + (1-u)^p}, & 0 < u < 1 \\ 1, & u \ge 1 \end{cases}, \ p > 0, \tag{2.8}$$

where $\Sigma(\cdot, p) \in C^{[p]}(\mathbb{R})$ and $[p]$ denotes the integer part of p. We need the following definition:

Definition 2.5. *$R^*[u] = \{x | u(x) > h + \tau\}$ is called a maximally excited region, and $R^-[u] = \{x | h < u(x) < h + \tau\}$ is an incompletely excited region,* [7].

Following [7], we next define the bump solutions corresponding to the firing rate function (2.7) as follows:

Definition 2.6. *An equilibrium solution $u(x)$ of* (1.1) *with f given by* (2.7) *is called a bump if $R^*[u]$ is the interval surrounded by an incompletely excited region $R^-[u]$, i.e., $R[u] = R^*[u] \cup R^-[u]$ being another interval,* [7].

Thus, by Definition 2.6 the function $u(x)$ displayed graphically in Fig.2 can be a bump when $\tau = \tau_1$, whereas for $\tau = \tau_2$ it can not be a bump.

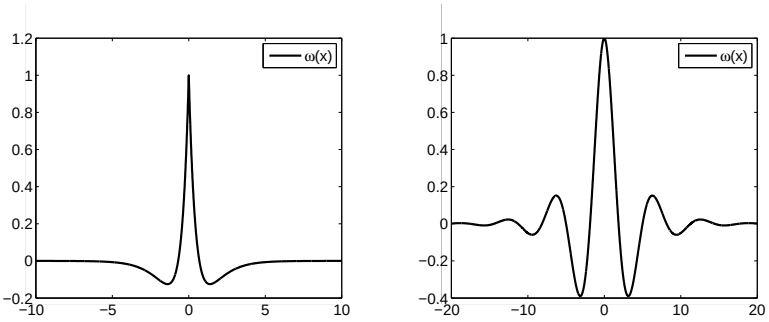

(a) (b)

FIGURE 1. The examples of the connectivity function ω: (a) The 'Mexican-hat' function (2.1), and (b) the function (2.2), with the parameters given in the text.

Let $f_0(u) = \theta(u)$ and $f_\tau(u) = \theta(u - \tau)$. Then the following inequality holds true

$$f_\tau(u) \le f(u) \le f_0(u).$$

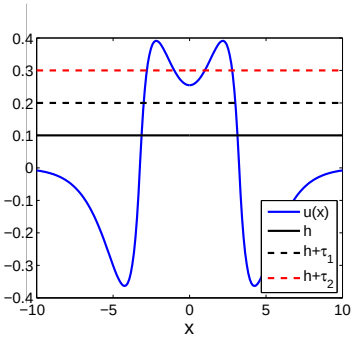

FIGURE 2. The graphic of a function $u(x)$ which satisfy Definition 2.6 when $\tau = \tau_1$ and does not satisfy it when $\tau = \tau_2$.

We use similar terminology as introduced in [7]: The neural field with the output functions f_0, f_τ, and f is called a f_0-field, f_τ-field, and f-field, respectively. Notice here that the f_τ- field is equivalent to the f_0-field with the new threshold value $h + \tau$.

The original idea of Kishimoto and Amari [7] was to use bump solutions of the f_0- and $f_\tau-$fields to prove the existence (and stability) of bumps in the $f-$field. If ω has a 'Mexican-hat' shape (see Fig. 1(a)) then the f_0-field ($f_\tau-$field) possesses two symmetric bumps for small and moderate values of h, one stable and one unstable bump. In [7] it was shown, using the Schauder fixed point theorem, that there exists a bump solution of $f-$field if both f_0- and $f_\tau-$ fields possess stable bumps and ω has a 'Mexican-hat' shape (i.e., the connectivity function can have the shape like in Fig.1(a) but not like in Fig.1(b)). Moreover, if ϕ is a differentiable function it was shown that the $f-$ field bump is stable. Notice that the differentiability of ϕ can be replaced by a weaker assumption, namely differentiability almost everywhere, i.e., $\phi \in W^{1,1}[0, \tau]$. Then, the firing rate function (2.7) can be represented as in [8] i.e.

$$f(u) = \int_{-\infty}^{+\infty} \rho(\xi)\theta(u - \xi)d\xi, \tag{2.9}$$

with θ given by (2.5), $\text{supp}\{\rho\} = [0, \tau]$, and ρ is positive and normalized $\int_{-\infty}^{\infty} \rho(x)dx = 1$.

In this paper we introduce two iteration methods to construct a bump of the $f-$field. We do not require the connectivity function to have a 'Mexican hat' shape as it is assumed in many studies, e.g., [4, 7]. Moreover, we do not require ω to be given by means of the expression (2.2) as for example in [11, 12], but we keep our assumptions on ω to be as general as possible. We also do not demand the bumps of the f_0- and $f_\tau-$field bumps be stable in order to prove the existence of an $f-$field bump and construct it numerically. We use the following assumptions:

Assumption 1. *There exist $2\Delta_0$-solutions of the f_0-field model, and $2\Delta_\tau$-solutions of the f_τ-field model such that $\Delta_\tau < \Delta_0$.*

Let us assume that there is a bump solution of the f_0-field model, i.e., $\Phi(\Delta_0, \Delta_0) = h$, see Theorem 2.3. Then, by the inverse function theorem there exists a value $\tau > 0$ such that $\Phi(\Delta_\tau, \Delta_\tau) = h + \tau$ for some $\Delta_\tau < \Delta_0$, if $\omega(2\Delta) < 0$ in some vicinity of Δ_0. In this case both bumps are stable by Theorem 2.4. However, Assumption 1 can be satisfied even when the situation described above does not take place, i.e., the condition $\omega(2\Delta) < 0$ is not fulfilled for all $\Delta \in [\Delta_\tau, \Delta_0]$, see for example Fig.3.

Under Assumption 1 bumps for the f_0-field model and the f_τ-field model are, in according with Theorem 2.3, given as

$$u_0(x) = \Phi(x, \Delta_0) \quad u_\tau(x) = \Phi(x, \Delta_\tau).$$

Assumption 2. *The function $r(x, y) \geq 0$ for $x, y \in [\Delta_\tau, \Delta_0]$.*

We get the following relationship between u_τ and u_0:

Lemma 2.7. *Under Assumption 2 we have $u_\tau \leq u_0$ on $[\Delta_\tau, \Delta_0]$.*

Proof. We get

$$u_0(x) - u_\tau(x) = \int_0^{\Delta_0} r(x, y)dy - \int_0^{\Delta_\tau} r(x, y)dy = \int_{\Delta_\tau}^{\Delta_0} r(x, y)dy \geq 0.$$

□

In this paper we will only consider bump solutions of the $f-$field such that

$$u(x) > h + \tau, \ \forall x \in R[u_\tau - \tau], \quad u(x) < h \ \forall x \notin R[u_0]. \tag{2.10}$$

3. Mathematical Preliminaries

The theoretical foundation of the iteration schemes presented in Section 4 and Section 5 is based on the following general results:

Let E be a cone in a real Banach space $\mathcal{B}$ and $\leq$ be a partial ordering defined by E.

Theorem 3.1. *Let $w_0, v_0 \in \mathcal{B}$, $w_0 < v_0$ and $A : [w_0, v_0] \to \mathcal{B}$ be an increasing operator such that*

$$w_0 \leq Aw_0, \ Av_0 \leq v_0.$$

Suppose that one of the following two conditions is satisfied:

(H1) *E is normal and A is condensing;*

(H2) *E is regular and A is semicontinuous, i.e., $x_n \to x$ strongly implies $Ax_n \to Ax$ weakly.*

Then A has a maximal fixed point x^* and a minimal fixed point x_* in $[w_0, v_0]$; moreover

$$x^* = \lim_{n\to\infty} v_n, \ x_* = \lim_{n\to\infty} u_n,$$

where $v_n = Av_{n-1}$ and $w_n = Aw_{n-1}$, $n = 1, 2, 3...$, and

$$w_0 \leq w_1 \leq ... \leq w_n \leq ... \leq v_n \leq ... \leq v_1 \leq v_0.$$

See [14].

From Theorem 3.1 we get the following result.

Corollary 3.2. *If under the conditions of Theorem 3.1 $x^* = x_* = \tilde{x}$, then $\tilde{x}$ is the unique fixed point of the operator A in $[w_0, v_0]$.*

Theorem 3.3. *The cone $E = \{u \in \mathcal{B} | u(x) \geq 0\}$ is normal but not regular in $\mathcal{B} = C(\bar{D})$, and regular in $\mathcal{B} = L_p(D), \ 1 \leq p < \infty$, where D is a bounded set and $\bar{D}$ is a closed bounded set.*

See [14].

Theorem 3.4. *The Hammerstein operator*

$$(Af)(x) = \int_a^b k(x, y)\psi(y, f(y))dy$$

is continuous and compact in $C([a, b])$ if $k(x, y)$ and $\psi(x, y)$ are continuous functions on $[a, b] \times [a, b]$.

Proof. The operator A can be represented as the superposition, $A = LN$, where L is the linear operator

$$(Lg)(x) = \int_a^b k(x,y)g(y)dy,$$

and N is the Nemytskii operator

$$(Nf)(x) = \psi(x, f(x)).$$

The linear operator $L : C([a,b]) \to \mathbb{R}$ is continuous and compact if $k(x,y)$ is continuous [16]. Obviously, the Nemytskii operator $N : C([a,b]) \to C([a,b])$ is continuous and bounded if $\psi(x,y)$ is continuous. Thus, the Hammerstein operator A is completely continuous as the superposition of the continuous and bounded operator N, and completely continuous operator L. □

4. Iteration Scheme I: Direct Iteration.

In this section we consider the direct iteration scheme for construction bumps. This scheme is based on [7]. We start out by observing that a bumps solution of an $f-$field satisfying (2.10) can be rewritten as

$$u(x) = u_\tau(x) + \int_{\Delta_\tau}^{\Delta_0} r(x,y)f(u(y) - h)dy.$$

We have the following theorem:

Theorem 4.1. *Let ω satisfy Assumption 1 and 2. Let the operator $T_f : [u_\tau, u_0] \subset \mathcal{B} \to \mathcal{B}$ be defined as*

$$(T_f u)(x) = u_\tau(x) + \int_{\Delta_\tau}^{\Delta_0} r(x,y)f(u(y) - h)dy \tag{4.1}$$

where $\mathcal{B}$ is chosen to be either $L_2([\Delta_\tau, \Delta_0])$ or $C([\Delta_\tau, \Delta_0])$. Then the operator T_f has a fixed point in $[u_\tau, u_0]$. Moreover, the sequences $\{T_f^n u_\tau\}$ and $\{T_f^n u_0\}$ converge to the minimal and maximal fixed point of the operator T_f, respectively.

Proof. We base our proof on Theorem 3.1. The set $E = \{u \in \mathcal{B} | u(x) \geq 0\}$ is a normal cone in $\mathcal{B} = C([\Delta_\tau, \Delta_0])$ and a regular cone in $\mathcal{B} = L_p([\Delta_\tau, \Delta_0])$, $1 \leq p < \infty$, see Theorem 3.3. By Assumptions 1-2 there exist u_τ and u_0 such that $0 \leq u_\tau \leq u_0$ on $[\Delta_\tau, \Delta_0]$.

First we describe the properties of T_f which are common for both spaces. The operator T_f is positive and monotone due to Assumption 2 and monotonicity of f, i.e.,

$$u_1(x) \leq u_2(x) \Rightarrow (T_f u_1)(x) \leq (T_f u_2)(x).$$

Moreover, T_f is continuous because f is continuous and $r(x,y)$ is bounded.

Define a non-linear operator T_g associated with the non-negative function $g(x)$ by

$$(T_g u)(x) = u_\tau(x) + \int_{\Delta_\tau}^{\Delta_0} r(x,y)g(u(y) - h)dy.$$

Then u_0 and u_τ are fixed points of the operators T_{f_0} and T_{f_τ}, respectively:

$$T_{f_0} u_0 = u_0, \quad T_{f_\tau} u_\tau = u_\tau.$$

From Assumption 2 we can easily deduce that

$$g(x) \leq m(x) \;\Rightarrow\; (T_g u)(x) \leq (T_m u)(x),$$

and, therefore,

$$(T_{f_\tau} u)(x) \leq (T_f u)(x) \leq (T_{f_0} u)(x).$$

Thus,

$$T_f u_\tau \geq T_{f_\tau} u_\tau = u_\tau, \quad T_f u_0 \leq T_{f_0} u_0 = u_0.$$

From Theorem 3.1 we conclude that $T_f : [u_\tau, u_0] \to L_2([\Delta_\tau, \Delta_0])$ has a fixed point in $[u_\tau, u_0]$ which can be found by iterations. However, for the case $\mathcal{B} = C([\Delta_\tau, \Delta_0])$ it remains to show that T_f is condensing. Applying Theorem 3.4 to the Hammerstein operator on the right hand side of (4.1), i.e., to the operator $\tilde{T}_f : [u_\tau, u_0] \to C[\Delta_\tau, \Delta_0]$ defined as

$$\tilde{T}_f u = \int_{\Delta_\tau}^{\Delta_0} r(x,y) f(u(y) - h) dy,$$

we find that $T_f : [u_\tau, u_0] \to C([\Delta_\tau, \Delta_0])$ is compact and, thus, condensing. This completes the proof.

□

In Fig.3 we have plotted $\omega(x)$ given by (2.2) with the marked points $(2\Delta_0, \omega(2\Delta_0))$, $(2\Delta_\tau, \omega(2\Delta_\tau))$, and $(2\Delta_\tau^{st}, \omega(2\Delta_\tau^{st}))$. Here Δ_0 is defined as $u_0(\Delta_0) = h$, and Δ_τ, Δ_τ^{st} are obtained as solutions of $u_\tau(\Delta) = h + \tau$, for $h = 0.3$, $\tau = 0.1$. The values are given as follows: $\Delta_0 = 1.3932$, $\Delta_\tau = 0.6562$, and $\Delta_\tau^{st} = 1.2410$. According to Theorem 2.4 the function u_0 is a stable bump. The bump u_τ is stable when $\Delta = \Delta_\tau^{st}$ and unstable if $\Delta = \Delta_\tau$. We denote these bumps as u_τ and u_τ^{st}, respectively. We have checked that Assumption 2 is satisfied on $[\Delta_\tau, \Delta_0] = [0.6562, 1.3932]$. Thus, we can apply Theorem 4.1. In Fig.4(a) we have plotted the solution $u^*(x)$ on $[\Delta_\tau, \Delta_0]$ obtained by iterations from $u_\tau(x)$ and $u_0(x)$ when f is given as in (2.8), $p = 2$. From Corollary 3.2 we conclude that u^* is a unique solution of the fixed point problem for (4.1). We have plotted u_0, u_τ, and u_τ^{st} on the same figure to illustrate the inequality

$$u_\tau^{st} \le u^* \le u_0. \tag{4.2}$$

In Fig.4(b) we have plotted the numerical errors calculated as

$$\begin{aligned} \varepsilon_1(n) &= \max_x |(T^n u_\tau)(x) - (T^{n-1} u_\tau)(x)|, \quad T^0 u_\tau \equiv u_\tau \\ \varepsilon_2(n) &= \max_x |(T^n u_0)(x) - (T^{n-1} u_0)(x)|, \quad T^0 u_0 \equiv u_0 \end{aligned} \quad , n = 1, 2, ..., N, \tag{4.3}$$

where N denotes the total number of iterations.

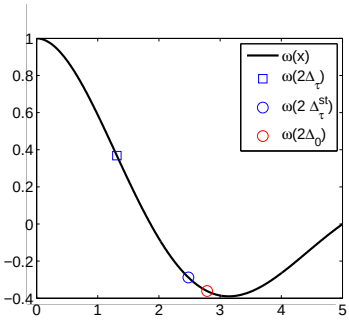

FIGURE 3. The connectivity function $\omega(x)$ given as in (2.2) with $b = 0.3$. The black square indicates an unstable bump of the $f_\tau-$field , the black circle indicates a stable bump of $f_\tau-$field, and the red circle indicates a stable bump of the f_0-field. The parameters are fixed and given as $h = 0.3$, $\tau = 0.1$.

Next we show that the solution $u^* = T_f u^*$ can be extended to the solution u of (2.3) over $\mathbb{R}$ such that $u(x) \ge h + \tau$ for $x \in [0, \Delta_\tau]$ and $u(x) \le h$ for $x \in [\Delta_0, \infty)$. To do that we have to introduce some additional assumptions on the connectivity function ω. We do this in the following way:

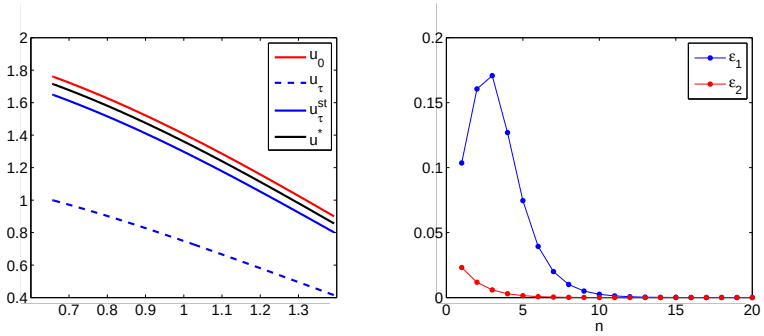

(a) (b)

FIGURE 4. (a) A fixed point of the operator (4.1), $u^*(x)$, the stable bump u_0 of the f_0-field, and stable, u_τ^{st} and unstable, u_τ bump of $f_\tau-$field, for $x \in [\Delta_\tau, \Delta_0]$. The connectivity function ω is given as in (2.2), $b = 0.3.$, f is defined by (2.8) with $p = 2$, $h = 0.3$, $\tau = 0.1$. (b) The errors given as in (4.3).

Assumption 3. *u_0 is a decreasing function on the interval $[\Delta_\tau, \Delta_0]$ which is equivalent to*

$$\frac{\partial \Phi}{\partial x}(x, \Delta_0) < 0, \ \forall x \in [\Delta_\tau, \Delta_0],$$

and u_τ is a decreasing function on $[\Delta_\tau, \Delta_0]$ which is equivalent to

$$\frac{\partial \Phi}{\partial x}(x, \Delta_\tau) < 0, \ \forall x \in [\Delta_\tau, \Delta_0].$$

From this assumption the transversality of the intersections $u_0(x)$ with h, and $u_\tau(x)$ with $h + \tau$ follows. Thus, the assumption always can be satisfied if, for example, we choose a small τ provided $|\Delta_0 - \Delta_\tau|$ is sufficiently small.

Assumption 4.

$$\int_{\Delta_\tau}^{\Delta_0} \mid \frac{\partial r}{\partial x}(x, y) \mid dy < -\frac{\partial \Phi}{\partial x}(x, \Delta_\tau), \ \forall x \in [\Delta_\tau, \Delta_0].$$

Instead of Assumption 4 we can introduce the following assumption:

Assumption 4 $'$.

$$\int_{\Delta_\tau}^{\Delta_0} \mid \frac{\partial r}{\partial x}(x, y) \mid f(u_0(y) - h)dy < -\frac{\partial \Phi}{\partial x}(x, \Delta_\tau), \ \forall x \in [\Delta_\tau, \Delta_0].$$

Although this assumption is less restrictive than Assumption 4, it implicitly contains a restriction on the firing rate function, f.

Assumption 4 (or 4$'$) is technical and used only to prove that $u^*(x)$ is a decreasing function on $[\Delta_\tau, \Delta_0]$.

Lemma 4.3. *The fixed point $u^*(x)$ is differentiable and decreasing on the interval $[\Delta_\tau, \Delta_0]$.*

Proof. We get

$$(u^*(x))' = u_\tau'(x) + I, \quad I = \int_{\Delta_\tau}^{\Delta_0} \frac{\partial r}{\partial x}(x, y) f(u^*(y) - h)dy.$$

In order to prove that $(u^*(x))' < 0$ we need to show that $I < -u'_\tau(x)$ where

$$u'_\tau(x) = \frac{\partial \Phi}{\partial x}(x, \Delta_\tau) < 0$$

by Assumption 3.

We get the following chain of inequalities for $|I|$

$$|I| \le \int_{\Delta_\tau}^{\Delta_0} \mid \frac{\partial r}{\partial x}(x,y) \mid f(u^*(y) - h)dy \le$$
$$\le \int_{\Delta_\tau}^{\Delta_0} \mid \frac{\partial r}{\partial x}(x,y) \mid f(u_0(y) - h)dy.$$

Thus, by Assumption 4 (or 4′) we have $|I| < -u'_\tau(x)$ and therefore $I < -u'_\tau(x)$. □

Finally, we introduce the following assumption which by Definition 2.6 allow us to view the extended solution u of u^* to be a bump:

Assumption 5. *The function Φ is such that*

(i) $\Phi(x,z) \le h,\ \forall x > \Delta_0,\ z \in [\Delta_\tau, \Delta_0]$,

(ii) $\Phi(x,z) \ge h + \tau,\ \forall x \in [0, \Delta_\tau],\ z \in [\Delta_\tau, \Delta_0]$.

Theorem 4.4. *Under Assumptions 3, 4 (or 4′), and 5 the fixed point u^* defined on the interval $[\Delta_\tau, \Delta_0]$ can be extended to a bump solution $u(x)$ of* (2.4) *defined on $\mathbb{R}$ such that $u(x) > h + \tau$ $\forall x \in [0, \Delta_\tau)$ and $u(x) < h$ $\forall x \in (\Delta_0, \infty)$.*

Proof. From Theorem 4.1 and Lemma 4.3 it follows that there exist unique δ_τ, $\delta_0 : \Delta_\tau < \delta_\tau < \delta_0 < \Delta_0$ such that

$$u^*(\delta_\tau) = h + \tau, \quad u^*(\delta_0) = h.$$

Let us introduce the function F defined by

$$F(y) = \begin{cases} 1, & 0 \le y < \delta_\tau \\ f(u^*(y) - h), & \delta_\tau \le y \le \delta_0 \\ 0, & y > \delta_0. \end{cases}$$

Then, according to Lemma 4.3 $F(y)$ is monotonically decreasing function on $[\delta_\tau, \delta_0]$ with $F(\delta_0) = 0$ and $F(\delta_\tau) = 1$. From (2.3) we get

$$u(x) = \int_0^{\delta_0} r(x,y)F(y)dy = -\int_0^{\delta_0} r(x,y) \int_y^{\delta_0} F'(z)dz.$$

By changing the order of integration, we have

$$u(x) = -\int_{\delta_\tau}^{\delta_0} \int_0^z r(x,y)dyF'(z)dz = \int_{\delta_\tau}^{\delta_0} \int_0^z r(x,y)dyd(1 - F(z)),$$

or

$$u(x) = \int_0^1 \int_0^{z(\xi)} r(x,y)dyd\xi = \int_0^1 \Phi(x, z(\xi))d\xi, \ \text{ where } \xi = 1 - F(z).$$

It remains to show that $\Phi(x,z) < h$ for $x > \Delta_0$, $z \in [\delta_\tau, \delta_0]$, and $\Phi(x,z) > h + \tau$ for $0 \le x < \Delta_\tau$, $z \in [\delta_\tau, \delta_0]$. Assumption 5 guarantees that these inequalities on a larger interval for z. Moreover, $u(-x) = u(x)$ due to symmetry of ω. Thus, the proof is completed. □

The proof of Theorem 4.1 is a modification of the theorem used in [7]. The modification is caused by the fact that our assumptions on the connectivity functions ω are different from ones used in [7].

We have checked numerically that Assumptions 3-5 are satisfied for the same parameters as we chose in Fig.4(a). In Fig.5 we have plotted the graph of a bump in $f-$field. Moreover, we can conclude that due to (4.2) the constructed solution is stable, see [7].

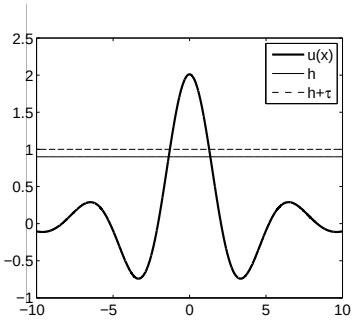

FIGURE 5. The bump solution of the $f-$ field constructed from u^*, see Fig.4(a).

5. ITERATION SCHEME II: BUMPS WIDTH ITERATION

In [8] an iteration procedure for construction of bumps of the f-field has been worked out. However, a mathematical verification of the procedure has not been given. In the present section we introduce an iteration scheme which is based on the idea introduced in [8] and give a mathematical verification of this approach.

Let $t \in [0, \tau]$ and assume that there exist $\Delta(t)$ such that a bump solution, $u_\Delta(x)$, satisfies

$$u_\Delta(\pm\Delta(t)) = t + h.$$

Then $u_\Delta(x)$ can be described by

$$u_\Delta(x) = \int_0^\tau \rho(\xi) \int_0^{\Delta(\xi)} r(x, y) dy d\xi \tag{5.1}$$

using the representation (2.9).

If a bump of the $f-$field is given by (2.10) then $\Delta(t) \in [\Delta_\tau, \Delta_0]$. The excitation width Δ satisfies the fixed point problem

$$\Delta = A\Delta, \quad (A\Delta)(t) = \Delta(t) + k\left(u_\Delta(\Delta(t)) - t - h\right), \quad k = \text{const} \in \mathbb{R}. \tag{5.2}$$

Theorem 5.1. *The operator A is Fréchet differentiable in $L_2[0, \tau]$ if $f \in W^{1,\infty}(\mathbb{R})$.*

Proof. Let us define the operator

$$(G\Delta)(t) = u_\Delta(\Delta(t)).$$

We calculate the Fréchet derivative of the operator $G\Delta$. To do this we first compute its Gáteaux derivative

$$g(\delta) = \lim_{\lambda \to 0} \frac{G(\Delta + \lambda\delta) - G(\Delta)}{\lambda}.$$

For any $\delta \in L_2[0, \tau]$ let us consider

$$G(\Delta + \lambda\delta) - G(\Delta) = \int_0^\tau \rho(\xi) I_1(\xi) d\xi, \tag{5.3}$$

where

$$I_1(\xi) = \int_0^{\Delta(\xi)+\lambda\delta(\xi)} r(\Delta(t)+\lambda\delta(t), y)dy - \int_0^{\Delta(\xi)} r(\Delta(t), y)dy.$$

Making use of the Taylor expansion of $r(\Delta(t)+\lambda\delta(t), y)$ as a function of λ at $\lambda = 0$ we have

$$\begin{aligned} I_1(\xi) &= \int_0^{\Delta(\xi)+\lambda\delta(\xi)} \left(r(\Delta(t), y) + \lambda \frac{\partial r}{\partial x}(\Delta(t), y)\delta(t) + o(\lambda) \right) dy - \int_0^{\Delta(\xi)} r(\Delta(t), y)dy \\ &= \int_{\Delta(\xi)}^{\Delta(\xi)+\delta(\xi)} r(\Delta(t), y)dy + \lambda\delta(t) \int_0^{\Delta(\xi)+\lambda\delta(\xi)} \frac{\partial r}{\partial x}(y, \Delta(t))dy + o(\lambda) \end{aligned}$$

Plugging I_1 into (5.3) and making use of the mean value theorem we get the following formula

$$g(\Delta, \delta(t)) = \int_0^\tau \rho(\xi)\delta(\xi) r(\Delta(t), \Delta(\xi))d\xi + \delta(t) \int_0^\tau \rho(\xi) \frac{\partial \Phi}{\partial x}(\Delta(t), \Delta(\xi))d\xi. \tag{5.4}$$

Hence, we arrive at the conclusion that the Gáteaux derivative is a linear operator. In order to prove Fréchet differentiability of the operator G we show in accordance with [15] that $g(\cdot, \delta) : L_2[0,\tau] \to L_2[0,\tau]$ is a continuous operator for all $\delta \in L_2[0,\tau]$. The proof of this fact is technical and we therefore formulate it as a separate lemma.

Lemma 5.2. *The operator $g(\cdot, \delta) : L_2[0,\tau] \to L_2[0,\tau]$ is continuous for all $\delta \in L_2[0,\tau]$.*

Proof. We consider the first and the second integral of (5.4) separately as the operators of Δ. Using the Cauchy-Schwarz and Minkowski inequalities we show that these operators are continuous and, thus, $g(\cdot, \delta)$ is continuous as well, for any $\delta \in L_2[0,\tau]$. We present the proof for the first integral operator. The proof of continuity for the second term proceeds in the same way and is omitted. Introduce

$$(F\Delta)(t) = \int_0^\tau \rho(\xi)\delta(\xi) r(\Delta(t), \Delta(\xi))d\xi.$$

We get

$$\begin{aligned} (F\Delta_1 - F\Delta_2)(t) = \int_0^\tau \rho(\xi)\delta(\xi) \big(& r(\Delta_1(t), \Delta_1(\xi)) - r(\Delta_1(t), \Delta_2(\xi)) + \\ & + r(\Delta_1(t), \Delta_2(\xi)) - r(\Delta_2(t), \Delta_2(\xi)) \big) d\xi = I_1(t) + I_2(t) \end{aligned}$$

where by the mean value theorem I_1 and I_2 can be defined as

$$I_1(t) = \int_0^\tau \rho(\xi)\delta(\xi) \frac{\partial r}{\partial y}(\Delta_1(t), \tilde{\Delta}_1(\xi))(\Delta_1(\xi) - \Delta_2(\xi))d\xi$$

$$I_2(t) = \int_0^\tau \rho(\xi)\delta(\xi) \frac{\partial r}{\partial x}(\tilde{\Delta}_2(t), \Delta_2(\xi))(\Delta_1(t) - \Delta_2(t))d\xi$$

with $\tilde{\Delta}_k = \lambda_k\Delta_1 + (1-\lambda_k)\Delta_2$, for some $\lambda_k \in [0,1]$, $k = 1, 2$.

We consider the norm of the difference. Using the Minkowski inequality we get

$$\begin{aligned} ||F\Delta_1 - F\Delta_2||_{L_2[0,\tau]} &= \left(\int_0^\tau (I_1(t) + I_2(t))^2 dt \right)^{1/2} \leq \\ &\leq \left(\int_0^\tau |I_1(t)|^2 dt \right)^{1/2} + \left(\int_0^\tau |I_2(t)|^2 dt \right)^{1/2} \end{aligned}$$

Applying the Cauchy - Schwarz inequality to each of the terms we have

$$||F\Delta_1 - F\Delta_2||_{L_2[0,\tau]} \leq$$
$$\leq \left(\int_0^\tau \int_0^\tau \left| \rho(\xi)\delta(\xi) \frac{\partial r}{\partial y}(\Delta_1(t), \tilde{\Delta}_1(\xi)) \right|^2 d\xi \int_0^\tau |\Delta_1(\xi) - \Delta_2(\xi)|^2 d\xi \, dt \right)^{1/2} +$$
$$+ \left(\int_0^\tau \int_0^\tau \left| \rho(\xi)\delta(\xi) \frac{\partial r}{\partial y}(\Delta_1(t), \tilde{\Delta}_1(\xi)) \right|^2 d\xi \int_0^\tau |\Delta_1(t) - \Delta_2(t)|^2 d\xi \, dt \right)^{1/2}$$

Since $r \in W^{1,\infty}(\mathbb{R} \times \mathbb{R})$, $\rho \in L_\infty(\mathbb{R})$, and $\delta \in L_2[0,\tau]$ the following estimate is valid

$$\int_0^\tau \left| \rho(\xi)\delta(\xi) \frac{\partial r}{\partial y}(\Delta_1(t), \tilde{\Delta}_1(\xi)) \right|^2 d\xi \leq C^2/2$$
$$\int_0^\tau \left| \rho(\xi)\delta(\xi) \frac{\partial r}{\partial x}(\tilde{\Delta}_2(t), \Delta_1(\xi)) \right|^2 d\xi \leq C^2/2$$

where

$$C^2 = 2||\rho||_{L_\infty(\mathbb{R})} \max\{||\frac{\partial r}{\partial x}||_{L_\infty(\mathbb{R}\times\mathbb{R})}, ||\frac{\partial r}{\partial y}||_{L_\infty(\mathbb{R}\times\mathbb{R})}\} ||\delta||^2_{L_2[0,\tau]}.$$

Therefore, we get

$$||F\Delta_1 - F\Delta_2||_{L_2[0,\tau]} \leq |C|\sqrt{\tau}||\Delta_1 - \Delta_2||_{L_2[0,\tau]}$$

from which the continuity of F follows. □

For convenience we redefine $g(\Delta, \delta) = G'_\Delta \delta$. Obviously, the operator A is Fréchet differentiable in any $\Delta \in L_2[0,\tau]$ and

$$A'_\Delta = I + kG'_\Delta \tag{5.5}$$

□

We get the following lemma:

Lemma 5.3. *The operator $A'_\Delta \delta \geq 0$ for $\delta \geq 0$ and $\Delta \in [\Delta_\tau, \Delta_0]$ under Assumption 2 and 3 and $0 < k < 1/m$, where*

$$m = -\min_{t,\xi \in [0,\tau]} \frac{\partial \Phi}{\partial x}(\Delta(t), \Delta(\xi)). \tag{5.6}$$

Proof. First of all, we notice that $\partial\Phi/\partial x \in BC(\mathbb{R}) \times BC(\mathbb{R})$. Thus, there exists a finite minimum of $\partial\Phi/\partial x$ on the given set. Moreover, this minimum is negative according to Assumption 3. Therefore, m given by (5.6) is finite and positive, and the operator A'_Δ preserves positivity for $0 < k < 1/m$. □

Lemma 5.4. *The operator $A : [\Delta_\tau, \Delta_0] \to D \in L_2[0,\tau]$ is monotonically increasing under the conditions of Lemma 5.3.*

Proof. Let $\Delta_2 \geq \Delta_1$. Then $A\Delta_2 - A\Delta_1 = A'_\Delta(\Delta_2 - \Delta_1)$ where $\Delta \in [\Delta_1, \Delta_2] \subset [\Delta_\tau, \Delta_0]$. We apply Lemma 5.3 to complete the proof. □

Theorem 5.5. *If the conditions of Theorem 5.1 and Lemma 5.4 are satisfied then the operator $A : [\Delta_\tau, \Delta_0] \to D \subset L_2[0,\tau]$ has a fixed point in $[\Delta_\tau, \Delta_0]$. Moreover, the sequences $\{A^n\Delta_\tau\}$ and $\{A^n\Delta_0\}$ converge to the smallest and greatest fixed point of the operator A, respectively.*

Proof. The operator A is monotonically increasing (see Lemma 5.4) and Frechet differentiable, and hence continuous, in $L_2[0,\tau]$ (see Lemma 5.1). Moreover, we have the following inequalities

$$(A\Delta_0)(t) = \Delta_0 + k(u_{\Delta_0}(\Delta_0) - t - h) = \Delta_0 + k(u_0(\Delta_0) - t - h) = \Delta_0 - kt \leq \Delta_0.$$

and

$$(A\Delta_\tau)(t) = \Delta_\tau + k(u_{\Delta_\tau}(\Delta_\tau) - t - h) = \Delta_\tau + k(u_\tau(\Delta_\tau) - t - h) = \Delta_0 + k(\tau - t) \geq \Delta_\tau.$$

We now apply Theorem 3.1 since all the conditions for the operator A are satisfied. This completes the proof. □

Remark 5.6. *We prove Theorem 5.5 for the case when $D \in L_2[0,\tau]$ but do not consider the case $D \in C[0,\tau]$. The cone of positive functions in $C[0,\tau]$ is not regular. Therefore additional assumptions on the operator A are required (see Theorem 3.1). We notice that A is not compact in $C[0,\tau]$. Indeed, the operator A is a Fréchet differentiable with A'_Δ defined as in* (5.5) *where A'_Δ is a sum of the identity operator and a compact operator, thus is not compact. Therefore, A is not a compact operator, see* [15]. *The operator A does not seem to be condensing either, at least with respect to the Hausdorff measure. The case of more general measures of noncompactness* [14, 17] *is not considered here.*

Assumption 3′. *The partial derivative of Φ with respect to x is negative for $x = \Delta(t), y = \Delta(s)$ for $t, s \in [0,\tau]$ and $\Delta(t)$ is a fixed point of* (5.2)*, i.e.,*

$$\frac{\partial \Phi}{\partial x}(\Delta(t), \Delta(s)) < 0, \ \forall t, s \in [0,\tau].$$

Lemma 5.8. *The fixed point $\Delta(t)$ of operator A is monotonically decreasing and differentiable on $[0,\tau]$ under Assumption 3′.*

Proof. Since $\Delta(t)$ is a solution of the fixed point problem (5.2) then $u_\Delta(\Delta(t)) = t + h$. We prove the lemma by direct differentiation of the last equality with respect to t. We obtain

$$\int_0^\tau \rho(\xi) \frac{\partial \Phi}{\partial x}(\Delta(t), \Delta(\xi)) \Delta'(t) d\xi = 1.$$

Thus,

$$\Delta'(t) = \left(\int_0^\tau \rho(\xi) \frac{\partial \Phi}{\partial x}(\Delta(t), \Delta(\xi)) d\xi \right)^{-1} < 0$$

as $\dfrac{\partial \Phi}{\partial x}(\Delta(t), \Delta(\xi)) < 0$ by Assumption 3′. □

Assumption 3′ requires an apriori knowledge of $\Delta(t)$ and therefore can not be checked before $\Delta(t)$ is found. Thus, we suggest to replace this assumption with the following assumption:

Assumption 3″. *The partial derivative of Φ with respect to x is negative for all $x, y \in [\Delta_\tau, \Delta_0]$, i.e.,*

$$\frac{\partial \Phi}{\partial x}(x, y) < 0, \ \forall x, y \in [\Delta_\tau, \Delta_0].$$

The fulfillment of Assumption 3″ is required so that Assumption 3 and Assumption 3′ are satisfied.

The Assumptions 1,2, and 3″ hold true when $\omega(x)$, and Δ_τ, Δ_0 are chosen as in Section 4. In Fig.6(a) we illustrate the result of the iteration process based on Theorem 5.5. The minimal and maximal fixed points are the same, $\Delta(t)$, and thus, the fixed point is unique. Moreover, it belongs to $[\Delta_\tau^{st}, \Delta_0]$. In Fig.6(b) we have plotted the errors

$$\begin{array}{ll} \varepsilon_1(n) = \max\limits_t |(A^n\Delta_\tau)(t) - (A^{n-1}\Delta_\tau)(t)|, & A^0\Delta_\tau \equiv \Delta_\tau \\ \varepsilon_2(n) = \max\limits_t |(A^n\Delta_0)(t) - (A^{n-1}\Delta_0)(t)|, & A^0\Delta_0 \equiv \Delta_0 \end{array} , n = 1, 2, ..., N, \tag{5.7}$$

where N denotes the total number of iterations.

It remains to show that u_Δ, where Δ is the fixed point of (5.2), is a bump. We introduce the following assumption:

Assumption 5′. *The function Φ is such that*

(i) $\Phi(x,y) \le h,\ \forall x > \Delta(0),\ y \in [\Delta(\tau), \Delta(0)]$,

(ii) $\Phi(x,y) \ge h+\tau,\ \forall x \in [0, \Delta(\tau)],\ y \in [\Delta(\tau), \Delta(0)]$.

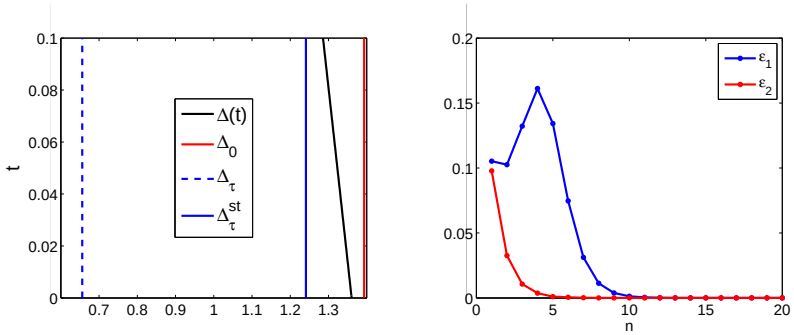

(a) (b)

FIGURE 6. (a) A fixed point of (5.2), $\Delta(t)$, vertical lines Δ_0, Δ_τ, andΔ_τ^{st} as defined in Fig. 3. The connectivity function ω is given as (2.2) with $b = 0.3$, f is defined by (2.8) with $p = 2$, $h = 0.3$, $\tau = 0.1$. (b) The errors given as in (5.7).

Theorem 5.11. *Let Δ be a fixed point of the problem* (5.2) *then u_Δ defined as* (5.1) *is a bump solution of* (1.1) *under Assumption 5′.*

Proof. We rewrite (5.1) as

$$u_\Delta(x) = \int_0^\tau \rho(\xi)\Phi(x, \Delta(\xi))d\xi.$$

Next, we make use of Assumption 5′. Keeping in mind the normalization property of ρ we show that

$$u_\Delta(x) \le h, \qquad \forall x > \Delta(0),\ y \in [\Delta(\tau), \Delta(0)],$$

$$u_\Delta(x) \ge h+\tau, \quad \forall x \in [0, \Delta(\tau)],\ y \in [\Delta(\tau), \Delta(0)].$$

□

Knowing $\Delta(t)$ we now reconstruct the bump by means of the formula (5.1). The reconstructed bump coincides with the bump solution we found in Section 4. See Fig. 5.

Remark 5.12. *For operator T_f we use Assumptions 1-5 and Assumptions 1-2, 3″ and 5′ for the operator A. Assumptions 3″ and 5′ are more restrictive than Assumptions 3 and 5. Moreover Assumption 5 needs information about the fixed point $\Delta(t)$ which is a disadvantage. On the other hand, the operator T_f needs one extra assumption, Assumption 4.*

6. DISCUSSION

We have introduced two iteration schemes for finding a bump solution in the $f-$field of the Wilson-Cowan model: The first scheme is based on the fixed point problem formulated by Kishimoto and Amari [7]. The second one is described by the fixed point problem formulated for the interface dynamics of the bump. The latter formulation became possible due to the special representation of the firing rated function introduced by Coombes and Schmidt [8].

We have proved using the theory of monotone operators in Banach spaces that both iteration schemes converge under Assumption 1 and 2. From the iterative procedures we obtain the solution on the finite interval $[\Delta_\tau, \Delta_0]$ (see Section 4), and on $[\Delta(0), \Delta(\tau)]$ (see Section 5). Then it has been shown that under some additional assumptions on the connectivity function ω this solution determines a bump of the $f-$field on $\mathbb{R}$.

The assumptions imposed for the first method (see Section 4) differ from the ones imposed for the second method (see Section 5). The evident disadvantage of Assumption $3'$ and $5'$ is that they contain information about the output of the interaction procedure, $\Delta(t)$. Assumption $3'$ can be substituted by more restrictive Assumption $3''$, but not Assumption $5'$. Thus, Assumption $5'$ can not be checked in advance. On the other hand, the set of assumptions for the fixed point problem (5.2) is in general less restrictive. All assumptions (except Assumption $5'$) are quite easy to check if $\omega(x)$ is given.

We show by a numerical example that both iterative schemes converge to the same solution. Moreover, from numerics it follows that this solution is unique and stable. Indeed, the maximal and minimal fixed points turn out to be equal for any trials and choice of parameters. Thus, by Corollary 3.2, the fixed point is unique. Moreover, the constructed fixed point solution is stable since it is located between stable solutions of f_0- and $f_\tau-$field, [7]. Notice that we have not given a mathematical verification of these observations.

Notice also that we have looked for the bump solutions under the assumption $\Delta_\tau < \Delta_0$ and (2.10). Thus, even if the constructed solution is unique, it does not necessarily mean that there are no other stable or unstable solution. However, the same type of reasoning as we performed here are not longer valid if we relax on these assumptions. Therefore we leave this problem for a future study.

7. ACKNOWLEDGEMENTS

The authors would like to thank Professor Stephen Coombes (School of Mathematical Sciences, University of Nottingham, United Kingdom), and Professor Vadim Kostrykin (Johannes Gutenberg-University, Mainz, Germany) for many fruitful and stimulating discussions during the preparation of this paper. John Wyller and Anna Oleynik also wish to thank the School of Mathematical Sciences, University of Nottingham for the kind hospitality during the stay. This research was supported by the Norwegian University of Life Sciences. The work has also been supported by The Research Council of Norway under the grant No. 178892 (eNEURO-multilevel modeling and simulation of the nervous system) and the grant No. 178901 (Bridging the gap: disclosure, understanding and exploitation of the genotype-phenotype map).

REFERENCES

[1] H. R. Wilson and J. D. Cowan, *Excitatory and inhibitory interactions in localized populations of model neurons*, Biophysical Journal, 12:1-24, 1972.

[2] H. R. Wilson and J. D. Cowan, *A mathematical theory of the functional dynamics of cortical and thalamic nervous tissue*, Kybernetik, 13:55-80, 1973.

[3] S Amari, *Homogeneous nets of neuron-like elements. Biological Cybernetics*, 17:211-220, 1975.

[4] S. Amari, *Dynamics of Pattern Formation in Literal-Inhibition Type Neural Fields*, Biol. Cybernetics, 27:77-87, 1977.

[5] S. Coombes, *Waves, bumps, and patterns in neural field theories*, Biological Cybernetics,93(91), 2005.

[6] S.Coombes and M.R.Owen *Evans functios for integral field equations with Heavisite firing rate function* SIAM Journal on Applied Dynamical Systems, 34:574-600,2004.
[7] K. Kishimoto, S. Amari, *Existence and Stability of Local Excitations in Homogeneous Neural Fields*, J.Math. Biology, 7:303-318, 1979.
[8] S. Coombes, H. Schmidt *Neural Fields with Sigmoidal Firing Rates: Approximate Solutions*,Discrete and Continuous Dynamical Systems, 28:1369-1379, 2010.
[9] O. Faugeras, F.Grimbert, and J.-J. Slotine, *Absolute stability and complete synchronization in a class of neural field models*, SIAM J. Appl. Math., 63:205-250, 2008.
[10] P.S. Goldman-Rakic, *Cellular basis of working memory,* Neuron, 14:477-485, 1995.
[11] A.J. Elvin, C.R. Laing, R.I.McLachlan, and M.G.Roberts, *Exploiting the Hamiltonian structure of a neural field model,* Physica D, 239:537-546, 2010.
[12] C.R.Laing amd W.C.Troy *PDE methods for nonlocal models,* Siam Journal on Applied Dynamical Systems, 2:487-516,2003.
[13] C.R. Laing, W.C. Troy, B. Gutkin, G.B. Ermentrout, *Multiple bumps in a neuronal network model of working memory*, SIAM J. Appl. Math., 63 (2002) 62–97.
[14] Dajun Guo and V.Lakshmikantham, *Nonlinear problems on Abstract Cones*,Academic Press, Inc., 1988.
[15] E. Zeidler, *Nonlinear Functional Analysis, Vol.1: Fixed-Point Theorems*, Springer, 1986.
[16] A.N. Kolmogorov and S.V. Fomin, *Introductory Real Analasis*,Dover publications Inc., 1975
[17] R. R. Akhmerov, M. I. Kamenskii, A. S. Potapov and B. N. Sadovskii, *Condensing operators*, Journal of Mathematical Sciences, 18(4): 551-592, 1982.

A. OLEYNIK, DEPARTMENT OF MATHEMATICAL SCIENCES AND TECHNOLOGY AND CENTER FOR INTEGRATIVE GENETICS, NORWEGIAN UNIVERSITY OF LIFE SCIENCES, N-1432 ÅS, NORWAY
E-mail address: anna.oleynik@umb.no

A. PONOSOV,DEPARTMENT OF MATHEMATICAL SCIENCES AND TECHNOLOGY AND CENTER FOR INTEGRATIVE GENETICS, NORWEGIAN UNIVERSITY OF LIFE SCIENCES, N-1432 ÅS, NORWAY
E-mail address: arkadi.ponossov@umb.no

J. WYLLER,DEPARTMENT OF MATHEMATICAL SCIENCES AND TECHNOLOGY AND CENTER FOR INTEGRATIVE GENETICS, NORWEGIAN UNIVERSITY OF LIFE SCIENCES, N-1432 ÅS, NORWAY, AND, SCHOOL OF MATHEMATICAL SCIENCES, UNIVERSITY OF NOTTINGHAM, NG7 2RD, UK
E-mail address: john.wyller@umb.no

Paper II

Physica D 239 (2010) 1766–1780

Contents lists available at ScienceDirect

Physica D

journal homepage: www.elsevier.com/locate/physd

The weakly nonlocal limit of a one-population Wilson–Cowan model

Anna Oleynik [a,*], John Wyller [a], Igor Wertgeim [b]

[a] Department of Mathematical Sciences and Technology, Norwegian University of Life Sciences and Centre for Integrative Genetics (CIGENE), P.O. Box 5003, N-1432 Ås, Norway
[b] Institute of Continuous Media Mechanics, Ural Branch, Russian Academy of Sciences, 1, Akad. Korolyov Street Perm, 614039, Russia

ARTICLE INFO

Article history:
Received 11 February 2010
Received in revised form
26 May 2010
Accepted 28 May 2010
Available online 8 June 2010
Communicated by A. Mikhailov

Keywords:
Neural field models
Nonlocal
Wavelet–Galerkin method

ABSTRACT

We derive the weakly nonlocal limit of a one-population neuronal field model of the Wilson–Cowan type in one spatial dimension. By transforming this equation to an equation in the firing rate variable, it is shown that stationary periodic solutions exist by appealing to a pseudo-potential analysis. The solutions of the full nonlocal equation obey a uniform bound, and the stationary periodic solutions in the weakly nonlocal limit satisfying the same uniform bound are characterized by finite ranges of pseudo energy constants. The time dependent version of the model is reformulated as a Ginzburg–Landau–Khalatnikov type of equation in the firing rate variable where the maximum (minimum) points correspond stable (unstable) homogeneous solutions of the weakly nonlocal limit. Based on this formulation it is also conjectured that the stationary periodic solutions are unstable. We implement a numerical method for the weakly nonlocal limit of the Wilson–Cowan type of model based on the wavelet–Galerkin approach. We perform some numerical tests to illustrate the stability of homogeneous solutions and the evolution of the bumps.

1. Introduction

Various types of mathematical models are used to describe the signal processing properties of networks of neurons. These model types are distinguished by their scope and the amount of biophysical detail incorporated in the description. The modeling approaches are divided into three main categories: *compartmental modeling, simplified spiking models* and *firing rate models*. For an overview of different modeling approaches; see [1,2]. The firing rate modeling approach has the coarsest level of detail. Here only the probability for action-potential firing is modeled. Then the "activity level" (for example, membrane potential in the cell body) is typically converted to a firing rate via a nonlinear sigmoidal function. The number of neurons in the brain is immensely large. Hence, if the typical spatial and temporal scales are much larger than the corresponding neuronal scales, mean field theoretical versions of the rate equations are appropriate. For a review on firing rate models; see the Refs. [2–6].

The key topics in neural field models are existence and stability of coherent structures like bumps and traveling fronts and pulses, pattern formation and experimental detection of coherent structures. Different levels of biophysical realism are incorporated in the models such as two-population models of excitatory and inhibitory neurons [2,7–10], micro structure in the connectivity functions [11], spike frequency adaptation (SFA) [12], finite dendritic and axonal delay effects [13–16], and 2D spatial effects [17].

The methods used to study rate equation models include different techniques from applied mathematics like construction of explicit representations for coherent structures like bumps and traveling fronts in the Heaviside limit of the firing rate function, stability analysis of these wave phenomena using the Evans functions techniques [6] (and the references therein), and detailing the dynamical evolution of the neural field states by means of different numerical methods.

The numerical methods used to solve the rate equations are of different degree of complexity. The time evolution is in most cases resolved by means of finite difference schemes. For example, the program XPPAUT, developed by Ermentrout [18], which aims at solving finite order rate equation models is based on 4th order Runge–Kutta in time. This has for example been used in [10]. In [9] a variant of the 4th order Runge–Kutta method is formulated for the temporal development of localized solutions where the pulse widths of the solutions are determined at each time step. However, when attempting to resolve problems with steep gradients or presence of a multiplicity of very different spatial and temporal scales, numerical approaches such as spectral methods and finite difference schemes lead to the development of numerical instabilities or loss of the accuracy of the solutions; see [19,20]. In order to overcome these type of problems the wavelet–Galerkin method seems to be quite promising. Wavelet basis functions which possess no singularities and, which are

* Corresponding author.
E-mail address: anna.oleynik@umb.no (A. Oleynik).

0167-2789/$ – see front matter © 2010 Elsevier B.V. All rights reserved.
doi:10.1016/j.physd.2010.05.011

localized both in physical and Fourier spaces give possibilities with less computational efforts to describe such processes connected to the interaction of localized structures of different spatial scales [19,20]. In particular, the advantages with wavelet bases have been demonstrated for the solutions of some physical problems, e.g., hydrodynamic problems (see [20], Chapter 4 by Farge et al.), atomic physics and solid state physics problems (see [20, Chapter 8], by Antoine et al.) and the famous Burgers equation [21–23].

We aim at studying the properties of the *weakly nonlocal limit* of the Wilson–Cowan type of model

$$\tau \partial_t u(x,t) = -u(x,t) + \int_{-\infty}^{\infty} \omega(y-x) P(u(y,t)-\theta)\mathrm{d}y \tag{1}$$

both analytically and numerically. Here u denote the electrical activity level, ω the connectivity function, P the firing rate function, θ the threshold value, τ the time constant, x spatial coordinate and t the temporal coordinate. The model (1) has been studied in several papers (see for example [5]).

The weakly nonlocal limit is obtained from (1) when the characteristic spatial scale length of the variation of the firing rate variable $v = P(u-\theta)$ is assumed to be much larger than the typical length scale for the connectivity function (*synaptic footprint*). The resulting equation is a nonlinear diffusion equation. The solutions of (1) obey the uniform bound $0 \le u(x,t) \le 1$ for all x and t for positive normalized connectivity functions. We reformulate the weakly nonlocal limit to the Ginzburg–Landau–Khalatnikov type of equation, see [24] or [25], in the firing rate variable $v = P(u-\theta)$. This formulation allows us to find a condition to have solutions within the same bound as the solutions of (1). Finally, we use the wavelet–Galerkin method for the numerical study of the weakly nonlocal limit. We choose the Daubechies wavelets as the wavelet basis due to the localized character of the expected solutions [5].

The present paper is organized as follows: In Section 2 we introduce the one-population neuronal field model. It is shown that the instability of a homogeneous background state in the Wilson–Cowan model is of the finite bandwidth type and that the instability structure consists of a set of well separated bands in a wavenumber space. In Section 3 we derive the weakly nonlocal limit from the model (1). It is shown that instability structure of the full model (1) continuously deforms to a single unstable band in the weakly nonlocal limit, which can be detected by direct stability analysis of the weakly nonlocal limit. We will refer to this instability structure as *gain band structure* in accordance with the terminology used in [10]. It is shown that in the stationary case the weakly nonlocal limit can be transformed to a pseudo-potential problem in the firing rate variable $v = P(u-\theta)$. It then turns out that the time dependent version of this equation assumes the form of the Ginzburg–Landau–Khalatnikov equation where the stability of the homogeneous background can be inferred from the properties of extreme points of the pseudo-potential. We review the wavelet–Galerkin numerical method in Section 4. The organization of this section is as follows. We start out by formulating the general framework for Galerkin expansion of model equations. Next we discuss the advantages of using wavelet functions as a Galerkin basis and introduce the definition of multiresolution analysis (MRA). Then we describe the wavelet–Galerkin expansion scheme and the way we treat boundary conditions. Finally, we implement the wavelet–Galerkin method for the weakly nonlocal limit of the one-population neural field model. We demonstrate numerically the evolution of a saw tooth initial condition and a bump initial condition for two choices of the firing rate function. We compare the outcome of these simulations with the analysis in Section 3. In Section 5 we summarize the findings of this paper and point out the directions of future research.

2. Properties of a one-population neural model

2.1. The model

We consider a one-population model in a one dimensional strip of cortical tissue. It is assumed that (i) all neurons receive synaptic inputs from, in principle, all neurons in the network, (ii) the synaptic weights depend only on absolute spatial distance between pre- and postsynaptic neurons, (iii) the net activity level in each neuron depends on a weighted sum over the past firing activity in the presynaptic neurons, and (iv) the neuronal firing rate at a certain time is modeled by means of an non-decreasing nonlinear function which assumes values between zero and one [2].

Let $u = u(x,t)$ denote the electrical activity level at the spatial point x and at time t. The field theoretical version of the input–output model reads

$$u = \langle P(u-\theta)\rangle \tag{2}$$

where the operator $\langle\cdot\rangle$ denotes the spatio-temporal average of $P(u-\theta)$ defined as

$$\begin{aligned}\langle P(u-\theta)\rangle(x,t) &= [\alpha * \omega \otimes P(u-\theta)](x,t)\\ &= \int_{-\infty}^{t} \alpha(t-s) \int_{-\infty}^{\infty} \omega(y-x)\\ &\quad \times P(u(y,s)-\theta)\mathrm{d}y\mathrm{d}s.\end{aligned} \tag{3}$$

Here $*$ and $\otimes$ denote the temporal and spatial convolutions defined as

$$(\alpha * \beta)(t) = \int_{-\infty}^{t} \alpha(t-s)\beta(s)\mathrm{d}s,$$

and

$$(\omega \otimes f)(x) = \int_{-\infty}^{\infty} \omega(y-x) f(y)\mathrm{d}y,$$

respectively.

The parameter θ models the *threshold value for firing*, which by assumption is constant and satisfies the inequality $0 < \theta < 1$.

The function P models the *firing rate function* and satisfies the following conditions:

(i) $P : \mathbb{R} \to [0,1]$.
(ii) P is continuous on $\mathbb{R}$ and differentiable almost everywhere.
(iii) P is an non-decreasing function.
(iv) The functions P constitute a one-parameter family of functions, parameterized by a steepness parameter β

$$P(u) = S(\beta u).$$

Here S plays the role of a *scaling function of the firing rate function*. The parameter $\beta > 0$ measures the steepness of the firing rate function such that $P(u)$ converges to the Heaviside-step function $H(u)$ as β tends to infinity.

In this paper we model the firing rate function with the smooth function

$$P(u) = S(\beta u), \qquad S(u) = \frac{1}{2}(1+\tanh(u)), \tag{4}$$

the piecewise linear function

$$P(u) = S(\beta u), \qquad S(u) = \begin{cases} 0, & \text{if } u \le -1 \\ (u+1)/2, & \text{if } -1 < u < 1 \\ 1, & \text{if } u \ge 1 \end{cases} \tag{5}$$

and the function

$$P(u) = S(\beta u),$$
$$S(u) = \begin{cases} 0, & \text{if } u \le -1 \\ -1/2 + \sqrt{u+5/4}, & \text{if } -1 < u < 1 \\ 1, & \text{if } u \ge 1. \end{cases} \tag{6}$$

The firing rate function (4) is used to illustrate essential features of the model while the choice of the expressions (5) and (6) is motivated by the wavelet–Galerkin method. Notice that expressions (5) and (6) are concrete examples of the general firing rate function used in [26] for the purpose of studying the existence and stability of stationary solutions of the Wilson–Cowan model.

The function ω is called a *connectivity function* and is real valued, symmetric, positive, bounded and normalized, i.e., $\int_{-\infty}^{\infty}\omega(x)\mathrm{d}x = 1$. Moreover, it constitutes a one-parameter family of functions, i.e., it can be expressed as

$$\omega(x) = \frac{1}{\sigma}\Phi(\xi), \quad \xi = \frac{x}{\sigma}. \tag{7}$$

Here Φ is a non-dimensional scaling function and σ is the *synaptic footprint*, which measures the width of the nonlocal connectivity of the network. As $\sigma \to 0, \omega(x) \to \delta(x)$ where δ is the Dirac function. This limit case represents a switch-off of the connectivity of the network. The examples of w are the Gaussian function

$$\Phi(\xi) = \frac{1}{\sqrt{\pi}}\mathrm{e}^{-\xi^2}, \tag{8}$$

and the exponential decay function

$$\Phi(\xi) = \frac{1}{2}\mathrm{e}^{-|\xi|}. \tag{9}$$

The function α in (3) is a weight function which measures the memory of the network. This function is real valued, positive, bounded and normalized. Moreover, α is parameterized by means of the time constant, τ, which we set to one without any loss of generality.

The properties imposed on the firing rate function, P, the connectivity function, ω, and the temporal kernel, α, imply that any solution of the model (2) obeys the uniform bound

$$0 \le u(x,t) \le 1 \tag{10}$$

for all x and $t \ge 0$.

Another important property of the model (2) is that spatially symmetric, localized stationary solutions (*bumps*), u_b, exist in the Heaviside limit of the firing rate function P for $0 < \theta < 1/2$ and are given as

$$u_b(x) = W(a+x) + W(a-x) \tag{11}$$

where

$$W(x) = \int_0^x \omega(y)\mathrm{d}y$$

where a is the unique positive solution of the equation $W(2a) = \theta$.

In the present study we restrict ourselves to the case when the temporal kernel α is an exponentially decaying function

$$\alpha(t) = \mathrm{e}^{-t}.$$

By using the linear chain trick [27] we find that the activity level u of (2) evolves according to the Wilson–Cowan type of model

$$\partial_t u = -u + \omega \otimes P(u-\theta). \tag{12}$$

In Potthast et al. [29] it is shown that globally bounded solutions of (12) exist provided that the connectivity function ω is absolute integrable, the firing rate function P has a smooth bounded derivative, and the initial condition is bounded and continuous.

For the Cauchy problem of (12) we can deduce the bounds

$$u_0(x)\exp(-t) \le u(x,t) \le 1 + (u_0(x)-1)\exp(-t) \quad \text{for all } t \ge 0 \tag{13}$$

for the solution u, consistent with the results of Potthast et al. [29]. Here u_0 denote the initial condition for (12) and $0 \le u_0(x) \le 1$ for all x in order to be consistent with (10).

2.2. Turing instability and pattern formation

The next issue to be addressed is the Turing type of instability as a pattern forming mechanism, [13,28]. First, we investigate the possibility of having homogeneous solutions $u(x,t) = u_{eq}$, u_{eq} is a constant, of the problem (12). Such solutions must satisfy

$$u_{eq} = P(u_{eq} - \theta) \tag{14}$$

where, from (10), $0 \le u_{eq} \le 1$. In order to study the existence of homogeneous states, we introduce

$$F(u) = u - P(u-\theta), \qquad F : [0,1] \to \mathbb{R}.$$

Since $F(0) = -P(-\theta) < 0, F(1) = 1 - P(1-\theta) > 0$ and F is continuous on $[0,1]$, the equation $F(u) = 0$ has at least one solution.

Theorem 2.1. *The Wilson–Cowan model (12) has at least one homogeneous state given by (14).*

We address the uniqueness issue for the homogeneous state in detail in Section 3.

Now we consider the linear stability of u_{eq} by assuming

$$u(x,t) = u_{eq} + \phi(x,t), \quad |\phi(x,t)| \ll 1.$$

Notice that the stability analysis below does not use the positivity of the connectivity function. The linearized evolution equation for ϕ reads

$$\partial_t \phi = -\phi + \beta S' \omega \otimes \phi \tag{15}$$

where we assume that S is differentiable at $u = \beta(u_{eq} - \theta)$ and

$$S' = \frac{\mathrm{d}S}{\mathrm{d}u}|_{u=\beta(u_{eq}-\theta)}.$$

The Fourier transform of (15) is

$$\partial_t \widetilde{\phi}(k,t) = (-1 + \beta S' \widetilde{\omega}(k))\widetilde{\phi}(k,t)$$

where $\widetilde{\phi}$ and $\widetilde{\omega}$ are the Fourier transforms of ϕ and ω, respectively, and k denotes the wave number of the perturbation imposed on u_{eq}. Since by assumption the connectivity function ω is real and symmetric, the same holds true for the Fourier transform $\widetilde{\omega}$. The growth (decay) rate $\lambda(k)$ of the perturbation is given by

$$\lambda(k) = -1 + \beta S' \widetilde{\omega}(k). \tag{16}$$

From (16) we get the following stability result.

Theorem 2.2. *The homogeneous state, u_{eq}, of (12) is stable if $\beta S' \widetilde{\omega}(k) < 1$ for all k, while it becomes unstable if $\beta S' \widetilde{\omega}(k) > 1$ for at least one k.*

Let us then consider some limiting cases.

In the local limit, when $\sigma \to 0$, the connectivity function ω is modeled by means of the Dirac δ-function. Hence, we get $\widetilde{\omega}(k) = 1$ and Theorem 2.2 can be simplified.

Theorem 2.3. *The homogeneous state u_{eq} of (12) in the local limit is stable if $\beta S' < 1$ and unstable if $\beta S' > 1$.*

This means that the slope of the firing rate function evaluated at u_{eq} must exceed a certain threshold to get instability. Now, since the connectivity function ω is normalized, we have $\widetilde{\omega}(0) = 1$. Hence, the long wavelength limit of the problem ($k \to 0$) coincides with the local limit.

For connectivity functions satisfying $\widetilde{\omega}(k) \le 1$ for all k, such as for example the Gaussian (8) and the exponential decay function (9), we get the same conditions as in Theorem 2.3 for stability and instability.

Let us return to the general case. Since ω is absolute integrable, Riemann–Lebesque lemma implies that $\widetilde{\omega}$ is a continuous function

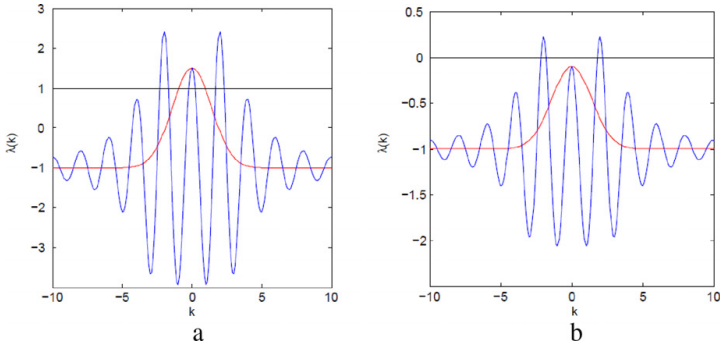

Fig. 1. The function λ given by (16) with $\widetilde{\omega}(k) = \exp(-k^2/4)$ (red curve) and $\widetilde{\omega}(k) = 10(k^2+5)\cos(\pi k)/(k^4+50)$ (blue curve), (a) $\lambda(k)$ is plotted for the case $\beta S' = 2.5$ (b) $\lambda(k)$ is plotted for the $\beta S' = 0.9$. (For interpretation of the references to colour in this figure legend, the reader is referred to the web version of this article.)

and that $\lim_{|k|\to\infty} \widetilde{\omega}(k) = 0$. From (16), we then get that $\lim_{|k|\to\infty} \lambda(k) = -1$. Hence, if there exist $\lambda = 0$ then there is a value $k_* > 0$ such that

$$\widetilde{\omega}(\pm k_*) = \frac{1}{\beta S'}, \qquad \widetilde{\omega}(k) < \frac{1}{\beta S'} \quad \text{for } |k| > k_*.$$

This means that a possible instability is of the finite band width type.

The instability structure can be investigated in a similar way as in Wyller et al. [10]. Wave number intervals satisfying $\widetilde{\omega}(k) > 1/\beta S'$ correspond to unstable modes. These intervals are referred to as *gain bands*.

Since $\lambda(0) = -1 + \beta S'$, the condition $\beta S' > 1$ guarantees that at least one gain band (containing $k = 0$) exists. We refer to this gain band as the *fundamental gain band*. Fig. 1(a) shows that higher order gain bands can exist for spectra $\widetilde{\omega}$ which execute oscillations in k-space.

For the case $\beta S' < 1$ we get $\lambda(0) < 0$. This implies that no fundamental gain band exists but there is a possibility of having higher order gain bands for spectra oscillating in k-space, Fig. 1(b). We can determine the number of gain bands if all solutions of the equation $\widetilde{\omega}(k) = 1/\beta S'$ are distinct and isolated. In order to study this problem, we proceed in the same way as in [10]. We assume that

$$\int_{-\infty}^{\infty} x\omega(x)\mathrm{d}x < \infty.$$

The Riemann–Lebesque lemma then implies that $\widetilde{\omega}$ is a smooth function. Assume that the transversal crossing condition $\widetilde{\omega}(k) = 1/\beta S'$, $\widetilde{\omega}'(k) \neq 0$ is fulfilled. According to Wyller et al. [10] the equation $\widetilde{\omega}(k) = 1/\beta S'$ in this case has a finite number of distinct and isolated solutions. The total number n of transversal crossings $\widetilde{\omega}(k) = 1/\beta S'$, $\widetilde{\omega}'(k) \neq 0$ is given as $n = 2N, N = 0, 1, 2, 3, \ldots$, where N is the number of gain bands. The condition $N = n = 0$ corresponds to a stable situation and might arise only when $\beta S' < 1$ (the red curve in Fig. 1(b)). The condition $N = 1$ corresponds to the instability consisting only of the fundamental gain band and appears when $\beta S' > 1$ (the red curve in Fig. 1(a)). The multiple gain band structure could emerge both for $\beta S' > 1$ (the blue curve in Fig. 1(a)) and for $\beta S' < 1$ (the blue curve in Fig. 1(b)).

We summarize the main results of the discussion above in the following theorem.

Theorem 2.4. *If $\omega(x) \in L^1(\mathbb{R})$ then the possible instability for u_{eq} is of finite band width type. Moreover, if $x\omega(x) \in L^1(\mathbb{R})$ and all solutions of the equation $\widetilde{\omega}(k) = 1/\beta S'$, where $\widetilde{\omega}'(k) \neq 0$ are distinct and isolated, then the gain band structure can be two types:* (i) *For the case $\beta S' > 1$ the gain band consists of one fundamental gain band plus a finite set (including the empty set) of higher order well separated gain bands. The relation between the number of solutions, n, of $\widetilde{\omega}(k) = 1/\beta S'$ to the number of gain bands, N, is expressed by $n = 2N, N = 1, 3, 5, \ldots$.* (ii) *For the case $\beta S' < 1$ we can only have higher order gain bands and $n = 2N, N = 2, 4, 6, \ldots$. For $N = n = 0$ we get a stable homogeneous solution u_{eq}.*

Notice, however, that due to the bound (10) or (13) any instability must be saturated.

3. Weakly nonlocal limit

The parameterization of the connectivity functions, (7), enables us to study the so called *weakly nonlocal limit* of the Wilson–Cowan model (12). The Fourier transform $\widetilde{\omega}$ of ω can be expressed in terms of the Fourier transform $\widetilde{\Phi}$ of Φ

$$\widetilde{\omega}(k) = \widetilde{\Phi}(\sigma k).$$

Then, by imposing the long wavelength condition

$$|\sigma k| \ll 1 \tag{17}$$

and assuming $\widetilde{\omega}$ at least three times differentiable at $k = 0$, we Taylor-expand $\widetilde{\omega}$ and retain the two lowest order terms, i.e.,

$$\widetilde{\omega}(k) = 1 - \gamma(\sigma k)^2, \qquad \gamma = -\frac{1}{2}\widetilde{\Phi}''(0) > 0. \tag{18}$$

Let $\widetilde{P}(u-\theta)$ denote the Fourier transform of the firing rate function $P(u-\theta)$. By Fourier transforming the evolution Eq. (12) we get

$$\partial_t \widetilde{u} = -\widetilde{u} + \widetilde{\omega}\widetilde{P}(u-\theta).$$

Then, by making use of the approximation (18) we get

$$\partial_t \widetilde{u} = -\widetilde{u} + (1 - \gamma(\sigma k)^2)\widetilde{P}(u-\theta).$$

Applying the inverse Fourier theorem we obtain the nonlinear diffusion equation

$$\partial_t u = -u + (1 + \gamma\sigma^2\partial_x^2)S(\beta(u-\theta)). \tag{19}$$

The model (19) is referred to as the *weakly nonlocal limit* of the Wilson–Cowan model (12).

This procedure has been extensively used in nonlocal nonlinear optics [30,31] and in mathematical biology [32].

Theorem 3.1. (i) *The model (19) possesses the same homogeneous background u_{eq} as the model (12).* (ii) *u_{eq} is stable if $\beta S' \leq 1$ and unstable otherwise. The possible instability is of finite bandwidth type and consists of one single gain band.*

Proof. The proof of (i) follows simply by assuming that the solutions of (19) are space and time independent. In order to prove (ii) we notice that the growth (decay) rate

$$\lambda(k) = \beta S' - 1 - \beta S' \gamma \sigma^2 k^2. \tag{20}$$

The eigenvalues $\lambda(k) < 0$ for all k if $\beta S' \leq 1$. For the complementary regime, $\beta S' > 1$ we obtain the range of the wave number k which provides positive $\lambda(k)$ as $0 \leq k^2 \leq k_*^2$ where $k_*^2 = (\beta S' - 1)/(\beta S' \gamma \sigma^2)$. This means that instability consists of one gain band. □

Notice that the *moderate steepness condition* $1 < \beta S' \ll \gamma$ implies that the assumption (17) is satisfied for all wave numbers k belonging to the unstable range.

3.1. Nonlinear diffusion equation for the firing rate variable

By introducing the change of variables $\xi = x/(\sqrt{\gamma}\sigma)$, $\tau = t$ we can rewrite the weakly nonlocal limit Eq. (19) on the form

$$\partial_\tau u = -u + (1 + \partial_\xi^2) S(\beta(u - \theta)).$$

We transform this equation to the nonlinear diffusion equation

$$\frac{1}{\beta}(S^{-1})'(v)\partial_\tau v = -\theta - \frac{1}{\beta}S^{-1}(v) + \left(1 + \partial_\xi^2\right) v \tag{21}$$

by introducing the new firing rate variable $v = S(\beta(u - \theta))$. Here we have exploited the fact that S is a smooth monotonically increasing function, as for example (4), from which it follows that it has a smooth inverse denoted by S^{-1}.

For each $u \in [0, 1]$ there is unique $v \in [v_0, v_1]$, where

$$v_0 = S(-\beta\theta), \qquad v_1 = S(\beta(1 - \theta)).$$

We will be searching for solutions of (21) fulfilling the property

$$v_0 \leq v(\xi, \tau) \leq v_1 \tag{22}$$

uniformly in ξ and τ. Notice, however, that we in general cannot guarantee that the solutions of the initial value problem of (21) satisfy the bounds (22) globally in time τ. This leads naturally to the following definition.

Definition 3.1. Solutions of (21) are called *proper solutions* if they satisfy (22) for all τ.

Notice that the interval for the proper solutions is contained in the unit interval, i.e., $[v_0, v_1] \subset [0, 1]$.

The functions (5) and (6) do not give a one-to-one correspondence between the firing rate variable $v \in [v_0, v_1]$ and the activity level $u \in [0, 1]$. Therefore, we have to restrict S to its oblique part, i.e., we require $-1 < \beta(u - \theta) < 1$. We add this requirement in the definition of a proper solution for these cases of S.

In the time independent case, solutions of (21) satisfy conservation law for the Hamiltonian H

$$H[v; \theta, \beta] \equiv \frac{1}{2}(\partial_\xi v)^2 + U(v; \theta, \beta) = E, \tag{23}$$

where the pseudo-potential, U, is given by

$$U(v; \theta, \beta) = \frac{1}{2}v^2 - \theta v - \frac{1}{\beta}\int S^{-1}(v)\mathrm{d}v, \tag{24}$$

and E is an energy constant. The range of the energy constant governs the range of v. We have to impose some constraints on E to get proper solutions of the pseudo-potential Eqs. (23)–(24). For example, if we assume that the pseudo-potential (24) has a minimum in some point $v_{\min}$ such that $v_0 < v_{\min} < v_1$, then the range of E giving proper, stationary, periodic solutions is given by

$$U(v_{\min}) \leq E \leq \min\{U(v_0), U(v_1)\}. \tag{25}$$

The system (23)–(24) allows us to predict the temporal evolution of the system. We have the following important result.

Theorem 3.2. *Extreme points of the pseudo-potential U given by (24) are constant solutions of (21) which correspond to the equilibrium $u = u_{eq}$ given by (14). Moreover, a local maximum corresponds to a stable solution, a local minimum to an unstable solution.*

Proof. The time dependent Eq. (21) can be reformulated as

$$f(v)\partial_\tau v = \frac{\delta H}{\delta v} \equiv -\theta - \frac{1}{\beta}S^{-1}(v) + \left(1 + \partial_\xi^2\right) v, \tag{26}$$

where we have made the identification $f(v) \equiv \beta^{-1}(S^{-1})'(v) > 0$ with H given by (23) and introduced the operator

$$\frac{\delta}{\delta v} \equiv \frac{\partial}{\partial v} + \frac{\partial}{\partial \xi}\left(\frac{\partial}{\partial v_\xi}\right), \quad v_\xi = \partial_\xi v.$$

The Eq. (26) has the form of the Ginzburg–Landau–Khalatnikov equation in kinetic theory [24,25] and the stability issue for constant solutions of (26) can be rephrased in terms of the extreme points of the pseudo-potential U.

Let v_* denote an extreme point of U, i.e., $U'(v_*) = 0$, $U''(v_*) \neq 0$. We linearize (26) and get

$$f(v_*)\partial_\tau w = U''(v_*)w + \partial_\xi^2 w.$$

By Fourier transforming this equation we find that

$$f(v_*)\partial_\tau \widetilde{w} = U''(v_*)\widetilde{w} - k^2\widetilde{w}$$

where k denotes the wave number of the perturbation w imposed on the background v_*. The growth (or decay) rate of this equation satisfies

$$\lambda f(v_*) = U''(v_*) - k^2 \tag{27}$$

from which follows that $v = v_*$ is stable if v_* is a local maximum of the pseudo-potential U whereas it is unstable when v_* is a local minimum of the potential U. Moreover, the instability is of the finite band width type where the wave numbers producing growing modes are restricted to the interval $0 \leq k^2 \leq U''(v_*)$. Notice that both the growth rate (27) and the corresponding bandwidth is just the same instability result as obtained in the previous section, i.e., (20). □

Notice that in [33,34] the Hamiltonian structure of the time independent Wilson–Cowan model is exploited in the study of stationary solutions. The analysis presupposes, however, that the connectivity functions have Fourier transforms given by rational functions.

The Ginzburg–Landau–Khalatnikov formulation (26) is expected to make it possible to study the stability of proper stationary, periodic solutions of the weakly nonlocal limit (21). Let us assume that we have identified a proper stationary periodic solution through the pseudo-potential U denoted by $\hat{v}$. We introduce the perturbation

$$v(\xi, \tau) = \hat{v}(\xi) + \varphi(\xi, \tau).$$

By taking into account that $\partial_\xi^2 \hat{v} + U'(\hat{v}) = 0$ we then end up with

$$f(\hat{v})\partial_\tau \varphi = \partial_\xi^2 \varphi + U''(\hat{v})\varphi$$

when linearizing about the stationary state $\hat{v}$. Now, by assuming the separation

$$\varphi(\xi, \tau) = g(\xi)\exp(\lambda\tau)$$

where λ plays the role as growth (decay) rate and exploiting the fact that

$$U''(\hat{v}) = 1 - f(\hat{v})$$

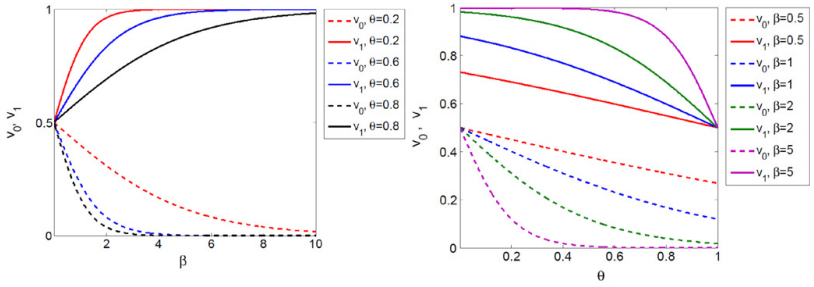

Fig. 2. The case of the sigmoid firing rate function (4): (a) Bounding values of v as functions of β for fixed θ. (b) Bounding values of v as functions of θ for fixed β.

with $f(\hat{v}) < 1$, we end up with the Sturm–Liouville problem

$$\partial_\xi^2 g + (1 - (\lambda + 1) f(\hat{v}))g = 0. \tag{28}$$

Due to the fact that the proper periodic stationary solutions exist for energy constants restricted to the interval (25) and that the potential minimum point $v_{\min}$ of the pseudo-potential U represents a proper stationary periodic solution $\hat{v}$ with an infinite short period, we expect by continuity that proper stationary solutions $\hat{v}$ are unstable, at least for small but finite wavelength oscillations, i.e., that the spectrum of the Sturm–Liouville problem (28) consists of at least one strictly positive eigenvalue. The following argument based on simple asymptotical analysis of (28) clearly supports this conclusion. For short wave length oscillations we have that $\hat{v} \approx v_{\min}$ where $v_{\min}$ denotes the minimum point of the pseudo-potential. Then the problem (28) is approximated with a constant coefficient problem. The square integrable eigenfunctions of the latter problem assume the form $g(\xi) \sim \exp(-\Omega|\xi|)$ where $\Omega^2 = (\lambda + 1) f(v_{\min}) - 1 > 0$, $\Omega > 0$. Hence, since $f(v_{\min}) < 1$, we find the estimate $\lambda > (1 - f(v_{\min}))/f(v_{\min}) > 0$. It is an open question whether this result extends to all proper stationary solutions. We do not pursue this aspect of the model in the present paper, however.

In Sections 3.1.1–3.1.3 we investigate the homogeneous solutions for the firing rate functions given by (4)–(6) by means of the Ginzburg–Landau–Khalatnikov formulation.

3.1.1. Smooth firing rate function

For the case of the smooth function (4) the bounds v_0 and v_1 are

$$v_0 = \frac{1}{2}(1 - \tanh(\beta\theta)), \qquad v_1 = \frac{1}{2}(1 + \tanh(\beta - \beta\theta)).$$

Notice that v_0 and v_1 asymptotically approach 0 and 1, respectively, as $\beta \to \infty$. We have plotted v_0 and v_1 as a function of β for fixed values θ in Fig. 2(a) and as a function θ for fixed values of β in Fig. 2(b).

The pseudo-potential U is given as

$$U(v; \theta, \beta) = \frac{1}{2}v^2 - \theta v - \frac{1}{2\beta}F(v),$$
$$F(v) = v\ln(v) + (1 - v)\ln(1 - v) - 1.$$

We introduce the open subsets, D and D_i, $i = 0, 1, 2$, of the parameter set $\{(\beta, \theta)\}$ as

$$D_0 = \{(\beta, \theta) : 0 < \beta < 2, 0 < \theta < 1\},$$
$$D = \{(\beta, \theta) : 2 < \beta < +\infty, \theta_-(\beta) < \theta < \theta_+(\beta)\},$$
$$D_1 = \{(\beta, \theta) : 2 < \beta < \infty, \theta_+(\beta) < \theta < 1\},$$
$$D_2 = \{(\beta, \theta) : 2 < \beta < \infty, 0 < \theta < \theta_-(\beta)\},$$

where $\theta_\pm$ are defined as

$$\theta_\pm(\beta) = \frac{1}{2}\left(1 \pm \sqrt{1 - 2/\beta}\right) - \frac{1}{\beta}\ln\left(\sqrt{\frac{\beta}{2}}\left(1 \pm \sqrt{1 - 2\beta}\right)\right). \tag{29}$$

Theorem 3.3. *Let* $\mathbf{a} = (\beta, \theta)$ *and assume* S *to be given by* (4). (i) *If* $\mathbf{a} \in D_i, i = 0, 1, 2$, *there exists a proper unique homogeneous solution of* (21) *that is stable.* (ii) *If* $\mathbf{a} \in D$, *the Eq.* (21) *has three homogeneous proper solutions,* $v^{(1)} < v^{(2)} < v^{(3)}$, *where* $v^{(1)}$, $v^{(3)}$ *are stable, and* $v^{(2)}$ *is an unstable solution.*

Proof. Firstly, we study the existence and stability property of the homogeneous solutions. Secondly, we show that these solutions are proper.

We find that the condition $U'(v) = 0$ is equivalent to

$$\theta = v - \frac{1}{2\beta}\ln\left(\frac{v}{1 - v}\right). \tag{30}$$

We have analyzed the convexity properties of U as a function of v in Fig. 3.

We divide our discussion into two cases:

1. Let $0 < \beta < 2$. Simple computation shows that θ given by (30) is a continuous strictly decreasing function of v, $0 < v < 1$, in this parameter regime; see Fig. 4(a). Hence, there is one-to-one correspondence between θ and v. Moreover, we find that $U''(v; \beta, \theta) < 0$ independently of v and θ, Fig. 3. This means that U has a global maximum for $\mathbf{a} \in D_0$; see Fig. 4(b). According to Theorem 3.2 this maximum is a stable equilibrium.
2. Next, let us consider the case $\beta > 2$. The function (30) changes its monotonicity twice in the points
$$v_\pm = \frac{1 \pm \sqrt{1 - 2/\beta}}{2}.$$
Therefore, the function (30) gives us either three or one intersection with the horizontal line $\theta = \text{const}$. We get three solutions $v^{(1)} < v^{(2)} < v^{(3)}$ when $\theta_-(\beta) < \theta < \theta_+(\beta)$ and one solution when $0 < \theta < \theta_-$ or $\theta_+ < \theta < 1$, Fig. 4(a). We obtain $\theta_\pm(\beta)$ as (29) if one inserts $v_\pm$ in (30). Thus, U has local maxima in $v^{(1)}$ and $v^{(3)}$ for $\mathbf{a} \in D$, while it has a local minimum in $v^{(2)}$ for $\mathbf{a} \in D$. The solutions $v^{(1)}$ and $v^{(3)}$ correspond to the stable equilibrium, while $v^{(2)}$ is gives the unstable state. Each of the parameter regimes D_1 and D_2 produces a maximum of U and indicates the existence of a unique stable solution. The sets D, D_1, and D_2 are plotted in Fig. 4(b).

Now we want to show that all the homogeneous solutions v satisfy the inequality $v_0 \le v \le v_1$ in order to be proper. For each fixed θ the solution v satisfies the expression

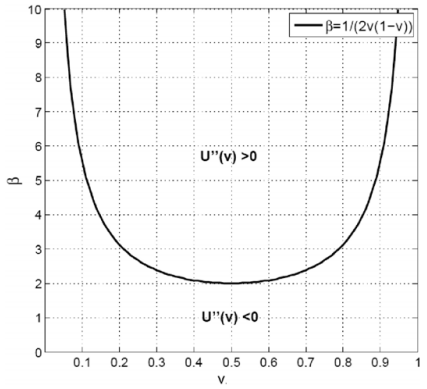

Fig. 3. The sets of constant signs of $U''(v)$ in terms of (v, β), where $\beta = 1/(2v(1-v))$ corresponds to $U''(v) = 0$.

$$\beta = \beta_v = \frac{1}{2(v-\theta)} \ln\left(\frac{v}{1-v}\right).$$

The upper bound, v_1, satisfies $v_1 \geq 1/2$ and can be represented as

$$\beta = \beta_1 = \frac{1}{2(1-\theta)} \ln\left(\frac{v}{1-v}\right).$$

The lower bound, v_0, obeys $v_0 \leq 1/2$ and can be rewritten as

$$\beta = \beta_0 = -\frac{1}{2\theta} \ln\left(\frac{v}{1-v}\right).$$

Simple analysis shows that $\beta_v \geq \beta_0$ and $\beta_v \geq \beta_1$. These properties cause that all homogeneous solutions of (21), in the framework of the smooth firing rate function (4), are proper. □

Theorem 3.4. *The weakly nonlocal limit (21) with the firing rate function modeled by means of (4) has proper stationary periodic solutions for the steepness parameter β exceeding a certain threshold.*

Proof. Consider the limit case, i.e., $\beta \to \infty$. Since $\lim_{v\to 0^+} F(v) = -1$ and $\lim_{v\to 1^-} F(v) = -1$, the function F can be extended to a continuous function on the closed, bounded interval [0, 1]. The convergence

$$\lim_{\beta\to\infty} U(v;\theta,\beta) = U_*(v) \equiv \frac{1}{2}v^2 - \theta v \tag{31}$$

is uniform and the homogeneous solution depends continuously on β. Hence, U has a minimum for $v = v_{\min} = \theta + \mathcal{O}(1/\beta)$ asymptotically as $\beta \to \infty$. The restrictions on the energy constants E permitting proper stationary periodic solutions is now given by the bound (25) for the steepness parameter β exceeding a certain threshold, since in this case the pseudo-potential U has a global minimum $v_{\min}$ with $v_0 < v_{\min} < v_1$. □

3.1.2. Piecewise linear firing rate function

The model (21) with the function (5) becomes linear, i.e.,

$$\partial_\tau v = \frac{\beta}{2}\partial_\xi^2 v + \frac{\beta-2}{2}v + \frac{1-\theta\beta}{2}. \tag{32}$$

This simplifies the analysis and serves as a good testing example for the numerical experiments. We compute the pseudo-potential U in this case for the oblique part of the firing rate function and get the quadratic function

$$U(v) = \left(\frac{1}{2} - \frac{1}{\beta}\right)v^2 - \left(\theta - \frac{1}{\beta}\right)v,$$

where v satisfies the bounds $v_0 \leq v \leq v_1$ with

$$v_0 = \begin{cases} \frac{1}{2}(1-\beta\theta), & \beta\theta \leq 1 \\ 0, & \beta\theta > 1, \end{cases}$$

$$v_1 = \begin{cases} \frac{1}{2}(1+\beta-\beta\theta), & \beta(1-\theta) \leq 1 \\ 1, & \beta(1-\theta) > 1. \end{cases}$$

We have plotted v_0 and v_1 for fixed values of θ in Fig. 5(a) and fixed values of β in Fig. 5(b).

Let us define the sets

$$D_1 = \{(\beta,\theta) : 0 < \beta < 2, 1 - 1/\beta \leq \theta < 1 - 1/\beta\},$$
$$D_2 = \{(\beta,\theta) : \beta > 2, 1/\beta < \theta \leq 1 - 1/\beta\}.$$

These sets are displayed in Fig. 6. Moreover, we have marked that U is concave for $\beta < 2$ and convex for $\beta > 2$ independently of θ. We formulate the following theorem which can be proven in a similar way as Theorem 3.4 in Section 3.1.1.

Theorem 3.5. *The Eq. (21) with the piecewise firing rate function (5) has the unique homogeneous proper solution $v = v_{\text{const}}$, $v_{\text{const}} = (\theta\beta - 1)/(\beta - 2)$, for all values $\mathbf{a} = (\beta,\theta) \in D_1 \cup D_2$. The solution is stable if $\mathbf{a} \in D_1$, and unstable if $\mathbf{a} \in D_2$.*

This rather simple case allows us to derive time independent solutions and analyze their stability. For $\mathbf{a} \in D_1$ we obtain a stable solution in the form

$$v(\xi) = A\exp(\varpi x) + B\exp(-\varpi x) + v_{\text{const}}, \qquad AB = \frac{\hat{E}}{4\varpi^2}, \tag{33}$$

and for $\mathbf{a} \in D_2$ an unstable solution in the form

$$v(\xi) = A\sin(\varpi x) + B\cos(\varpi x) + v_{\text{const}}, \quad A^2 + B^2 = \frac{\hat{E}}{\varpi^2}, \tag{34}$$

where $\varpi^2 = |1 - 2/\beta|$ and $\hat{E} = 2E + (1 - 2/\beta)v_{\text{const}}$.

However, the solution (33) is not proper for all constants A and B except $A = B = 0$, so $v(\xi) = v_{\text{const}}$ is the only proper solution in this case. For the case in (34) the pseudo-potential, U, has the global minimum $v = v_{\text{const}}$ according to Theorem 3.5. Moreover, $v_0 < v_{\text{const}} < v_1$ for $\mathbf{a} \in \text{int}(D_2)$. Thus, we can apply a restriction on the energy constant as in (25) to keep the solution within the bounds. We get the following estimate

$$-\frac{1}{2}\left(1 - \frac{2}{\beta}\right)v_{\text{const}}^2 \leq E \leq \min\left\{0, \frac{1}{2} - \theta\right\}. \tag{35}$$

We summarize all the results above as the following theorem.

Theorem 3.6. *The Eq. (21) with the piecewise firing rate function (5) has the unique stable time independent proper solution $v = v_{\text{const}}$, $v_{\text{const}} = (\theta\beta - 1)/(2 - \beta)$, for all values $\mathbf{a} = (\beta,\theta) \in D_1$, and unstable time independent solutions in the form (34) with the range of the energy constant given by (35) if $\mathbf{a} \in \text{int}(D_2)$.*

3.1.3. The piecewise nonlinear function

Another possibility which enables us to use the wavelet–Galerkin method is to approximate the firing rate function with a piecewise nonlinear function containing a square root function (6). Then, from (21) we obtain

$$(1+2v)\partial_\tau v = \beta\partial_\xi^2 v - v^2 + (\beta - 1)v + (1 - \beta\theta). \tag{36}$$

The bounds (22) are now given as

$$v_0 = \begin{cases} -1/2 + \sqrt{-\beta\theta + 5/4}, & \beta\theta \leq 1 \\ 0, & \beta\theta > 1, \end{cases} \tag{37}$$

$$v_1 = \begin{cases} -1/2 + \sqrt{\beta(1-\theta) + 5/4}, & \beta(1-\theta) \leq 1 \\ 1, & \beta(1-\theta) > 1. \end{cases} \tag{38}$$

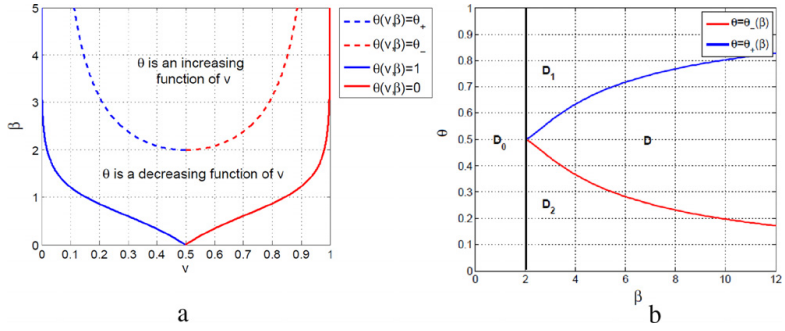

Fig. 4. (a) The intervals of monotonicity for θ given by (30). (b) The sets D, D_i, $i = 0, 1, 2$, where $\theta_\pm$ is given by (29).

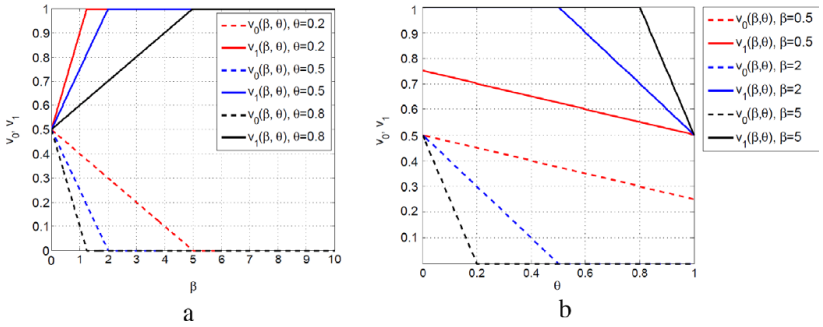

Fig. 5. The case of the piecewise linear firing rate function (5): (a) Bounding values of v as functions of β for fixed θ. (b) Bounding values of v as functions of θ for fixed β.

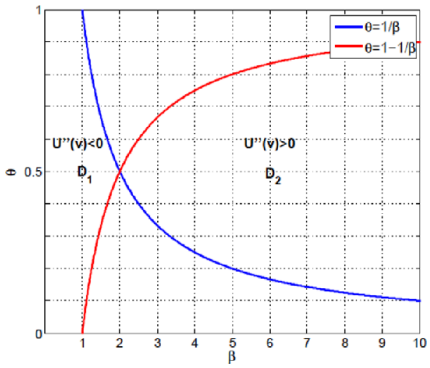

Fig. 6. The sets D_1 and D_2 in the case of the piecewise linear firing rate function (5).

The graphs of the bounds are plotted in Fig. 7(a) and (b) for fixed θ and β, respectively.

For the pseudo-potential U with this choice of firing rate function we get a cubic polynomial

$$U(v) = -\frac{1}{3\beta}v^3 + \frac{1}{2}\left(1 - \frac{1}{\beta}\right)v^2 + \left(\frac{1}{\beta} - \theta\right)v. \tag{39}$$

We have analyzed the convexity property of (39) and the number of its critical points satisfying the bounds (37)–(38). The result is represented in Fig. 8. The pseudo-potential U is convex when $v > (\beta - 1)/2$ and concave for $v < (\beta - 1)/2$; see Fig. 8(a). We introduce the sets

$$D_1 = (0, 1) \times (0, 1) \cup \{(\beta, \theta) : 1 < \beta < 2, \\ 1/\beta \le \theta < (1 - 1/\beta)\},$$

$$D_2 = \{(\beta, \theta) : (2 < \beta < 3, 1/\beta \le \theta < 1/\beta) \\ \cup (3 < \beta < \infty, 1/\beta \le \theta \le 1/\beta)\},$$

$$D_3 = \{(\beta, \theta) : 1 < \beta < 5, f(\beta) \le \theta < 1\},$$

$$D = \{(\beta, \theta) : (1 < \beta \le 2, (1 - 1/\beta) \le \theta < f(\beta)) \\ \cup (2 < \beta < 3, 1/\beta \le \theta < f(\beta))\}$$

where $f(\beta) = (\beta^2 - 2\beta + 5)/(4\beta)$. These sets are plotted in Fig. 8(b).

Theorem 3.7. *Let* $\mathbf{a} = (\beta, \theta)$ *and assume* S *to be given by* (6). (i) *If* $\mathbf{a} \in D_1$ *there exists a unique proper homogeneous solution of* (21), $v^{(+)}$, *which is stable.* (ii) *If* $\mathbf{a} \in D_2$ *the Eq.* (21) *has an unstable unique proper homogeneous solutions,* $v^{(-)}$. (iii) *For* $\mathbf{a} \in D$, *the Eq.* (21) *has two proper homogeneous solutions,* $v^{(-)} < v^{(+)}$, $v^{(-)}$ *is unstable while* $v^{(+)}$ *is stable. Here solutions* $v^{(\pm)}$ *are given as*

$$v^{(\pm)} = \frac{1}{2}\left((\beta - 1) \pm \sqrt{(\beta - 1)^2 + 4(1 - \beta\theta)}\right).$$

Proof. Any value $\mathbf{a} \in (0, \infty) \times (0, 1) \setminus D_3$ gives a minimum $v = v^{(-)}$ and a maximum $v = v^{(+)}$ of U. From Theorem 3.2 it follows that $v^{(-)}$ is unstable and $v^{(+)}$ is stable. However, it is possible to show that the solution $v^{(-)}$ is proper for $\mathbf{a} \in D_1 \cup D$ and not proper everywhere else where it exists. The solution $v^{(+)}$ is proper for $\mathbf{a} \in D_2 \cup D$ and does not respect the bounds otherwise. However, the proof of these facts is quite technical and is thus omitted. □

Non-constant stationary solutions of (36) at any values of parameters β and θ appear to be expressed in terms of Weierstrass elliptic function, which diverges at least in one location, so such expression cannot be a proper solution.

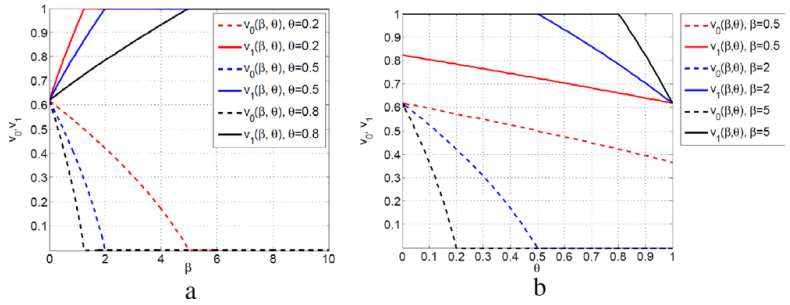

Fig. 7. The case of the piecewise nonlinear firing rate function (6): (a) Bounding values of v as functions of β for fixed θ. (b) Bounding values of v as functions of θ for fixed β.

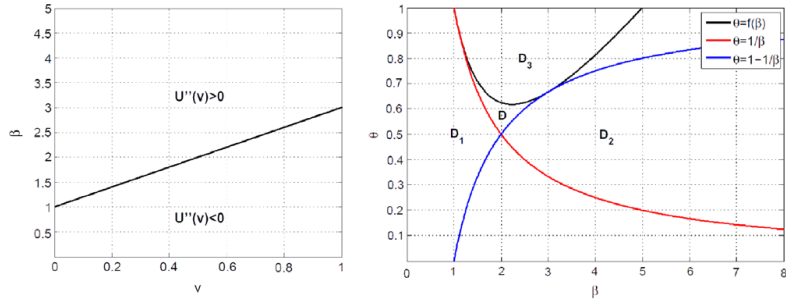

Fig. 8. The case of the piecewise nonlinear firing rate function (6): (a) The sets of constant signs of $U''(v)$ in terms of (v, β), where $v = (\beta - 1)/2$ corresponds to $U''(v) = 0$. (b) The sets D, D_i, $i = 1, 2, 3$.

4. Wavelet–Galerkin solution of the Ginzburg–Landau–Khalatnikov problem

In this section we describe the wavelet–Galerkin method for solving the model Eq. (21) with the firing rate function given by (5) and (6). We recall the main notations and definitions related to the method and list some properties of Daubechies wavelets, which have been chosen as basis functions for a Galerkin expansion. For the numerical study we restrict the spatial variable ξ to $[X_1, X_2]$ where $|X_2 - X_1|$ is sufficiently large. We treat boundary conditions by means of modification of the fictitious boundary approach as worked out in [35].

4.1. The Galerkin method and choice of basis functions

Galerkin methods have been known since 1915 and are currently widely used for solving nonlinear differential and integro–differential equations in numerous scientific areas and engineering applications [36]. The efficiency of these methods is substantially connected with the choice of the system of basis functions, which are used for the expansion of the solution.

The general form of the Galerkin expansion in an arbitrary orthonormal basis $\{g_k\}$ is given as

$$z(x, t) = \sum_k a_k(t) g_k(x), \qquad \langle g_k, g_l \rangle = \delta_{kl}, \qquad a_k(t) = \langle z(\cdot, t), g_k \rangle, \; k \in \mathbb{Z}, \tag{40}$$

where $z(x, t)$ is a general notation for the unknown quantity, and $\langle \cdot, \cdot \rangle$ denotes the inner product in a corresponding space.

The correct choice of $\{g_k\}$ provides a maximal level of the approximation of a real solution with a minimal number of basis functions. The choice of basis functions $g_k(x)$ depends to a large extent on the expected solutions of the given differential or integro–differential equations. The neural field equations have solutions that possess a spatial localization property [5]. This observation serves as the main motivation for using wavelets as basis functions. Moreover, a wavelet basis has some advantages compared with other basis functions, e.g., localization in both physical and Fourier space, almost block-diagonal representation of most differential operators, availability of fast algorithms of discrete wavelet transform and multiresolution analysis, and others.

The known examples of successful usage of wavelets basis in the Galerkin approach are numerous. They include application to nonlinear differential equations of different types [23,37,38] as well as some pedagogical examples of integro–differential equations [39,40].

The important task in the wavelet–Galerkin method is computation of *connection coefficients*. The connection coefficients are integrals of products of wavelet basis functions, their derivatives, their translates, and so on.

We have chosen Daubechies wavelets [41] as a basis for our problem. These functions have compact support and are well known as very useful tools in numerical solutions of ordinary and partial differential equations [23,42], and integro–differential equations [37]. The algorithms for and the calculated values of connection coefficients for Daubechies wavelets are available in numerous publications [23,43,44]. The calculation of connection coefficients for the partial differential equation (21) and therefore their reduction to an ordinary differential equation for the coefficients of the Galerkin expansion ($a_k(t)$ in (40)) is possible when (21) has the form

$$P_n(z(x, t))\partial_t z(x, t) = Lz(x, t) + Nz(x, t), \tag{41}$$

where $P_n(z)$ is a polynomial of degree n, L is a linear operator, N is nonlinear operator. In order to use (41) we have chosen the firing rate functions as (5) and (6).

4.2. Multiresolution analysis (MRA)

MRA is a technique based on an iterative procedure of approximation of an arbitrary function $f(x) \in L^2(\mathbb{R})$ with successively more accurate resolutions. The procedure of building such successive approximations of a given function involves two important special families of functions localized in both physical and Fourier spaces, which are *wavelets* and *scaling functions*. For the sake of completeness we review some fundamental properties of MRA; see [45].

Definition 4.1. The MRA of $L^2(\mathbb{R})$ is a sequence of closed subspaces $V_j \subset L^2(\mathbb{R})$

$$\cdots \subset V_{-2} \subset V_{-1} \subset V_0 \subset V_1 \subset V_2 \subset \cdots$$

with the following properties:

(i) $V_j \subset V_{j+1}$, $\forall j \in \mathbb{Z}$
(ii) $f(x) \in V_j \Leftrightarrow f(2x) \in V_{j+1}$, $\forall j \in \mathbb{Z}$
(iii) $\bigcup_{j\in\mathbb{Z}} V_j$ is dense in $L^2(\mathbb{R})$
(iv) $\bigcap_{j\in\mathbb{Z}} V_j = \{0\}, f(x) \in V_0 \Leftrightarrow f(x+1) \in V_0$
(v) There exists a *scaling function* $\varphi \in V_0$, such that $\{\varphi_k(x)\} = \{\varphi(x-k)\}$ is an orthonormal basis for V_0.

The dilated, translated, and normalized scaling functions φ_{jk} defined as

$$\varphi_{jk}(x) = 2^{j/2}\varphi(2^j x - k), \quad j, k \in \mathbb{Z}$$

constitute an orthonormal basis for V_j for every fixed j.

Let W_j denote an orthogonal complement of subspace V_j in V_{j+1}, i.e., $V_{j+1} = V_j \oplus W_j$.

Definition 4.2. A function ψ is called a *mother wavelet* if W_0 is spanned by the translations $\psi(x-k)$. Moreover, we require the *wavelets* $\psi(x-k)$ to be an orthonormal basis for W_0.

The dilated, translated, and normalized wavelets ψ_{jk} defined as

$$\psi_{jk}(x) = 2^{j/2}\psi(2^j x - k), \quad j, k \in \mathbb{Z}$$

form an orthonormal basis for W_j for each fixed j.

The projection, $P_{V_{j+1}}f$, of f onto the space V_{j+1} is then given as the unique decomposition

$$P_{V_{j+1}}f(x) = P_{V_j}f(x) + P_{W_j}f(x) = \sum_{k=-\infty}^{+\infty} c_{jk}\varphi_{j,k}(x) + \sum_{k=-\infty}^{+\infty} d_{jk}\psi_{j,k}(x) \tag{42}$$

where

$$c_{jk} = \langle f, \varphi_{j,k}\rangle, \qquad d_{jk} = \langle f, \psi_{j,k}\rangle. \tag{43}$$

4.3. Wavelet–Galerkin expansion scheme

Let $z_J(x,t)$ be a projection of $z \in L^2(\mathbb{R})$ onto V_J for any t. Then (40) can be rewritten using (42) as the following wavelet–Galerkin expansion scheme

$$z_J(x,t) = \sum_{k\in\mathbb{Z}} c_{J,k}(t)\varphi_{J,k}(x) + \sum_{k\in\mathbb{Z}}\sum_{j=J}^{\infty} d_{j,k}(t)\psi_{j,k}(x), \tag{44}$$

where $c_{J,k}$ and $d_{J,k}$ is given by (43). The choice of J is determined by the coarsest scale in the representation of $z(x,t)$. In the computations we have to use a finite upper limit for the sum, say J'. Choosing $J = J'$, the second term of (44) disappears, i.e.,

$$z_J(x,t) = \sum_{k\in Z} c_{J,k}(t)\varphi_{J,k}(x). \tag{45}$$

See also [45].

4.4. General properties of Daubechies wavelets and connection coefficients

Daubechies wavelets are compactly supported orthonormal wavelets which are characterized by a maximal number of vanishing moments for the given support. Let L be an even number that denotes the length of the support, then the number of the vanishing moments, M, is equal $L/2$. For our numerical experiments we use $L = 6$. A Daubechies scalar function, φ, and a mother wavelet, ψ, do not have explicit representation, but can be obtained through the two-scale relation

$$\varphi(x) = \sum_{k=0}^{L-1} h_k\varphi(2x-k), \qquad \operatorname{supp}(\varphi) = [0, L-1],$$

and

$$\psi(x) = \sum_{k=2-L}^{1} h_{1-k}\psi(2x-k), \qquad \operatorname{supp}(\psi) = \left[1 - \frac{L}{2}, \frac{L}{2}\right],$$

where h_k are *the wavelet filter coefficients*. Here we only list the main properties of Daubechies scaling functions and expression for connection coefficients needed for our calculations, i.e.,

(i) $\int_{-\infty}^{+\infty} \varphi(x)\mathrm{d}x = 1$
(ii) $\int_{-\infty}^{+\infty} \varphi(x-k)\varphi(x-l)\mathrm{d}x = \delta_{kl}$
(iii) $\int_{-\infty}^{+\infty} \varphi(x-k)\varphi(x-l)\varphi(x-m)\mathrm{d}x = \delta_{kl}\delta_{km}$
(iv) $\int_{-\infty}^{+\infty} \varphi^{(m)}(x)\varphi^{(n)}(x-k)\mathrm{d}x = \Lambda_k^{m,n}$, where $\varphi^{(m)}(x) = d^m\varphi/\mathrm{d}x^m$, $\varphi^{(n)}(x) = d^m\varphi/\mathrm{d}x^n$. For our model we use only $m = 0$, $n = 1$.

The algorithm for the calculation of $\Lambda_k^{m,n}$ can be found in [23,43], and is not reproduced here.

4.5. Boundary conditions

Let $z(x,t)$ be defined on $[X_1, X_2] \times (0,\infty)$ and assume that it belongs to $L^2[X_1, X_2]$ for any t. We assume that $z(x,t) = 0$ when x is outside of the interval $[X_1, X_2]$ such that $z(\cdot,t) \in L^2(\mathbb{R})$. For the partial differential equation (41), we define the wavelet expansion for the projection $z_J(x,t)$ as

$$z_J(x,t) = \sum_k z_{J,k}(t)\cdot\varphi_{J,k}(x) = 2^{J/2}\sum_k z_{J,k}(t)\varphi\left(2^J x - k\right) \tag{46}$$

where k goes from $k_1 = 2 - L + 2^J X_1$ to $k_N = 2^J X_2 - 1$.

Notice that the support of the expansion (46), $z_J(\cdot,t)$, is $[X_1', X_2'] = \left[(2-L)/2^J + X_1, (L-2)/2^J + X_2\right]$ while the support of $z(\cdot,t)$ is given by $[X_1, X_2]$. Moreover $z_J(x,t)$ and $\partial z_J(x,t)/\partial x$ are equal to zero on the boundaries of the extended interval, since

$$z_J(X_1', t) = z_{J,k_1}\varphi(0) = 0, \qquad z_J(X_2', t) = z_{J,k_N}\varphi(L-1) = 0, \tag{47}$$

$$\begin{aligned} \frac{\partial}{\partial x}z_J(X_1', t) &= z_{J,k_1}\frac{\partial\varphi}{\partial x}(0) = 0, \\ \frac{\partial}{\partial x}z_J(X_2', t) &= z_{J,k_N}\frac{\partial\varphi}{\partial x}(L-1) = 0. \end{aligned} \tag{48}$$

In order to use the Galerkin method directly, namely when the selected basis satisfies the boundary conditions, we reset the analytical boundaries X_1, X_2 to the boundaries $X_1' = (2-L)/2^J + X_1$

and $X_2' = (L-2)/2^J + X_2$ and impose Dirichlet boundary conditions (47), Neumann boundary conditions (48), or other linear boundary conditions such as for example a Robin boundary condition [46].

We approximate the solutions of the partial differential equation (41), $z(x,t)$, on the interval $[X_1, X_2]$ with these boundary conditions by $z_J(x,t)$ on the interval $[X_1', X_2']$ noticing that as $J \to +\infty$, $|X_n' - X_n| = \mathcal{O}(2^{-J})$ for $n = 1, 2$ and $z_J \to z$.

We consider the Eq. (21) on the symmetric interval, i.e., $-X_1 = X_2 = X$, with homogeneous boundary conditions

$$v_J(-X,t) = v_J(X,t) = b, \tag{49}$$

and the initial condition

$$v_J(\xi,0) = v_0(\xi). \tag{50}$$

4.6. Piecewise linear firing rate function case

By change of the variable $z(\xi,\tau) = v_J(\xi,\tau) - b$ we get

$$\partial_\tau z = \frac{\beta}{2}\partial_\xi^2 z + \frac{\beta-2}{2} z + \frac{(\beta-2)b + 1 - \theta\beta}{2}, \tag{51}$$

with

$$z(\pm X,\tau) = 0, \qquad z(\xi,0) = v_0(\xi) - b,$$

from the Eq. (32). This formulation allows us to apply the result from Section 4.5.

Substituting (46) into (51) and then applying the Galerkin discretization scheme, we get the system of ordinary differential equations for the coefficients

$$\sum_k a_{lk}\frac{\mathrm{d}z_{Jk}}{\mathrm{d}\tau} = \sum_k \left(\frac{\beta-2}{2}a_{lk} + \frac{\beta}{2}c_{lk}\right) z_{Jk} + \frac{(\beta-2)b + 1 - \theta\beta}{2} d_l, \tag{52}$$

for all $l = k_1, k_1+1, \ldots, k_N$, where

$$a_{lk} = \langle \varphi_{Jl}, \varphi_{Jk}\rangle = \delta_{kl}, \qquad c_{lk} = \left\langle \varphi_{Jl}, \frac{d^2\varphi_{Jk}}{\mathrm{d}\xi^2}\right\rangle = 2^{2J}\Lambda^{0,2}_{k-l},$$

$$d_l = \langle \varphi_{Jl}, 1\rangle = 2^{-J/2}.$$

We write (52) in matrix form

$$\frac{\mathrm{d}\mathbf{z}}{\mathrm{d}\tau} = \left(\frac{\beta}{2}\Lambda + \frac{\beta-2}{2} I\right)\mathbf{z} + \frac{(\beta-2)b + 1 - \theta\beta}{2}\mathbf{d}, \tag{53}$$

where $\mathbf{z}(\tau) = (z_{Jk})(\tau)$ is the $N \times 1$ vector function of the Galerkin expansion coefficients, $\Lambda = (c_{lk})$ is $N \times N$ matrix and $d = (d_l)$ is the $N \times 1$ vector with $N = 2^J(X_2 - X_1) + (L-2)$. We solve (53) using the MatLab© solver ode23TB, obtain z_J as (45), and finally get the approximative solution v_J.

4.6.1. Stationary periodic solution

First, we consider stationary solution of (32) with zero Dirichlet boundary conditions and $\beta > 2$. When applying the wavelet–Galerkin scheme we get the system of algebraic equations

$$\left(\frac{\beta}{2}\Lambda + \frac{\beta-2}{2} I\right)\mathbf{z} + \frac{1-\theta\beta}{2}\mathbf{d} = 0.$$

The exact stationary solution of (32) on the symmetric interval $[-X, X]$ is

$$v(\xi) = -\frac{\theta - 1/\beta}{(1-2/\beta)\cos\left(\sqrt{1-2/\beta}X\right)} \times \cos\left(\sqrt{1-2/\beta}\xi\right) + \frac{\theta - 1/\beta}{1-2/\beta}. \tag{54}$$

In Fig. 9(a) we have plotted the exact solution and the approximation obtained by the wavelet–Galerkin approach for the approximation level $J = 4$, and parameters $X = 10$, $\beta = 3$, and $\theta = 0.5$. For the approximation level $J = 6$ and above one hardly observes any difference between the analytical predictions and the outcome of the numerical runs. The error of the approximation evaluated in $L_2[-X, X]$, i.e.,

$$\varepsilon = \sqrt{\int_{-X}^{X} \left(v_J - v\right)^2 \mathrm{d}x}.$$

In Fig. 9(b) we show $\log_2 \varepsilon$ as a function of the approximation level J. The error points are marked with squares in this figure. These points apparently seem to lie on a straight line. However, we do not do any further analysis of the error estimates in this paper.

4.6.2. The time evolution of a 'saw tooth'

We consider the solutions of Eq. (32) with boundary conditions

$$v(-X,t) = v(X,t) = v_{\mathrm{const}},$$

where $v_{\mathrm{const}} = (\theta\beta - 1)/(\beta - 2)$ is a homogeneous solution of the equation (see Section 3.1.2). The initial condition is given as

$$v(\xi,0) = v_{\mathrm{const}} + \varsigma(\xi),$$

where ς is

$$\varsigma(\xi) = \begin{cases} 0, & \text{if } |\xi| > h \\ -\dfrac{A}{h}|\xi| + A, & \text{if } |\xi| \le h. \end{cases} \tag{55}$$

We refer to the profile (55) as a 'saw tooth' profile. We take $A = 0.01$ and $h = X/2$ for all the examples we are studying here.

We have made simulations for a set of parameters $(\beta,\theta) \in D_1$ and $(\beta,\theta) \in D_2$, see Fig. 6, with small A and $h < X$. We have found that the results reflect the conclusions of Section 3.1.2, i.e., if we interpret the initial condition as a perturbation of the constant solution v_{const} we see that v_{const} is stable for $(\beta,\theta) \in D_1$, Fig. 10(a), and unstable for $(\beta,\theta) \in D_2$, Fig. 10(b). Notice, however, that the analysis in Section 3.1.2 is done for the infinite interval. Therefore, the accuracy in the representation of the regions D_1 and D_2 in the finite case depends on the length of the interval $[X_1, X_2]$. To avoid additional complications we do not reproduce the analysis for the correction for D_1 and D_2 here. However, we have taken it into account for test examples.

In the unstable case, see Fig. 10(b), the following features are apparent in the numerical evolution of the saw tooth profile: First, the region of the pulse around $\xi = 0$ (the core) grows with time. Secondly, a broadening of the pulse takes place.

Notice, that an unstable solution with this choice of firing rate function exceeds boundaries of proper solutions.

4.6.3. The time evolution of the bump

The bump (11) in the firing rate variable is given as $v_b = S(\beta(u_b - \theta))$. Since the bump, u_b, is spatially symmetric and there is a one-to-one correspondence between u and v for the oblique part of the firing rate function, the representation v_b must also be spatially symmetric. Moreover, we have

$$\lim_{x\to\pm\infty} v_b(x) = v_0. \tag{56}$$

This naturally imposes the Dirichlet condition for the problem (32) with the bump initial condition, i.e.,

$$v(\xi,0) = v_b(\xi), \qquad v(\pm X,\tau) = v_0.$$

The limit (56) is the lower bound in the definition of proper solutions. We assume that ω is positive. Thus, we have $0 \le W(x) \le 1/2$ (by the normalization condition) so that $v_0 \le v_b(\xi) \le v_1$.

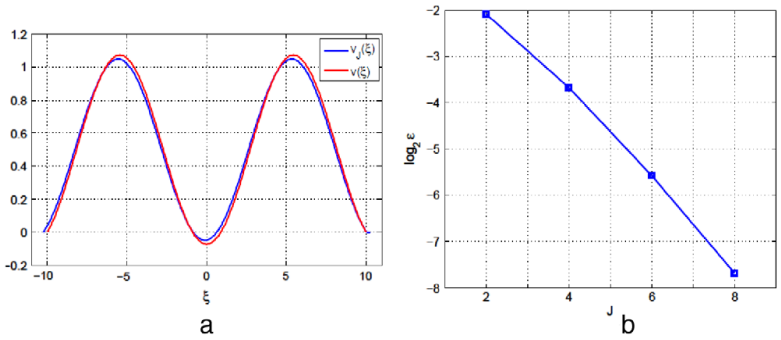

Fig. 9. (a) The exact solution (red line) and the approximation (blue line) of the stationary periodic solution of (32) with $\beta = 3, \theta = 0.5$, and $[-X, X] = [-10, 10]$. The approximation level is $J = 4$. (b) $\log_2 \varepsilon$ for different J. (For interpretation of the references to colour in this figure legend, the reader is referred to the web version of this article.)

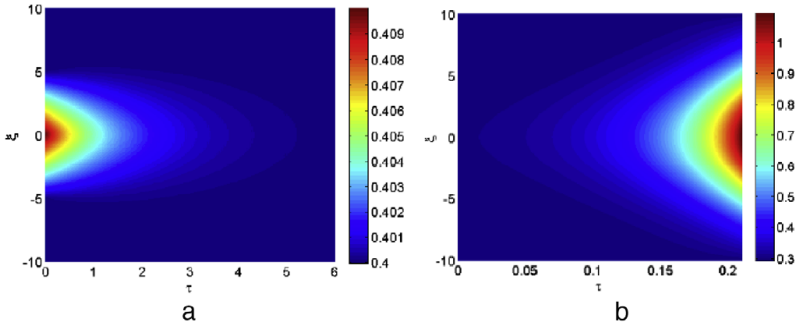

Fig. 10. The time evolution of the saw tooth profile (55) with (a) $\beta = 0.5, \theta = 0.8, v_{\text{const}} = 0.4$, (b) $\beta = 50, \theta = 0.3, v_{\text{const}} = 0.2917$.

We demand $-1 \le \beta(u_b(\xi) - \theta) \le 1$ for all ξ to stay in oblique part of the firing rate function. Under the positivity assumption for ω we get $0 \le u_b(\xi) \le 2W(a)$. Therefore, β is required to satisfy $\beta < 2/W(a)$, and θ is required to satisfy $\theta \le 1/\beta$ and $|\theta - 2W(a)| \le 1/\beta$.

The Heaviside limit of the firing rate function can be considered as an approximation of very steep firing rate functions. In accordance with previous results we expect that the profile v_b is unstable for larger β.

In Fig. 11(a) we have plotted $v_b(\xi) = 0.5(\beta(u_b(\xi) - \theta) + 1)$ with the Gaussian connectivity function, (8), $\sigma = 1, \theta = 0.01$, and $\beta = 50$. In Fig. 11(b) the time evolution of v_b when $\xi \in [-10, 10]$ is shown. The outcome of the numerical runs for the bump clearly demonstrates the same typical features as seen for the saw tooth profile in the high steepness regime: The core of the amplitude grows with time and at the same time a broadening takes place.

We notice that the growth of the core and the broadening of the profile for both the saw tooth and the bump in the unstable regime are to be expected since the evolution equation is given as (32). The Eq. (32) is a diffusion equation extended with a term $(\beta - 2)v/2$, which produces the growth of the core of the solution when $\beta > 2$. The broadening of the pulse is caused by the diffusion.

4.7. Piecewise nonlinear firing rate function case

The Eq. (36) with (49) and (50) transforms to

$$(1 + 2b + 2z)\,\partial_\tau z = \beta\partial_\xi^2 z - z^2 + (2f + \beta - 1)\,z + \left(1 - \beta\theta + (\beta - 1)b - b^2\right), \tag{57}$$

$$z(\pm X, \tau) = 0, \qquad z(\xi, 0) = v_0(\xi) - b, \tag{58}$$

by change of the variable $z(\xi, \tau) = v_J(\xi, \tau) - b$.

Applying the wavelet–Galerkin scheme and using the properties and formalism worked out in Section 4.4, we get the system of ordinary differential equations

$$(1 + 2b + 2^{J+1}z_{Jl})\frac{\mathrm{d}z_{Jl}}{\mathrm{d}\tau} = 2^{J/2}\beta\sum_k \Lambda^{0,2}_{k-l} z_{Jk} - 2^J z_{Jl}^2 + 2^{J/2}(2b + \beta - 1)z_{Jl} + (1 - \beta\theta + (\beta - 1)b - b^2),$$
$$l = k_1, k_1 + 1, \ldots, k_N.$$

In analogy with Section 4.6 we consider the problem (57)–(58) with the saw tooth and the bump as the initial conditions.

4.7.1. The time evolution of the saw tooth and the bump profile

We impose a small perturbation of the 'saw tooth' type to the constant solution, $v^{(-)}$ or $v^{(+)}$ i.e.,

$$v(-X, t) = v(X, t) = v^{(\pm)}$$

where $v^{(-)}$ and $v^{(+)}$ are the homogeneous solutions of the Eq. (36) (see Section 3.1.2), and

$$v(\xi, 0) = v^{(-)} + \varsigma(\xi), \tag{59}$$

or

$$v(\xi, 0) = v^{(+)} + \varsigma(\xi), \tag{60}$$

respectively, where ς is defined as (55).

In Fig. 12(a) we have plotted the evolution of $v(\xi, 0)$ given by (60), with $v^{(+)} = 0.5639$ for $(\beta, \theta) = (0.5, 0.8)$, which

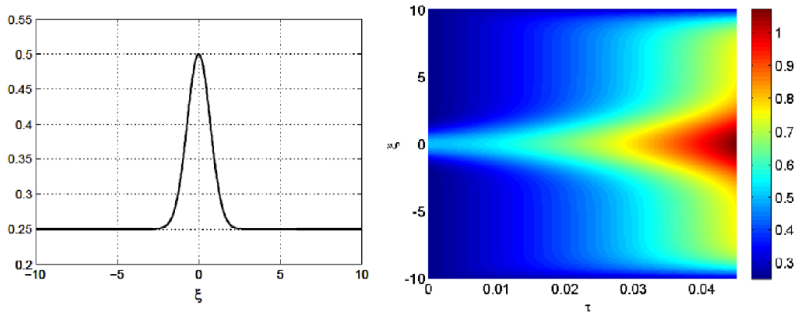

Fig. 11. (a) The bump $v_b(\xi) = 0.5(\beta(u_b(\xi) - \theta) + 1)$ with the Gaussian connectivity function, (8), $\sigma = 1$, $\theta = 0.01$, $\beta = 50$. (b) The time evolution of $v_b(\xi)$.

corresponds to the region D_1 in Fig. 8(b). In Fig. 12(b) the evolution of $v(\xi, 0)$ given by (59) with $v^{(-)} = 0.2874$ for $(\beta, \theta) = (50, 0.3)$ corresponding to the region D_2 in Fig. 8(b) is shown. In the former case the pulse dies out, while in the latter case the profile apparently develops into a saturated state. The maximum amplitude approaches the constant level $v^{(+)}$ in this case.

For the case $(\beta, \theta) \in D_2$, we have $v^{(+)} > v_0$ according to the analysis in Section 3.1.3, therefore, the pulse exceeds the upper bound of the proper solution after some time. However, for $(\beta, \theta) \in D$, $v^{(+)}$ is a proper solution and the pulse remains within the bounds.

We proceed in the same way as in Section 4.6.2. In Fig. 13(a) we have plotted $v_b(\xi) = -1/2 + \sqrt{\beta(u_b(\xi) - \theta) + 5/4}$ with the Gaussian connectivity function, (8), and the same set of parameters, $\sigma = 1, \theta = 0.01$, and $\beta = 50$. In Fig. 13(b) the time evolution of v_b when $\xi \in [-10, 10]$ is shown.

Again the evolution is characterized by a development into a saturated state.

Hence, the presence of nonlinearity in the oblique part of the firing rate function adds interesting features to the dynamics, namely the evolution to a saturated level where the maximum amplitude is given by $v^{(+)}$.

5. Concluding remarks and directions of further study

In the present paper we have derived a nonlinear diffusion equation from a one-population nonlocal neural field model of the Wilson–Cowan type by assuming that the typical spatial scale of variation of $v = P(u-\theta)$ is much larger than the synaptic footprint. The diffusion equation is termed the weakly nonlocal limit. We have tested the wavelet–Galerkin method on the weakly nonlocal limit. Our findings can be summarized as follows:

A homogeneous background is linearly unstable provided the slope of the firing rate function evaluated at the homogeneous state exceeds a certain threshold value. The instability structure consists of a finite gain band where the fastest growing mode is in the long wavelength limit.

The weakly nonlocal limit can be transformed to the Ginzburg–Landau–Khalatnikov type of equation in the firing rate variable where stationary states can be analyzed by means of a pseudo-potential formulation. Moreover we have shown that stationary, periodic solutions of this model satisfying the uniform bound $0 \leq u(x, t) \leq 1$ correspond to a finite range of pseudo energy constants E. Finally, we show that the stability of constant solutions of this model can be inferred from the properties of the extreme points of the pseudo-potential.

It is possible to construct wavelet–Galerkin expansion and discretization scheme for the model equation with Daubechies scaling functions as the basis functions. This choice of the basis seems to be quite good due to the localized character of the expected solutions.

The usage of wavelet–Galerkin expansion allows us to confirm results on stationary solutions of the actual neural field model and their linear stability properties, and to detail the evolution of disturbances numerically. In particular, we notice that when the firing rate function is modeled by a piece wise linear function a localized initial profile such as the bump and the saw tooth develops into a state characterized by a growth of the core and a broadening of the pulse in the unstable regime. In the case of a nonlinear firing rate function the bump and saw tooth develops into a saturated state in the unstable regime.

The weakly nonlocal limit can indeed be studied by using other numerical methods. However, we believe that it is important to test the wavelet–Galerkin method on simple neural model such as the weakly nonlocal model before studying more complicated neural field models by means of the same numerical approach. We expect that the wavelet-based spatial analysis of large scale 1D and 2D structures in neural field models will be an efficient tool in extracting information which is unavailable by other methods such as distribution of scales, localization of defects of the patterns and more smooth spectrum of scales than spectral methods can give. This is one of the main motivation for the present work.

Future work consists of applying the developed method to the numerical study of one- and two-population models of the Wilson–Cowan type. In addition, one should compare the outcome of the wavelet–Galerkin method with the outcome of other numerical schemes.

Acknowledgements

This research work was supported by Norwegian University of Life Sciences. The work was carried out in August 2008 and in May 2009, when I. Wertgeim was a visiting researcher at the Department of Mathematical Sciences and Technology, Norwegian University of Life Sciences. The authors would like to thank S. Coombes (University of Nottingham), A. Ponossov and G. Einevoll (Norwegian University of Life Sciences), N. Svanstedt (University of Gothenburg), V. Kostrykin (Johannes Gutenberg-University Mainz) and V.G. Zakharov (Institute of Continuous Media Mechanics, Ural Branch, Russian Academy of Sciences) for many fruitful and stimulating discussions during the preparation of this paper. The authors would also like to thank the reviewer for constructive remarks. The research work has also been supported by The

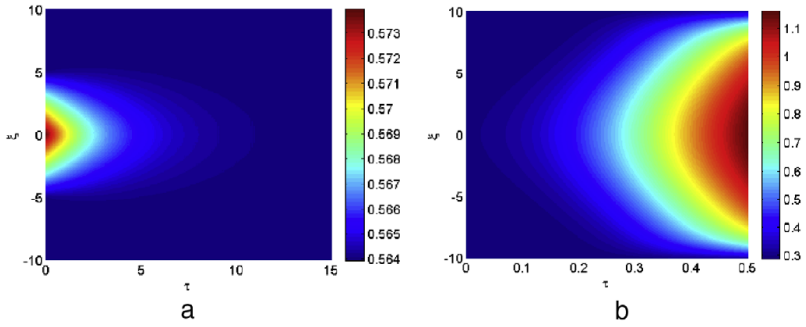

Fig. 12. (a) The time evolution of the saw tooth profile given by (60) with $v^{(+)} = 0.5639$ for $(\beta, \theta) = (0.5, 0.8)$. (b) The time evolution of the saw tooth profile given by (59) with $v^{(-)} = 0.2874$ for $(\beta, \theta) = (50, 0.3)$.

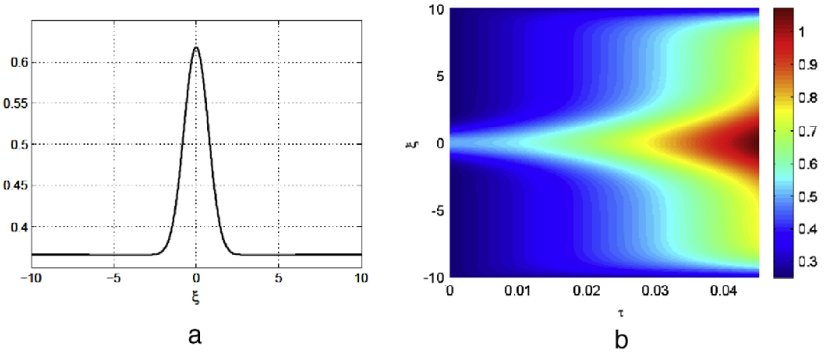

Fig. 13. (a) The bump $v_b(\xi) = -1/2 + \sqrt{\beta(u_b(\xi) - \theta) + 5/4}$ with the Gaussian connectivity function, (8), $\sigma = 1$, $\theta = 0.01$, and $\beta = 50$. (b) The time evolution of $v_b(\xi)$.

Research Council of Norway under grant No. 178892 (eNEURO-multilevel modelling and simulation of the nervous system) and grant No. 178901 (Bridging the gap: disclosure, understanding and exploitation of the genotype–phenotype map).

References

[1] P. Dayan, L.F. Abbott, Theoretical Neuroscience, MIT Press, Cambridge, MA, 2001.
[2] J. Wyller, P. Blomquist, G.T. Einevoll, On the origin and properties of two-population neural field models-a tutorial introduction, Biophys. Rev. Lett. 2 (2007) 79–98.
[3] B. Ermentrout, Neural networks as spatio-temporal pattern-forming systems, Rep. Progr. Phys. 61 (1998) 353–430.
[4] H.R. Wilson, J.D. Cowan, A mathematical theory of the functional dynamics of cortical and thalamic nervous tissue, Kybernetik 13 (1973) 55–80.
[5] S. Amari, Dynamics of pattern formation in lateral-inhibition type neural fields, Biol. Cybernet. 27 (1977) 77–87.
[6] S. Coombes, Waves, bumps, and patterns in neural field theories, Biol. Cybernet. 93 (2005) 91–108.
[7] D.J. Pinto, G.B. Ermentrout, Spatially structured activity in synaptically coupled neuronal networks: I. Traveling fronts and pulses, SIAM J. Appl. Math. 62 (2001) 206–225.
[8] D.J. Pinto, G.B. Ermentrout, Spatially structured activity in synaptically coupled neuronal networks: II. Lateral inhibition and standing pulses, SIAM J. Appl. Math. 62 (2001) 226–243.
[9] P. Blomquist, J. Wyller, G.T. Einevoll, Localized activity patterns in two-population neuronal network, Physica D 206 (2005) 180–212.
[10] J. Wyller, P. Blomquist, G.T. Einevoll, Turing instability and pattern formation in a two-population neuronal network model, Physica D 225 (2007) 75–93.
[11] Z.P. Kilpatrick, S.E. Folias, P.C. Bressloff, Traveling pulses and wave propagation failure in inhomogeneous neural media, SIAM J. Appl. Dyn. Syst. 7 (2008) 161–185.
[12] S. Coombes, M.R. Owen, Bumps, breathers, and waves in a neural network with spike frequency adaptation, Phys. Rev. Lett. (2005) 148102.
[13] A. Hutt, M. Bestehorn, T. Wennekers, Pattern formation in intracortical neuronal fields, Network 14 (2003) 351–368.
[14] A. Hutt, F.M. Atay, Analysis of nonlocal neural fields for both general and gamma-distributed connectivities, Physica D 203 (2005) 30–54.
[15] F.M. Atay, A. Hutt, Stability and bifurcations in neural fields with finite propagation speed and general connectivity, SIAM J. Appl. Math. 65 (2005) 644–666.
[16] N.A. Venkov, S. Coombes, P.C. Matthews, Dynamic instabilities in scalar neural field equations with space-dependent delays, Physica D 232 (2007) 1–15.
[17] M.R. Owen, C.R. Laing, S. Coombes, Bumps and rings in a two-dimensional neural field: splitting and rotational instabilities, New J. Phys. 9 (2007) 378.
[18] B. Ermentrout, Simulating, Analyzing, and Animating Dynamical Systems: A Guide to XPPAUT to Researchers and Students, SIAM, Philadelphia, PA, 2002.
[19] O.V. Vasilyev, D.A. Yuen, S. Paolucci, The solution of PDEs using wavelets, Comput. Phys. 11 (5) (1997) 429–435.
[20] J.C. van den Berg (Ed.), Wavelets in Physics, Cambridge University Press, Cambridge, 1999, p. 453.
[21] R. Vaillancourt, V.G. Zakharov, Biorthogonal wavelet bases for solving time-dependent PDEs, in: Scientific Proceedings of Riga Technical University 29, Boundary Field Problems and Computer Simulation 48th issue, 2006, pp. 25–52.
[22] E.B. Lin, X. Zhou, Connection coefficients on an interval and wavelet solutions of Burgers equation, J. Comput. Appl. Math. 135 (2001) 63–78.
[23] M.-Q. Chen, C. Hwang, Y.-P. Shih, The computation of wavelet–Galerkin approximation on a bounded interval, Internat. J. Numer. Methods Engrg. 39 (17) (1998) 2921–2944.
[24] H. Haken, Synergetics. An Introduction, Springer Verlag, Berlin, Heidelberg, New York, 1978.
[25] L.D. Landau, E.M. Lifshitz, in: E.M. Lifshitz, L.P. Pitaevskii (Eds.), Course of Theoretical Physics, in: Physical Kinetics, vol. 10, Pergamon Press, New York, 1981, p. 452.
[26] K. Kishimoto, S. Amari, Existence and stability of local excitations in homogeneous neural fields, J. Math. Biol. 7 (1979) 303–318.
[27] J.M. Cushing, Integrodifferential Equations and Delay Models in Population Dynamics, in: Lecture Notes in Biomathematics, Springer, New York, NY, 1977.
[28] A.J. Elvin, C.R. Laing, M.G. Roberts, Transient Turing patterns in a neural field model, Phys. Rev. E 79 (2009) 011911.
[29] R. Potthast, P.B. Graben, Existence and properties of solutions for the neural field equations, Math. Methods Appl. Sci. (2009).
[30] W. Królikowski, O. Bang, N.L. Nikolov, D. Neshev, J. Wyller, J.J. Rasmussen, D. Edmundsson, J. Opt. B 6 (2004) 288–294.
[31] W.Z. Królikowski, O. Bang, Phys. Rev. E 63 (2001) 016610.
[32] J.D. Murray, Mathematical Biology, Springer Verlag, 1993.

[33] C. Laing, W. Troy, B. Gutkin, B. Ermentrout, Multiple bumps in a neuronal model of working memory, SIAM J. Appl. Math. 63 (1) (2002) 62–97.
[34] A.J. Elvin, C.R. Laing, R.I. McLachlan, M.G. Roberts, Exploiting the Hamiltonian structure of a neural field model, Physica D 239 (2010) 537–546.
[35] D. Lu, T. Ohyoshi, L. Zhu, Threatment of boundary conditions in the applycation of wavelet–Galerkin method to a SH wave problem.
[36] C.A.J. Fletcher, Computational Galerkin Methods, Springer Verlag, Berlin, Heidelberg, New York, Tokyo, 1984.
[37] A. Avudainayagam, C. Vani, Wavelet–Galerkin solutions of quasilinear hyperbolic conservation equations, Comm. Numer. Methods Engrg. 15 (8) (1999) 589–601.
[38] I.I. Wertgeim, V.G. Zakharov, Numerical methods and parallel algorithms for study of Burgers' turbulence, in: B. Chetverushkin (Ed.), Parallel Computational Fluid Dynamics, in: Advanced Numerical Methods Software and Applications, 2004, pp. 227–234.
[39] B. Alpert, G. Beylkin, R. Coifman, V. Rokhlin, Wavelet-like bases for the fast solution of second-kind integral equations, SIAM J. Sci. Comput. 14 (1993) 159–184.
[40] A. Avudainayagam, C. Vani, Wavelet–Galerkin method for integro–differential equations, Appl. Numer. Math. 32 (2000) 247–254.
[41] I. Daubechies, Orthinormal bases of compactly supported wavelets, Comm. Pure Appl. Math. 41 (1988) 909–996.
[42] K. Amaratunga, J.R. Williams, S. Qian, J. Weiss, Wavelet–Galerkin solutions for one-dimensional partial differential equations, Internat. J. Numer. Methods Engrg. 27 (1994) 2703–2716.
[43] A. Latto, H.L. Resnikoff, E. Tenennbaum, The evaluation of connectivity coefficients of compactly supported wavelets, in: Y. Maday (Ed.), Proc. French-USA Workshop on Wavelets and Turbulence, Princeton Univercity, June 1991, Springer, New York, 1994.
[44] G. Beylkin, On the representation of operators in bass of compactly supported wavelets, SIAM J. Numer. Anal. 6 (1922) 1716–1740.
[45] J. Bergh, F. Ekstedt, M. Lindeberg, Wavelets, Studentlitteratur, Lund, Sweden, 1990.
[46] A. Tveito, R. Winther, Introduction to Partial Differential Equations: A Computational Approach, in: Text in Applied Mathematics, vol. 29, Springer-Verlag, New York, 1998.

Paper III

Nonlinear Analysis: Real World Applications 12 (2011) 3073–3094

Contents lists available at SciVerse ScienceDirect

Nonlinear Analysis: Real World Applications

journal homepage: www.elsevier.com/locate/nonrwa

Stability of bumps in a two-population neural-field model with quasi-power temporal kernels

Anna Oleynik [a,*], John Wyller [a,b], Tom Tetzlaff [a], Gaute T. Einevoll [a]

[a] Department of Mathematical Sciences and Technology and Center for Integrative Genetics, Norwegian University of Life Sciences, N-1432 Ås, Norway
[b] School of Mathematical Sciences, University of Nottingham, NG7 2RD, UK

ARTICLE INFO

Article history:
Received 3 February 2011
Accepted 8 May 2011

Keywords:
Stability of bumps
Integro-differential equations
Short term memory
Neuroscience

ABSTRACT

Neural-field models describing the spatio-temporal dynamics of the average neural activity are frequently formulated in terms of partial differential equations, Volterra equations or integro-differential equations. We develop a stability analysis for spatially symmetric bumps in a two-population neural-field model of Volterra form for a large class of temporal kernels. We find that the corresponding Evans matrix can be block-diagonalized, where one block corresponds to the symmetric part of the perturbations while the other block takes care of the antisymmetric part of these perturbations including the translational invariance of the bumps. For the class of quasi-power temporal kernels $\sim t^k \exp(-t)$ we show that the system of governing equations can be converted to a system of rate equations. We prove that for this class of temporal kernels the stability analysis based on the Evans function approach is equivalent to the phase-space reduction technique termed the generalized Amari approach. We illuminate these results by carrying out numerical simulations based on a fourth-order Runge–Kutta numerical scheme in time for the special mixed case modeled by α-functions in the excitatory equation and exponentially decaying functions in the inhibitory equation. Excellent agreement between analytical predictions from the stability analysis and numerical simulations is obtained. The generic picture consists of an unstable narrow bump pair and a broad bump pair. The broad bump pair is stable for small and moderate values of the relative inhibition time τ, is converted to a stable breather at a critical time constant, $\tau = \tau_{cr}$ (which is identified as a Hopf-bifurcation point), and becomes unstable as τ exceeds τ_{cr}.

1. Introduction

The macroscopic dynamics of neuronal tissue is often studied by means of *population* or *firing-rate* models. Rather than describing the activity of each individual neuron, they focus on the average activity, the firing rate, of populations of cells. The main purpose of such models is to reduce the dimensionality and complexity of the microscopic neural-network dynamics to obtain tools which allow mathematical treatment, efficient simulation and intuitive understanding. Since the seminal studies of [1,2], a number of population models have emerged in the literature. In the main, they have to be considered purely phenomenological descriptions. However, under simplifying assumptions, they can be derived or extracted from the single-neuron dynamics (see e.g. [3] and the references therein).

Neural population-rate models describe the temporal evolution of the firing rate r_m of a neuron population m. *Neural-field models* constitute a special class of population-rate models: here, the neuronal tissue is treated as a continuous structure.

* Corresponding author.
E-mail addresses: anna.oleynik@umb.no (A. Oleynik), john.wyller@umb.no (J. Wyller), tom.tetzlaff@umb.no (T. Tetzlaff), gaute.einevoll@umb.no (G.T. Einevoll).

1468-1218/$ – see front matter © 2011 Elsevier Ltd. All rights reserved.
doi:10.1016/j.nonrwa.2011.05.008

Each point x in space represents a subpopulation $m(x)$ of neurons. The spatial coupling between subpopulations $m(x)$, $n(x')$ is described by a *connectivity kernel* $\omega_{mn}(x, x')$ which is typically assumed to be distance dependent and homogeneous, i.e. $\omega_{mn}(x, x') = \omega_{mn}(|x - x'|)$. Notice that neural-field models where the connectivity kernels are not spatially translational invariant have been studied in a series of papers (see for example [4–9]). The time dependence of the interaction is frequently modeled by a *temporal kernel* $\alpha_{mn}(t)$. Given these ingredients, the dynamics of firing rates $r_n(x, t)$ of a system $\mathcal{N}$ of $N = |\mathcal{N}|$ populations is often described in terms of a Volterra equation system of type

$$\begin{aligned} u_n(x, t) &= \sum_{m\in\mathcal{N}} (\alpha_{mn} * \omega_{mn} \otimes r_m)(x, t) \\ r_n(x, t) &= P_n(u_n(x, t) - \theta_n) \quad (\forall n \in \mathcal{N}). \end{aligned} \tag{1}$$

Here, $u_n(x, t)$ denotes an (auxiliary) variable representing the activity of population n, $P_n(\cdot)$ the (typically sigmoidal) *firing-rate function* and θ_n the firing threshold. The index m represents the presynaptic (sender) and n the postsynaptic (target) population. The operators "$*$" and "$\otimes$" denote the temporal and spatial convolution integrals, respectively (see Section 2 for details).

The temporal kernel $\alpha_{mn}(t)$ denotes the impulse response (Green's function) of the target population n given a delta-shaped input from population m.[1] Several experimental [10–14] and theoretical studies [2,3,15–24] have shown that populations of (unconnected) neurons typically exhibit low-pass characteristics (at least if one takes into account that incoming spikes are low-pass filtered by the synapses): while the neuron ensembles can reliably track low-frequency fluctuations in the input, high-frequency components are damped. Most previous studies on neural-field models have taken this into account by considering exponential temporal kernels $\alpha_{mn}(t) = \exp(-t/\tau_n)/\tau_n$ with time constants τ_n, i.e. first-order low-pass filters. In this case, the Volterra system (1) can be transformed to a system of integro-differential equations (rate equations)

$$\begin{aligned} \tau_n \frac{\partial}{\partial t} u_n(x, t) &= -u_n(x, t) + \sum_{m\in\mathcal{N}} (\omega_{mn} \otimes r_m)(x, t) \\ r_n(x, t) &= P_n(u_n(x, t) - \theta_n) \quad (\forall n \in \mathcal{N}). \end{aligned} \tag{2}$$

Compared to the Volterra form (1), neural-field models in rate-equation form (2) are more amenable to mathematical and numerical analysis due to the fact that the latter category of equations is local in time, while the former is global in time. This is one reason that neural-field models in rate-equation form (2) have been more popular in theoretical neuroscience (e.g. [1,25,26]). The exact shape of the temporal kernel $\alpha_{mn}(t)$ is determined by a variety of factors, for example, by the dynamical properties of the postsynaptic neurons (see e.g. [20,21]), by the activity of the presynaptic neurons (e.g. excitation vs. inhibition; additive vs. multiplicative noise; see [11,14,17,22,24]), and by the properties of the synapses. Experiments have shown that the transfer of somatic input currents (currents which are directly injected into the cell body; the effect of synaptic filtering is thus neglected) to the response firing rate of a neuron population exhibits signs of higher-order low-pass or band-pass characteristics [12]. Furthermore, postsynaptic currents (the response of somatic input currents to presynaptic firing) are often much better described by second-order (alpha function kernels) or higher-order low-pass filters rather than by simple exponentials [27]. Therefore, the restriction to exponential temporal kernels in neural-field models can hardly be justified.

In this article, we exploit that neural-field models in Volterra form (1) can be transformed to a system of integro-differential equations similar to (2) not only for simple exponentials, but for the whole class of *quasi-polynomial* temporal kernels [28]

$$\alpha_{mn}(t) = \sum_{k=0}^{K} c_{mnk}\, t^k \exp(-t/\tau_{mnk})$$

with constants $c_{mnk},\ \tau_{mnk} \in \mathbb{R}$ and $K \in \mathbb{N}$ [29]. Neural-field models with general temporal kernels have been studied before (see Coombes [30] and the references therein). All these studies are, however, restricted to one-population models. Here, we extend this work by studying the dynamics of a two-population neural-field model ($N = 2$; $m, n \in \{e, i\}$) for the sub-class of 'quasi-power' temporal kernels (higher-order low-pass filters):

$$\alpha_{mn}(t) = \begin{cases} \dfrac{t^{k_n}}{(k_n)!} \exp(-t) & n = e \\ \dfrac{t^{k_n}}{\tau^{k_n+1}(k_n)!} \exp(-t/\tau) & n = i \end{cases} \qquad (k_n \in \mathbb{N}). \tag{3}$$

For convenience, time is measured here in units of the excitatory time constant (which is therefore set to 1).

Key topics in the study of neural-field models are the generation and/or stability of coherent activity structures, such as stationary bumps (pulses) [25,26,30–41] and stationary periodic patterns [42–47], spatio-temporal oscillatory

[1] Note that $\alpha_{mn}(t)$ corresponds to the impulse response of an *isolated* population n rather than to the impulse response of the entire network. In other words, it is the response of population n to a firing-rate fluctuation of population m in the absence of any feedback connections, i.e. for $\omega_{pq}(x, y) = 0\ \forall x, y \in \mathbb{R}$ and $\forall p, q \neq n$.

patterns [37,43,48–51], or traveling waves, pulses and fronts [30,35,37,44,49,50,52–56]. Commonly, one (excitatory) [26] or two (excitatory, inhibitory) [25,57] neuronal populations in a single spatial dimension have been described by a single or two coupled integro-differential equations of type (2).

In [25], the rate-equation system (2) with $N = 2$, $m, n \in \{e, i\}$, i.e., all temporal kernels are modeled by exponentially decaying functions, was considered. The closed-form expressions for the stationary localized solutions (bumps) were derived under the assumption that the firing-rate functions P_e and P_i are Heaviside functions. It was shown that there is always a set of threshold values θ_e, θ_i for which bumps exist. This set of threshold values is referred to as the *admissible set of threshold values*. The generic picture consists of two bump pairs for each pair of admissible threshold values. The stability problem in [25] was addressed by using two different approaches:

The first one, which is referred to as the *Amari approach*, describes the bumps by their *pulse width coordinates*, the coordinates of the crossing between the pulses and the threshold values. An autonomous system of ordinary differential equations, termed the *Amari system*, for the pulse width coordinates was derived from (2) under the assumption that imposed perturbation is symmetric. The second approach considered in [25] consists of a direct linearization of the rate-equation system (2) around the bump state. The growth/decay rate of the perturbation is determined by requiring the stability matrix to be singular. It was shown that the stability matrix can be block-diagonalized. The growth/decay rates obtained from the upper block are identical to the eigenvalues of the Jacobian matrix of the Amari system. The lower block predicts translational invariance. The Amari approach is based on the conjecture that the stability of bumps can be inferred from the stability of the equilibrium of the Amari system. However, in [25] it was shown that two stability approaches do not coincide.

The work presented in this article constitutes a generalization of [25] to a new general class of temporal kernels (3). In Section 2, we introduce the model and the necessary notation, and prove that the solutions of the initial value problem are uniformly bounded provided the firing-rate functions P_n are bounded. Thus, any instability will eventually be saturated. In the remainder of the paper, we restrict ourselves to firing-rate functions described by Heaviside functions. In Section 3, we review the existence theory for bumps [25]. Section 4 is devoted to the stability of spatially symmetric bumps within the framework of (1). The linearization procedure is applied directly to (1) for arbitrary temporal kernels $\alpha_{mn}(t)$. We refer to this approach as the *Evans function technique*. The growth/decay rate of the perturbation is determined by requiring the stability matrix to be singular. We refer to the stability matrix as *Evans matrix* [30], its determinant as the *Evans function*. We demonstrate that the Evans matrix of the system can be block-diagonalized. The resulting blocks correspond to symmetric and antisymmetric perturbations. We emphasize that this result is independent from the choice of the temporal kernels and does not require the rate-equation representation of (1) as in [25]. For quasi-power kernels (3), the Evans function is a rational function. Its roots can therefore be localized by means of the Routh–Hurwitz criterion. We derive a sufficient condition for bumps to be unstable, independently of the orders of the quasi-power kernels. In Section 5, we generalize the Amari approach to quasi-power temporal kernels, and show that it is, for this case, equivalent to the Evans function technique described in Section 4. In Section 6, we illustrate our results by means of an example. We consider the specific case of temporal kernels (3) with $k_e = 1$, $k_i = 0$, i.e., the temporal kernels of the excitatory and inhibitory population are modeled by an α-function and an exponentially decaying function, respectively. We study the stability of bumps for this case both analytically (Section 6.1) and numerically (Section 6.2). For the numerical simulations, we make use of the fact that the system can be described in terms of rate equations. The example of this type of temporal interaction ($k_e = 1$, $k_i = 0$) was studied in [58] (Model B). However, since spatial effects are not taken into account in the model considered in [58] is a compartment model and not a neural-field model.

The fact that the stability result from the generalized Amari approach is equivalent with the results of the Evans function technique for the quasi-power temporal kernels, apparently contradicts the conclusion in [25]. We discuss the cause of this result in Section 7. We also point out the advantage of the rate-equation representation of (1), and discuss advantages and disadvantages of the two stability approaches. Section 7 contains also the conclusions and an outlook. The appendices include details about the boundedness property for the solutions of the two-population form of (1) with temporal kernels (3) (Appendix A) and the detailed proof of the equivalence of the Evans function technique and the generalized Amari approach (Appendix B).

2. The model

For the construction of the two-population neural-field model we assume that (i) all neurons receive synaptic inputs from, in principle, all excitatory and inhibitory neurons in the network, (ii) the synaptic weights depend only on the type of pre- and postsynaptic neurons and their absolute spatial distance, (iii) the net activity level of each population depends on a weighted sum over the past firing activity in the presynaptic subpopulations, and (iv) the neuronal firing rates at a certain time are given by applying particular nonlinear functions to the neuronal activity levels at the same time [59].

The nonlocal model for the excitatory activity level u_e and the inhibitory activity level u_i in one spatial dimension reads [30,59]

$$u_e = \alpha_{ee} * \omega_{ee} \otimes P_e(u_e - \theta_e) - \alpha_{ie} * \omega_{ie} \otimes P_i(u_i - \theta_i) \tag{4a}$$

$$u_i = \alpha_{ei} * \omega_{ei} \otimes P_e(u_e - \theta_e) - \alpha_{ii} * \omega_{ii} \otimes P_i(u_i - \theta_i) \tag{4b}$$

with $\omega_{mn} \otimes P_m(u_m - \theta_m)$ defined as the spatial convolution integral

$$(\omega_{mn} \otimes P_m(u_m - \theta_m))(x, t) = \int_{-\infty}^{\infty} \omega_{mn}(y - x) P_m(u_m(y, t) - \theta_m) \mathrm{d}y,$$

and $\alpha_{mn} * f$ as the temporal convolution integral

$$(\alpha_{mn} * f)(x, t) = \int_{-\infty}^{t} \alpha_{mn}(t - s) f(x, s) \mathrm{d}s.$$

Here and in what follows we have $m, n = e, i$.

The spatial distribution of synaptic connection strength in the network is described by means of the *connectivity functions* ω_{mn}, which are assumed to be real-valued, bounded, symmetric, normalized and parameterized by means of *synaptic footprints* σ_{mn}, i.e.,

$$\omega_{mn}(x) = \sigma_{mn}^{-1} \Phi_{mn}(\xi_{mn}), \quad \xi_{mn} = x/\sigma_{mn}. \tag{5}$$

Here Φ_{mn} are scaling functions.

The impact of past neural firing on the present activity levels in the network is described by the temporal kernels $\alpha_{mn}(t)$ typically parameterized by a single time constant, say τ, which is the ratio between the inhibitory and excitatory time constants. We assume that α_{mn} are normalized i.e.,

$$\int_0^{\infty} \alpha_{mn}(t) \mathrm{d}t = 1. \tag{6}$$

The conversion of activity levels to action-potential firing activities of the neurons is modeled by means of the *firing-rate functions* denoted by P_e and P_i, respectively, for the excitatory and the inhibitory neurons. These functions are smooth, increasing and parameterized by an inclination parameter $\beta_m > 0$. Here, they are chosen to map the set of real numbers onto the unit interval (so that the true firing rates are obtained by multiplying the output of these functions with appropriate constants). The firing-rate functions approach the Heaviside function H as $\beta_m \to \infty$.

Finally, the parameters θ_m represent *threshold values for firing*, which by assumption satisfy $0 < \theta_m \leq 1$.

In [25,43,59], system (4) with

$$\alpha_{ee}(t) = \alpha_{ie}(t) = \mathrm{e}^{-t}, \qquad \alpha_{ei}(t) = \alpha_{ii}(t) = \frac{1}{\tau} \mathrm{e}^{-\frac{t}{\tau}}$$

has been investigated with respect to existence and stability of stationary, spatially localized solutions, the so-called *bumps* or *standing pulses* [25], and pattern formation through Turing type of instability [43]. The starting point of the analysis performed in [25,43,59] is the Wilson–Cowan type of equations

$$\begin{aligned} \partial_t u_e &= -u_e + \omega_{ee} \otimes P_e(u_e - \theta_e) - \omega_{ie} \otimes P_i(u_i - \theta_i) \\ \tau \partial_t u_i &= -u_i + \omega_{ei} \otimes P_e(u_e - \theta_e) - \omega_{ii} \otimes P_i(u_i - \theta_i), \end{aligned}$$

which are derived by means of the Linear Chain Trick (LCT)[29].

It is also possible to obtain a system of rate equations from (4) by the LCT when the temporal kernels are given by quasi-power functions (3). In this case, we get a system of $(k_e + k_i + 2)$ coupled equations with $(k_e + k_i)$ auxiliary variables. Then the initial value problem can be written in a compact vector form as

$$\partial_t \bar{U} = L\bar{U} + F\bar{U}, \qquad \bar{U}_{t=0} = \bar{U}^0. \tag{7}$$

Here $\bar{U}$ is the vector solution containing the activity levels u_m and the auxiliary variables $v_m^{(k)}$, $k = 1, \ldots, k_m$, $m = e, i$, as components, i.e.,

$$\bar{U} = (u_e, v_e^{(1)}, \ldots, v_e^{(k_e)}, u_i, v_i^{(1)}, \ldots, v_i^{(k_i)})^T.$$

Moreover, L is a linear operator represented by means of the matrix $\mathbf{L}$ which has a Jordan block form,

$$\mathbf{L} = \begin{pmatrix} \mathbf{J}_e & \mathbf{O}_e \\ \mathbf{O}_i & \frac{1}{\tau}\mathbf{J}_i \end{pmatrix}, \qquad \mathbf{J}_m = \begin{pmatrix} -1 & 1 & & & \\ & -1 & 1 & & \\ & & \ddots & \ddots & \\ & & & -1 & 1 \\ & & & & -1 \end{pmatrix}, \quad m = e, i. \tag{8}$$

Here the block $\mathbf{J}_m$ is a $(k_m+1) \times (k_m+1)$ matrix for $m = e, i$; $\mathbf{O}_e$ is a $(k_e+1) \times (k_i+1)$ zero matrix, and $\mathbf{O}_i$ is a $(k_i+1) \times (k_e+1)$ zero matrix.

Finally, F is a nonlocal nonlinear operator such that

$$F\bar{U} = \begin{pmatrix} 0 \\ \vdots \\ 0 \\ \omega_{ee} \otimes P_e(u_e - \theta_e) - \omega_{ie} \otimes P_i(u_i - \theta_i) \\ 0 \\ \vdots \\ 0 \\ \omega_{ei} \otimes P_e(u_e - \theta_e) - \omega_{ii} \otimes P_i(u_i - \theta_i) \end{pmatrix},$$

where non-zero elements of (2) are located in $(k_e + 1)$th and $(k_i + 1)$th rows. The initial condition vector, $\bar{U}^0$, is a continuous and bounded vector function.

One can prove that the initial value problem (7) is locally well posed in the space of bounded continuous functions in a way analogous to Potthast et al. [60] for one-population models and Faye et al. [61] for multipopulation models with axonal and dendritic delay effects incorporated.

Next, let us consider the boundedness of the solutions. The initial value problem (7) is equivalent to the fixed point problem, [62]

$$\bar{U}(x, t) = R(t)\bar{U}^0(x) + \int_0^t R(t - s)(F\bar{U})(x, s)\mathrm{d}s, \quad R(t) = \mathrm{e}^{tL}. \tag{9}$$

Notice that the spectrum of the operator L consists of two negative eigenvalues, -1 and $-1/\tau$, with the multiplicity $k_e + 1$ and $k_i + 1$, respectively. Moreover, $|F(\bar{U})| \leq 1$, since the range of P_m is $[0, 1]$ and w_{mn} is normalized. Therefore, the solutions of (9) are uniformly bounded and the following estimate is valid for all components of $\bar{U}$ (for details, see Appendix A)

$$|U_j(x, t)| \leq \|\bar{U}^0\|_\infty + \max\{k_e, k_i\tau\}, \quad j = 1, \ldots, N, \ N = k_e + k_i + 2. \tag{10}$$

The norm here is defined for a vector function $\bar{V}(x) = (V_1(x), \ldots, V_N(x))^T \in (C_b(\mathbb{R}))^N$, where $C_b(\mathbb{R})$ is the space of bounded continuous functions on $\mathbb{R}$, as

$$\|\bar{V}\|_\infty = \max_i(\sup_x |V_i(x)|). \tag{11}$$

Thus, if any instability occurs it has to be saturated. The boundedness result for the Wilson–Cowan models studied in this paper is analogous to the one obtained in [25,60].

From now we assume that the firing-rate functions P_m are approximated with the Heaviside function H.

3. Existence and uniqueness of bumps

For the sake of completeness, we summarize the results in [25] regarding the existence and uniqueness of pairs of excitatory and inhibitory bumps.

When approximating the firing-rate functions P_m with Heaviside functions H, one obtains closed-form expressions for excitatory, U_e, and inhibitory, U_i, bumps, that is

$$U_e(x) = W_{ee}(a - x) + W_{ee}(a + x) - W_{ie}(b - x) - W_{ie}(b + x), \tag{12a}$$

$$U_i(x) = W_{ei}(a - x) + W_{ei}(a + x) - W_{ii}(b - x) - W_{ii}(b + x), \tag{12b}$$

where

$$W_{mn}(x) = \int_0^x \omega_{mn}(y)\mathrm{d}y = \int_0^{x/\sigma_{mn}} \Phi_{mn}(y)\mathrm{d}y. \tag{13}$$

The coordinates a, b satisfy the equations

$$f_e(a, b) = \theta_e, \qquad f_i(a, b) = \theta_i \tag{14}$$

with f_e and f_i given as

$$\begin{aligned} f_e(a, b) &= W_{ee}(2a) - W_{ie}(b - a) - W_{ie}(a + b) \\ f_i(a, b) &= W_{ei}(a + b) + W_{ei}(a - b) - W_{ii}(2b). \end{aligned} \tag{15}$$

In the process of deriving (12), (14), it is assumed that we have a single bump structure of the stationary solutions. The parameters a, b, which are unique solutions of $U_e(\pm a) = \theta_e$ and $U_i(\pm b) = \theta_i$, measure the pulse widths of $U_e(x)$ and $U_i(x)$. It turns out that a typical situation consists of two pairs of pulses $(U_e(x), U_i(x))$ for each set of threshold values (θ_e, θ_i), one *broad* and one *narrow* pulse pair. This result has also been found for one-population models [26] and simpler two-population

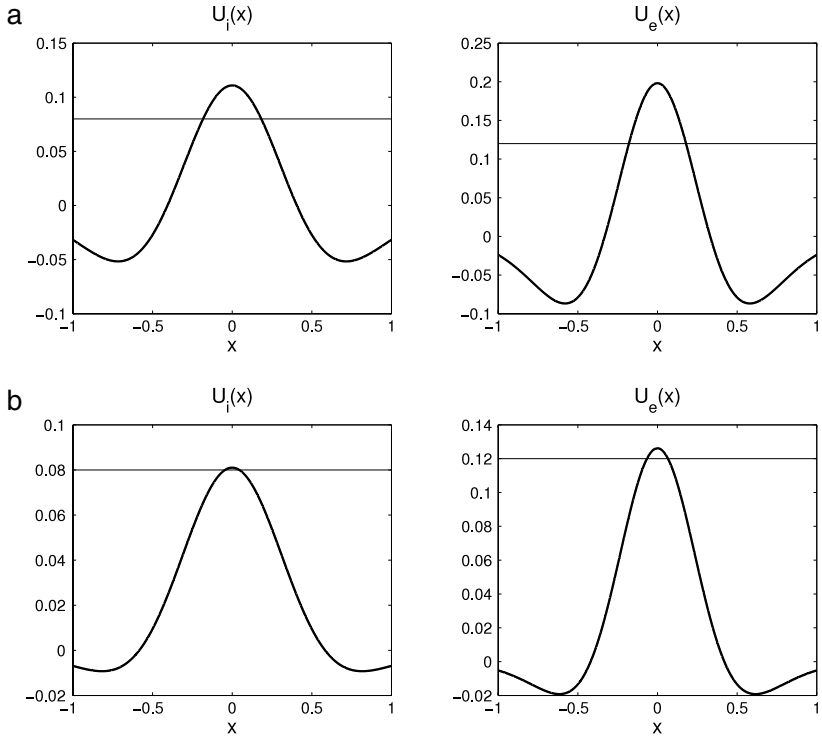

Fig. 1. A numerical example of (a) a broad excitatory (left) and inhibitory (right) pulse pair; and (b) a narrow excitatory (left) and inhibitory (right) pulse pair. The connectivity functions are Gaussian (5), (16) with synaptic footprints given by (17). The horizontal lines notify the corresponding threshold values given by (18).

models [32]. In addition, one finds that *an excitatory pulse may exist without an accompanying inhibitory pulse* but *the inhibitory cannot exist alone* [25]. From now on we refer to any solution of (14) as (a_0, b_0).

In Fig. 1, we display graphically the bumps when the connectivity functions are modeled by means of Gaussian functions, [25]

$$\Phi_{mn}(\xi_{mn}) = \frac{1}{\sqrt{\pi}} \exp(-\xi_{mn}^2) \tag{16}$$

with synaptic footprints

$$\sigma_{ee} = 0.35, \qquad \sigma_{ei} = 0.48, \qquad \sigma_{ie} = 0.60, \qquad \sigma_{ii} = 0.69, \tag{17}$$

and threshold values are

$$\theta_e = 0.12, \qquad \theta_i = 0.08. \tag{18}$$

The widths (a_0, b_0) for narrow pulse pair are (0.066, 0.045) and for the broad pulse pair are (0.179, 0.183). We will use this example in Section 6.2.

4. Stability of bumps for the two-population model: Evans function technique

In order to investigate the stability of the bumps, the Evans function technique is applicable (see for example [30]). We proceed in the standard way by assuming solutions of (4) on the form

$$u_e(x, t) = U_e(x) + \tilde{u}_e(x)e^{\lambda t},$$
$$u_i(x, t) = U_i(x) + \tilde{u}_i(x)e^{\lambda t},$$

where λ denotes the growth/decay rate and linearize the resulting equations about the bump state. We end up with the system of equations for the spatial part of the perturbations, $\tilde{u}_e$, $\tilde{u}_i$,

$$\begin{aligned} \tilde{u}_e(x) &= \tilde{\alpha}_{ee}(\lambda)\Omega_{ee}(x) - \tilde{\alpha}_{ie}(\lambda)\Omega_{ie}(x), \\ \tilde{u}_i(x) &= \tilde{\alpha}_{ei}(\lambda)\Omega_{ei}(x) - \tilde{\alpha}_{ii}(\lambda)\Omega_{ii}(x). \end{aligned} \tag{19}$$

Here $\tilde{\alpha}_{mn}$ denotes the Laplace transform of α_{mn}

$$\tilde{\alpha}_{mn}(\lambda) = \int_0^\infty \alpha_{mn}(t)\mathrm{e}^{-\lambda t}\mathrm{d}t$$

provided the integral exists. Here the functions Ω_{mn} are defined as $\Omega_{mn} = \omega_{mn} \otimes H'((U_m - \theta_m)\tilde{u}_m)$ where $H' = \delta$ and δ is the Dirac function.

The convolution integral Ω_{mn} is according to [25] given as

$$\Omega_{en}(x) = \frac{1}{|U_e'(a_0)|}(\omega_{en}(x + a_0)\tilde{u}_e(-a_0) + \omega_{en}(x - a_0)\tilde{u}_e(a_0)), \tag{20a}$$

$$\Omega_{in}(x) = \frac{1}{|U_i'(b_0)|}(\omega_{in}(x + b_0)\tilde{u}_i(-b_0) + \omega_{in}(x - b_0)\tilde{u}_i(b_0)). \tag{20b}$$

Let

$$\bar{X} = (\tilde{u}_e(a_0), \tilde{u}_e(-a_0), \tilde{u}_i(-b_0), \tilde{u}_i(b_0))^T.$$

The relations (19)–(20) imply

$$\tilde{u}_e(x) \equiv \tilde{u}_i(x) \equiv 0 \Leftrightarrow \bar{X} = \bar{0}.$$

We consider non-trivial disturbances and, thus, $\bar{X} \neq \bar{0}$. Plugging $x = \pm a_0$ into the first equation of (19) and $x = \pm b_0$ into the second we can write the result in the matrix form $J_E\bar{X} = \bar{0}$ where

$$\mathbf{J}_E = \begin{pmatrix} \dfrac{\tilde{\alpha}_{ee}(\lambda)\omega_{ee}(0)}{|U_e'(a_0)|} - 1 & \dfrac{\tilde{\alpha}_{ee}(\lambda)\omega_{ee}(2a_0)}{|U_e'(a_0)|} & -\dfrac{\tilde{\alpha}_{ie}(\lambda)\omega_{ie}(a_0 - b_0)}{|U_i'(b_0)|} & -\dfrac{\tilde{\alpha}_{ie}(\lambda)\omega_{ie}(a_0 + b_0)}{|U_i'(b_0)|} \\ \dfrac{\tilde{\alpha}_{ee}(\lambda)\omega_{ee}(2a_0)}{|U_e'(a_0)|} & \dfrac{\tilde{\alpha}_{ee}(\lambda)\omega_{ee}(0)}{|U_e'(a_0)|} - 1 & -\dfrac{\tilde{\alpha}_{ie}(\lambda)\omega_{ie}(a_0 + b_0)}{|U_i'(b_0)|} & -\dfrac{\tilde{\alpha}_{ie}(\lambda)\omega_{ie}(a_0 - b_0)}{|U_i'(b_0)|} \\ \dfrac{\tilde{\alpha}_{ei}(\lambda)\omega_{ei}(a_0 - b_0)}{|U_e'(a_0)|} & \dfrac{\tilde{\alpha}_{ei}(\lambda)\omega_{ei}(a_0 + b_0)}{|U_e'(a_0)|} & -\dfrac{\tilde{\alpha}_{ii}(\lambda)\omega_{ii}(0)}{|U_i'(b_0)|} - 1 & -\dfrac{\tilde{\alpha}_{ii}(\lambda)\omega_{ii}(2b_0)}{|U_i'(b_0)|} \\ \dfrac{\tilde{\alpha}_{ei}(\lambda)\omega_{ei}(a_0 + b_0)}{|U_e'(a_0)|} & \dfrac{\tilde{\alpha}_{ei}(\lambda)\omega_{ei}(a_0 - b_0)}{|U_e'(a_0)|} & -\dfrac{\tilde{\alpha}_{ii}(\lambda)\omega_{ii}(2b_0)}{|U_i'(b_0)|} & -\dfrac{\tilde{\alpha}_{ii}(\lambda)\omega_{ii}(0)}{|U_i'(b_0)|} - 1 \end{pmatrix}.$$

We call the matrix $\mathbf{J}_E$ the *Evans matrix* in accordance with the terminology used in [30].

The structure of the Evans matrix $\mathbf{J}_E$ allows us to introduce the block-diagonalization

$$\tilde{\mathbf{J}}_E = \mathbf{P}\mathbf{J}_E\mathbf{P}^{-1}, \qquad \mathbf{P} = \begin{pmatrix} \frac{1}{2} & \frac{1}{2} & 0 & 0 \\ 0 & 0 & \frac{1}{2} & \frac{1}{2} \\ \frac{1}{2} & -\frac{1}{2} & 0 & 0 \\ 0 & 0 & \frac{1}{2} & -\frac{1}{2} \end{pmatrix}, \qquad \tilde{\mathbf{J}}_E = \begin{pmatrix} \mathbf{J}_{11} & \mathbf{O} \\ \mathbf{O} & \mathbf{J}_{22} \end{pmatrix}$$

where $\mathbf{J}_{11}$ and $\mathbf{J}_{22}$ are given as

$$\mathbf{J}_{11} = \begin{pmatrix} \tilde{\alpha}_{ee}(\lambda)\dfrac{A + B}{p_1} - 1 & -\tilde{\alpha}_{ie}(\lambda)\dfrac{C + D}{p_2} \\ \tilde{\alpha}_{ei}(\lambda)\dfrac{E + F}{p_1} & -\tilde{\alpha}_{ii}(\lambda)\dfrac{G + H}{p_2} - 1 \end{pmatrix},$$

$$\mathbf{J}_{22} = \begin{pmatrix} \tilde{\alpha}_{ee}(\lambda)\dfrac{A - B}{p_1} - 1 & -\tilde{\alpha}_{ie}(\lambda)\dfrac{C - D}{p_2} \\ \tilde{\alpha}_{ei}(\lambda)\dfrac{E - F}{p_1} & -\tilde{\alpha}_{ii}(\lambda)\dfrac{G - H}{p_2} - 1 \end{pmatrix}.$$

Here we have conveniently introduced the following parameters which we will use throughout the paper.

$$\begin{aligned} &A = w_{ee}(0), \quad B = w_{ee}(2a_0), \quad C = w_{ie}(a_0 - b_0), \quad D = w_{ie}(a_0 + b_0), \\ &E = w_{ei}(a_0 - b_0), \quad F = w_{ei}(a_0 + b_0), \quad G = w_{ii}(0), \quad H = w_{ii}(2b_0), \end{aligned} \tag{21}$$

$$\begin{aligned} p_1 &= |U_e'(a_0)| = (A + D) - (B + C), \\ p_2 &= |U_i'(b_0)| = (E + H) - (F + G). \end{aligned} \tag{22}$$

Notice that $\tilde{\alpha}_{mn}(0) = 1$ since α_{mn} by assumption (6) are normalized functions. Thus, $\lambda = 0$ is the zero of $\det(\mathbf{J}_{22}) = 0$. This result indeed reflects the translation invariance property of the bump solutions.

The block-diagonalization of the Evans matrix $\mathbf{J}_E$ yields the factorization

$$\mathcal{E}(\lambda) = \mathcal{E}_S(\lambda)\mathcal{E}_{As}(\lambda)$$

of the Evans function $\mathcal{E}(\lambda) \equiv \det(\mathbf{J}_E)$. Here $\mathcal{E}_S(\lambda) = \det(\mathbf{J}_{11})$ and $\mathcal{E}_{As}(\lambda) = \det(\mathbf{J}_{22})$.

Since $\bar{X} \neq \bar{0}$, the eigenvalues λ must be the zeros of the Evans function i.e. $\mathcal{E}(\lambda) = \det(\mathbf{J}_E) = 0$. Due to the factorization of the Evans function (4) the set of eigenvalues consists of the zeros of $\mathcal{E}_S(\lambda)$ and $\mathcal{E}_{As}(\lambda)$. Notice that by construction, the matrix $\mathbf{J}_{11}$ corresponds to the symmetrical part of the perturbations while the matrix $\mathbf{J}_{22}$ reflects the antisymmetry in the perturbations imposed on the bumps.

Now, introduce the parameters

$$\begin{aligned} d_1 &= \frac{\partial f_e}{\partial a}(a_0, b_0)/|U_e'(a_0)| = (2B + C - D)/p_1, \\ d_2 &= \frac{\partial f_e}{\partial b}(a_0, b_0)/|U_i'(b_{eq})| = -(C + D)/p_2, \\ d_3 &= \frac{\partial f_i}{\partial a}(a_0, b_0)/|U_e'(a_0)| = (E + F)/p_1, \\ d_4 &= \frac{\partial f_i}{\partial b}(a_0, b_0)/|U_i'(b_{eq})| = -(2H + E - F)/p_2, \end{aligned} \tag{23}$$

where f_e and f_i are given as (15).

By letting $\lambda = 0$ we also get $\det(\mathbf{J}_{11}) = \gamma_S$ where

$$\gamma_S = d_1 d_4 - d_2 d_3, \tag{24}$$

which we require to be not equal to zero to avoid a multiple zero eigenvalue. The role of γ_S is not clear for the general choice of temporal kernels. However, we notice that γ_S is proportional (with the positive constant of proportionality) to the Jacobian obtained for the Amari system in [25] where the model (4) with exponentially decaying kernels has been studied. In that paper, it is shown that $\gamma_S < 0$ implies instability of bumps.

Let us consider the case when the temporal kernels are given as (3). The Laplace transforms are computed as

$$\tilde{\alpha}_{ee}(\lambda) = \tilde{\alpha}_{ie}(\lambda) = \frac{1}{(1+\lambda)^{k_e+1}}, \qquad \tilde{\alpha}_{ei}(\lambda) = \tilde{\alpha}_{ii}(\lambda) = \frac{1}{(1+\tau\lambda)^{k_i+1}}.$$

In this case, the factors $\mathcal{E}_S(\lambda)$ and $\mathcal{E}_{As}(\lambda)$ in the Evans function can be expressed as a rational function in λ:

$$\begin{aligned} \mathcal{E}_S(\lambda) &= (1+\lambda)^{-(k_e+1)}(1+\tau\lambda)^{-(k_i+1)}\mathcal{P}_S(\lambda), \\ \mathcal{E}_{As}(\lambda) &= (1+\lambda)^{-(k_e+1)}(1+\tau\lambda)^{-(k_i+1)}\lambda\mathcal{P}_{As}(\lambda), \end{aligned}$$

where $\mathcal{P}_S(\lambda)$ is the polynomial of the degree $(k_e + k_i + 2)$

$$\mathcal{P}_S(\lambda) = \lambda^2\tau P_{k_e}(\lambda)Q_{k_i}(\lambda) - d_4\lambda P_{k_e}(\lambda) - d_1\tau\lambda Q_{k_i}(\lambda) + \gamma_S, \tag{25}$$

and $\mathcal{P}_{As}$ is the polynomial of the degree $(k_e + k_i + 1)$

$$\mathcal{P}_{As}(\lambda) = \tau\lambda P_{k_e}(\lambda)Q_{k_i}(\lambda) + \frac{E-F}{p_2}P_{k_e}(\lambda) - \frac{C-D}{p_1}\tau Q_{k_i}(\lambda). \tag{26}$$

Here P_{k_e} and Q_{k_i} are defined by

$$\lambda P_{k_e}(\lambda) = (1+\lambda)^{k_e+1} - 1, \qquad \tau\lambda Q_{k_i}(\lambda) = (1+\tau\lambda)^{k_i+1} - 1. \tag{27}$$

From (25) and (27) it follows that the leading coefficient of the polynomial $\mathcal{P}_S$ is positive. It implies according to the Routh–Hurwitz criterion (see Appendix in [58]) that $\gamma_S < 0$ is sufficient for having at least one positive zero of $\mathcal{P}(\lambda)$. Thus, for the model (4) in the framework of the kernels (3) we conclude that $\gamma_S < 0$ is a sufficient condition for bumps to be unstable. We notice that γ_S does not depend on the powers k_e, k_i. Therefore, if $\gamma_S < 0$ is detected for some bumps in the framework of the model with some choice of quasi-power functions (3) then these bumps remain unstable for any other choices of (3).

The polynomial representation of $\det(\mathbf{J}_{22})$ allows us to calculate the constant coefficient of $\mathcal{P}_{As}$, that is,

$$\gamma_{As} = \frac{E-F}{p_2}(k_e+1) - \frac{C-D}{p_1}(k_i+1)\tau.$$

The leading coefficient of $\mathcal{P}_{As}$ is positive. Therefore, we arrive at the following conclusion: the bumps are unstable if at least one of the values γ_S or γ_{As} is negative.

5. Stability of bumps for the two-population model with quasi-power temporal kernels: generalized Amari approach

The Amari approach is based on the assumption that the solutions $(u_e(x,t), u_i(x,t))$ in a vicinity of the bump solution $(U_e(x), U_i(x))$ have a shape which is close to the shape of the bump solutions i.e. we assume that the perturbed solutions have exactly two intersections with the corresponding thresholds. Thus, there are time-dependent crossing coordinates $a_1, a_2 (a_1 < a_2)$ of the pulse u_e with the threshold θ_e and $b_1, b_2 (b_1 < b_2)$ with the pulse u_i with the threshold θ_i, [25]

$$u_e(a_j(t),t) = \theta_e, \qquad u_i(b_j(t),t) = \theta_i, \quad j = 1,2. \tag{28}$$

In the original work of Amari [26], the dynamical system for the crossing coordinates is obtained in the case of a one-population neural-field model. The equilibrium of this dynamical system is identified with the stationary bumps. It is conjectured that the stability of the bumps can be inferred from the stability of this equilibrium.

We exploit this idea and present a phase-space reduction technique termed the *generalized Amari approach* for the two-population neural-field model (4) under the assumption that the temporal kernels are modeled as (3). We prove that the stability problem can be resolved completely by means of the generalized Amari approach.

We differentiate (28) with respect to t in a way analogous to [26] and obtain

$$\begin{aligned} &\frac{\partial u_e}{\partial x}(a_j(t),t)\frac{da_j}{dt} + \frac{\partial u_e}{\partial t}(a_j(t),t) = 0, \\ &\qquad\qquad\qquad\qquad\qquad\qquad\qquad\qquad j = 1,2, \\ &\frac{\partial u_i}{\partial x}(b_j(t),t)\frac{db_j}{dt} + \frac{\partial u_i}{\partial t}(b_j(t),t) = 0 \qquad . \end{aligned}$$

We then apply the static slope approximation [25]

$$\frac{\partial u_e}{\partial x}(a_j(t),t) \approx (-1)^{j+1}p_1, \qquad \frac{\partial u_i}{\partial x}(b_j(t),t) \approx (-1)^{j+1}p_2.$$

By making use of (4) we aim at deriving expressions for $\partial u_e/\partial t(a_j(t),t)$ and $\partial u_i/\partial t(b_j(t),t)$ and thus, obtain the dynamical system for a_j, b_j. This can be easily done when the temporal kernels are given as (3), since the Volterra system (4) in that case can be converted to a system of rate equations by means of the LCT [29].

The case $k_e = k_i = 0$ which corresponds to exponentially decaying functions, has been analyzed in [25]. In that paper, however, only symmetric perturbations were considered within the framework of the Amari approach, i.e. $a_2 = -a_1$, $b_2 = -b_1$. It was shown that eigenvalues obtained by the Amari approach form a proper subset of an eigenvalue set obtained by the Evans function technique. In [63], the comparison of the Amari approach and the Evans function technique has been carried out for the one-population model with spike frequency adaptation [32,64] when the memory functions are assumed to be exponentially decaying. We show here that the generalized Amari approach coincides with the Evans function technique for the two-population model when there are no symmetry restrictions imposed on the perturbations and for the set of temporal kernels given by (3).

We make use of (28) and (7) and derive the dynamical system for the state vector

$$\bar{Z} = (a_1, z_1^{(1)}, \ldots, z_1^{(k_e)}, b_1, \mathrm{w}_1^{(1)}, \ldots, \mathrm{w}_1^{(k_i)}, a_2, z_2^{(1)}, \ldots, z_2^{(k_e)}, b_2, \mathrm{w}_2^{(1)}, \ldots, \mathrm{w}_2^{(k_i)})^T$$

where

$$\begin{aligned} &z_j^{(p)}(t) = v_e^{(p)}(a_j(t),t), \quad p = 1,\ldots,k_e, \\ &\mathrm{w}_j^{(q)}(t) = v_i^{(q)}(b_j(t),t), \quad q = 1,\ldots,k_i, \end{aligned} \tag{29}$$

for $j = 1, 2$, are auxiliary variables. For the auxiliary variables in (7) we also apply the static slope approximation, i.e.,

$$\frac{\partial v_e^{(p)}}{\partial x}(a_j(t),t) = (-1)^{j+1}p_1, \qquad \frac{\partial v_i^{(q)}}{\partial x}(b_j(t),t) = (-1)^{j+1}p_2,$$

where p and q are given as in (29).

Then we get a $2(k_e + k_i + 1)$-dimensional autonomous dynamical system which reads

$$\begin{aligned} &(-1)^{j+1}p_1\frac{da_j}{dt} = z_j^{(1)} - \theta_e \\ &\frac{dz_j^{(p)}}{dt} = \theta_e - z_j^{(1)} - z_j^{(p)} + z_j^{(p+1)}, \quad p = 1,\ldots,k_e - 1 \\ &\frac{dz_j^{(k_e)}}{dt} = \theta_e - z_j^{(1)} - z_j^{(k_e)} + f_e^{(j)}(a_1,a_2,b_1,b_2) \\ &(-1)^{j+1}p_2\tau\frac{db_j}{dt} = \mathrm{w}_j^{(1)} - \theta_e \\ &\tau\frac{d\mathrm{w}_j^{(q)}}{dt} = \theta_e - \mathrm{w}_j^{(1)} - \mathrm{w}_j^{(q)} + \mathrm{w}_j^{(q+1)}, \quad q = 1,\ldots,k_i - 1 \\ &\tau\frac{d\mathrm{w}_j^{(k_i)}}{dt} = \theta_e - \mathrm{w}_j^{(1)} - \mathrm{w}_j^{(k_i)} + f_i^{(j)}(a_1,a_2,b_1,b_2), \end{aligned} \tag{30}$$

where $j = 1, 2$, and the components $f_e^{(j)}$ and $f_i^{(j)}$ are defined as

$$f_e^{(j)} = (W_{ee}(a_2 - a_j) - W_{ee}(a_1 - a_j)) - (W_{ie}(b_2 - a_j) - W_{ie}(b_1 - a_j)),$$
$$f_i^{(j)} = (W_{ei}(a_2 - b_j) - W_{ei}(a_1 - b_j)) - (W_{ii}(b_2 - b_j) - W_{ii}(b_1 - b_j)).$$

The equilibrium of this system corresponding to the symmetric bump is given by

$$\bar{Z}_0 = (-a_0, \theta_e, \ldots, \theta_e, -b_0, \theta_i, \ldots, a_0, \theta_e, \ldots, \theta_e, b_0, \theta_i, \ldots, \theta_i)^T. \tag{31}$$

Now we analyze the linear stability of this equilibrium. We construct the Jacobian matrix $\mathbf{J}_A$ of the RHS of the system (30) evaluated at the equilibrium (31) and consider the matrix $\mathbf{J}_A - \lambda\mathbf{E}$. We get the following fundamental theorem which shows that the Evans function approach is equivalent to the generalized Amari approach.

Theorem 1. *Let the temporal kernels α_{mn} be given by the quasi-power function (3). Then*

$$\begin{aligned}\det(\mathbf{J}_A - \lambda\mathbf{E}) &= \tau^{-2(k_i+1)}\mathcal{P}_S(\lambda)\lambda\mathcal{P}_{\mathrm{As}}(\lambda)\\ &= (1+\lambda)^{-2(k_e+1)}(1/\tau+\lambda)^{-2(k_i+1)}\mathcal{E}_S(\lambda)\mathcal{E}_{\mathrm{As}}(\lambda).\end{aligned}$$

Therefore, eigenvalues obtained using the generalized Amari approach and the eigenvalues obtained by means of the Evans function technique are the same.

The proof of this equivalence theorem is given in Appendix B. Notice that although we have considered the general form of the dynamical system (30) for $k_e \geq 1$ and $k_i \geq 1$, it is easy to check that the same argument can be extended to the case when $k_e = 0$ and/or $k_i = 0$. We do not give a separate proof for this case.

6. Example: α-function for the excitatory target population and exponential decaying function for the inhibitory target population ($k_e = 1$ and $k_i = 0$)

In this section, we consider one particular example when $k_e = 1$ and $k_i = 0$, i.e.,

$$\alpha_{ee}(t) = \alpha_{ie}(t) = t\mathrm{e}^{-t}, \qquad \alpha_{ei}(t) = \alpha_{ii}(t) = \frac{1}{\tau}\mathrm{e}^{-\frac{t}{\tau}}.$$

In mathematical neuroscience, the temporal kernel obtained by letting $k_e = 1$ is referred to as an α-function. This means that the temporal kernel in the excitatory equation is modeled by means of an α-function, while the temporal kernel of the inhibitory equation assumes the form of an exponentially decaying function.

In this case, the rate-equation system in (7) is given as

$$\begin{aligned}&\partial_t u_e = -u_e + v_e^{(1)}\\ &\partial_t v_e^{(1)} = -v_e^{(1)} + \omega_{ee} \otimes P_e(u_e - \theta_e) - \omega_{ie} \otimes P_i(u_i - \theta_i)\\ &\tau\partial_t u_i = -u_i + \omega_{ei} \otimes P_e(u_e - \theta_e) - \omega_{ii} \otimes P_i(u_i - \theta_i).\end{aligned} \tag{32}$$

We study the stability of bumps (12) within the framework of this model. The bumps are represented by the stationary state $\bar{X} = (U_e, U_e, U_i)$. From (30) we find that the generalized Amari system for this case reads

$$\begin{aligned}&-p_1\frac{\mathrm{d}a_1}{\mathrm{d}t} = z_1^{(1)} - \theta_e\\ &\frac{\mathrm{d}z_1^{(1)}}{\mathrm{d}t} = \theta_e - 2z_e + f_e^{(1)}(a_1, a_2, b_1, b_2)\\ &-\tau p_2\frac{\mathrm{d}b}{\mathrm{d}t} = f_i^{(1)}(a_1, a_2, b_1, b_2) - \theta_i\\ &p_1\frac{\mathrm{d}a_2}{\mathrm{d}t} = z_2^{(1)} - \theta_e\\ &\frac{\mathrm{d}z_2^{(1)}}{\mathrm{d}t} = \theta_e - 2z_2^{(1)} + f_e^{(1)}(a_1, a_2, b_1, b_2)\\ &\tau p_2\frac{\mathrm{d}b}{\mathrm{d}t} = f_i^{(2)}(a_1, a_2, b_1, b_2) - \theta_i.\end{aligned} \tag{33}$$

Within this formalism the bumps correspond to $\bar{Z}_0 = (-a_0, \theta_e, -b_0, a_0, \theta_e, b_0)^T$.

6.1. Stability of bumps in the framework of (32)

In this section, we assume that the connectivity functions $\omega_{mn}(x)$ are decreasing for positive arguments. This assumption allows us to find the sign of parameters appearing in the Evans function.

We analyze separately the 'symmetric' and the 'antisymmetric' part, i.e., $\mathcal{P}_S(\lambda)$ and $\mathcal{P}_{As}(\lambda)$ given by (25) and (26). For the 'symmetric' part, we have

$$\mathcal{P}_S(\lambda) = \tau(\lambda^3 + c_1\lambda^2 + c_2\lambda + c_3)$$

with the coefficients

$$c_1 = 2 + |d_4|/\tau,$$
$$c_2 = 2|d_4|/\tau - |d_1|,$$
$$c_3 = \gamma_S/\tau$$

where γ_S is given by (24). According to the Routh–Hurwitz criterion, all the eigenvalues are located in the left half plane if and only if the determinants of the matrix

$$\mathbf{D} = (c_1), \qquad \mathbf{D}_2 = \begin{pmatrix} c_1 & c_3 \\ 1 & c_2 \end{pmatrix}, \qquad \mathbf{D}_3 = \begin{pmatrix} c_1 & c_3 & c_5 \\ 1 & c_2 & 0 \\ 0 & c_1 & c_3 \end{pmatrix},$$

are positive. See [58]. We calculate the determinants and get

$$\det(\mathbf{D}_1) = c_1,$$
$$\det(\mathbf{D}_2) = c_1c_2 - c_3,$$
$$\det(\mathbf{D}_3) = c_3\det(\mathbf{D}_2).$$

If $c_3 < 0 (\gamma_S < 0)$ we have either $\det(\mathbf{D}_2)$ or $\det(\mathbf{D}_3)$ negative. Thus, in this case the bumps are unstable, as expected. Assume now $c_3 > 0 (\gamma_S > 0)$. According to the general theory it is possible to have a bifurcation when

$$\det(\mathbf{D}_2) = (-2|d_1|\tau^2 + (4|d_4| - |d_2||d_3|)\tau + 2|d_4|^2)/\tau^2 = 0. \tag{34}$$

See Appendix in [58] for details. The roots of (34) are given as

$$\tau_\pm = \frac{4|d_4| - |d_2d_3|}{4|d_1|} \pm \sqrt{\left(\frac{4|d_4| - |d_2d_3|}{4|d_1|}\right)^2 + \frac{|d_4|^2}{|d1|}}.$$

One of the roots, τ_-, is always negative while the other one, τ_+, is positive. Moreover, $\det(\mathbf{D}_2)$ changes sign at $\tau = \tau_+$ from positive to negative which indicates the presence of a Hopf bifurcation. We fix the notation and define $\tau_S = \tau_+$.

Thus, from the 'symmetric' part we get two regimes: In the first regime, when $\gamma_S > 0$, the bumps are stable for $\tau < \tau_S$, unstable for $\tau > \tau_S$, and convert to breathers through the Hopf bifurcation when $\tau = \tau_S$. In the complementary regime, $\gamma_S < 0$, the bumps are unstable.

For the 'antisymmetric' part, we have

$$\mathcal{P}_{As}(\lambda) = \tau\lambda^2 + \lambda\left(\frac{E - F}{p_2} + 2\tau\right) + \gamma_{As}$$

where

$$\gamma_{As} = 2\frac{E - F}{p_2} - \frac{C - D}{p_1}\tau.$$

Notice that $E > F$ (as well as $C > D$) in accordance with the monotonicity requirement imposed on ω_{mn} for positive arguments. Therefore, if $\gamma_{As} > 0$ the bumps are stable, while for $\gamma_{As} < 0$ unstable. The case $\gamma_{As} = 0$ gives a value for the critical time τ_{As}, i.e.,

$$\tau_{As} = 2\frac{p_1}{p_2}\frac{E - F}{C - D}.$$

We can rephrase the conclusion in terms of τ, i.e., for all $\tau < \tau_{As}$ the bumps are stable, while for $\tau > \tau_{As}$ we have instability.

To determine the sign of γ_S and the relationship between τ_S and τ_{As} we need to have more information about the connectivity functions and some parameters. However, the case $\gamma_S < 0$ and $\tau < \tau_{As}$ corresponds to a saddle point. For the case with Gaussian connectivity functions (16)–(18) we have that $\gamma_S \approx -58.867 < 0$ for the narrow bump and $\gamma_S \approx 1.969 > 0$ for the broad bump. In the latter case we find that $\tau_S < \tau_{As}$, where $\tau_S \approx 5.705$ and $\tau_{As} \approx 8.728$. Therefore, it follows that

the broad bump pair is stable for $\tau < \tau_S$, unstable for $\tau > \tau_S$, and is converted to a breather through a Hopf bifurcation at $\tau = \tau_S$.

6.2. Numerics

We have run simulations of the system (32) based on the fourth-order Runge–Kutta algorithm developed in [25]. The initial condition is given as a perturbed bump pair. In this subsection, we assume that the unperturbed bumps are given by (12), (16)–(18); see Fig. 1. We perturb the bump solution by making the assumption

$$\begin{aligned} \tilde{U}_e(x) &= W_{ee}(a_2 - x) - W_{ee}(a_1 - x) - W_{ie}(b_2 - x) + W_{ie}(b_1 - x), \\ \tilde{U}_i(x) &= W_{ei}(a_2 - x) - W_{ei}(a_1 - x) - W_{ii}(b_2 - x) + W_{ii}(b_1 - x), \end{aligned} \tag{35}$$

where $\bar{a} = (a_1, a_2, b_1, b_2)^T$ is time dependent and chosen to be close to initial pulses crossing coordinates $\bar{a}_0 = (-a_0, a_0, -b_0, b_0)^T$ such that

$$\|\bar{a} - \bar{a}_0\| \le \epsilon, \tag{36}$$

for some positive tolerance ϵ, where $\|\cdot\|$ denotes the maximum norm in $\mathbb{R}^4$. Under the assumption (36) we get the error estimate

$$\|\tilde{U}_m - U_m\|_{C_b(\mathbb{R})} \le C_m \varepsilon, \qquad C_m = \max_{x\in\mathbb{R}}\{|\omega_{em}(x)|, |\omega_{im}(x)|\}, \quad m = e, i.$$

First, we impose the symmetric perturbation

$$\bar{a} = \bar{a}_0 + (-\varepsilon, \varepsilon, -\varepsilon, \varepsilon)^T \tag{37}$$

in the initial pulse width coordinates of (35).

In Fig. 2, we have plotted the evolution of the perturbed broad bump state $(\tilde{U}_e, \tilde{U}_i)$ when $\bar{a}$ is given by (37) with $\varepsilon = 0.01$. From the simulations we observe that $(\tilde{U}_e(x), \tilde{U}_i(x))$ is converted to breathers for a small range of the value τ, $\tau \in [5.6, 5.8]$, (whereas the stability analysis predicts that this conversion shall take place at $\tau = 5.705$). In Fig. 2(b), we have plotted the solution $(u_e(x, t), u_i(x, t))$ for the value $\tau = 5.6$, when the breather the first time appears. Below this critical value, $\tau < 5.6$ the state $(\tilde{U}_e(x), \tilde{U}_i(x))$ approaches the bumps and remain unchanged. We show this in Fig. 2(a) for $\tau = 3$. For $\tau > 5.8$ the pulse collapses. We illustrate this behavior of the solution in Fig. 2(c) for $\tau = 6$. Thus, we get excellent agreement between the predictions obtained from the stability analysis and the numerical simulations. It turns out that the sign of ε does not change the picture qualitatively for the broad bump case. Therefore, we do not present results for negative values of ε. Next, we consider the symmetric perturbation (35) with (37) on the narrow bumps. In this case, the sign of ε plays an important role in the evolution of $(\tilde{U}_e, \tilde{U}_i)$ as is evident from Figs. 3 and 4: for $\varepsilon > 0$ the narrow bumps initially approach the broad ones, and thereafter evolve into a broad stable bumps for the given τ, while for $\varepsilon < 0$, the narrow pulses collapse. We conjecture that this behavior is consistent with the fact that narrow bumps are identified as saddle points; cf. Section 6.1.

We have also solved the ODE system (33) numerically in order to predict the evolution of bumps and compared it with simulations for rate-equation system (32). The conclusion is, however, that the two approaches give qualitatively the same results, but exhibit significant quantitative differences. We conjecture that this discrepancy is due to the static slope assumption imposed in order to derive the finite dimensional generalized Amari system (33). In Fig. 5, we show the limit cycle in the pulse width coordinate plane obtained from simulations of (32) (Fig. 5(a)) and from simulations of (33) (Fig. 5(b)). Notice that there is a small discrepancy between the value for τ_S obtained by these two methods. This discrepancy is caused by numerical error which is larger for the simulation of the rate-equation system due to the incorporation of the spatial dynamics. The observation of the limit circle supports the idea that we get stable breathers at the critical inhibition time $\tau = \tau_S$, which corresponds to a supercritical Hopf bifurcation in the generalized Amari system (33). In order to study this problem one has to make a normal form expansion of the system (33) in the vicinity of the critical inhibition time $\tau = \tau_S$. We do not pursue any analysis of this problem here, however.

We then investigate the evolution of (35) when imposing an antisymmetric perturbation represented by

$$\bar{a} = \bar{a}_0 + (-\varepsilon, 0, 0, \varepsilon)^T. \tag{38}$$

Tracing the mean values

$$\xi_a(t) = (a_2(t) + a_1(t))/2, \qquad \xi_b(t) = (b_2(t) + b_1(t))/2,$$

we observe that for $\tau < \tau_S$, $(\tilde{U}_e, \tilde{U}_i)$ approaches a broad bump pair which is simply a rigid translation of the unperturbed symmetric broad bumps. In another words, after some finite time T we get $u_e(x, t) = U_e(x - x_0)$, $u_i(x, t) = U_i(x - x_0)$, for all $t > T$, i.e., the solution $(u_e(x, t), u_i(x, t))$ becomes symmetric with respect to the symmetric axis $Ox : x = x_0$. This axis can be found as the asymptotical mean values, i.e.,

$$Ox : x = x_0, \quad x_0 = \xi_a(t \to \infty) = \xi_b(t \to \infty). \tag{39}$$

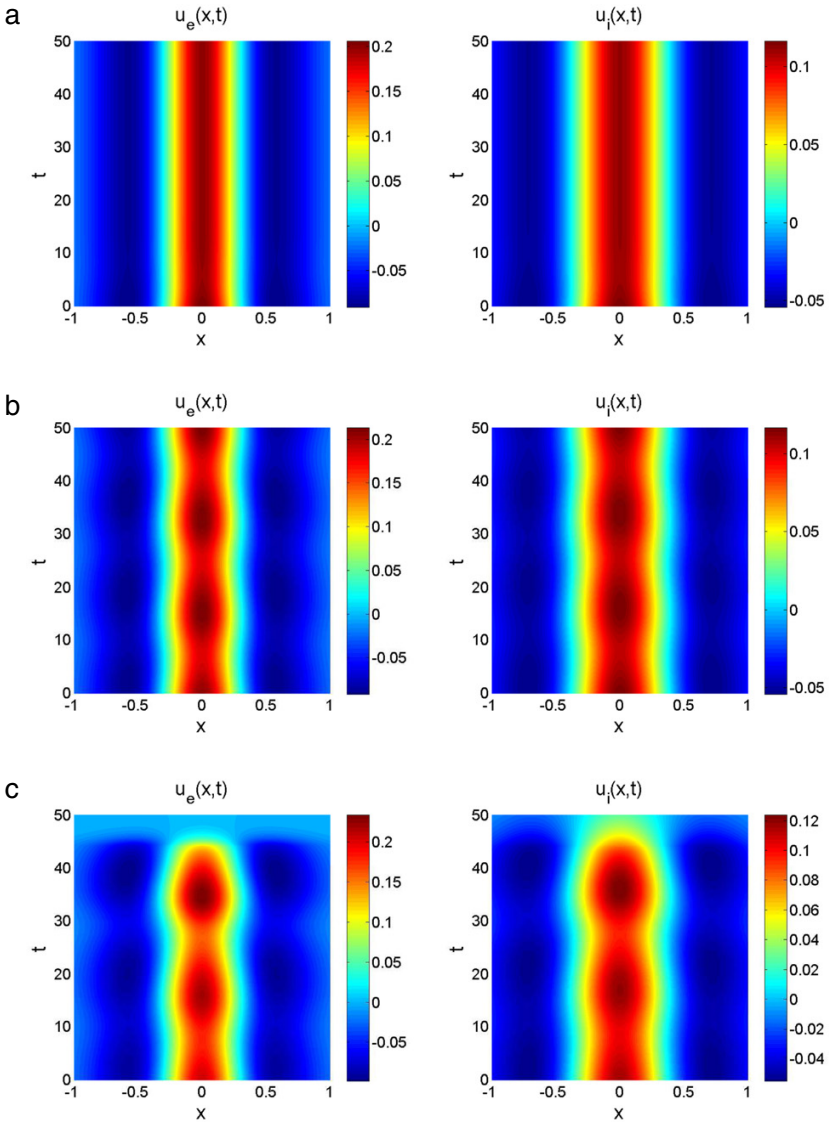

Fig. 2. The evolution of the symmetric perturbation of the broad bump pair (U_e, U_i) (Fig. 1(a)). The perturbed pulses are given by (35) with (37), $\varepsilon = 0.01$. (a) Broad excitatory (left) and inhibitory (right) pulses reach the stable symmetric bumps (U_e, U_i) when $\tau = 3$. (b) Broad excitatory (left) and inhibitory (right) pulses convert to breathers when $\tau = 5.6$. (c) Broad excitatory (left) and inhibitory (right) pulses collapse when $\tau = 6$.

We display this result in Fig. 6(a). We get the similar result for the case when the initial condition of (32) is given as the perturbation of the narrow bumps when $\varepsilon > 0$; see Fig. 7(a). The solution approaches a broad bumps pair which is symmetric with respect to some symmetry axes Ox. For $\tau \approx \tau_S$ we also see that $(u_e(x, t), u_i(x, t))$ (for the broad bump perturbation and for the narrow bump perturbation with $\varepsilon > 0$ as an initial condition of (32)) become symmetric with respect to the axis Ox given as in (39). We illustrate these results in Figs. 6(b), 7(b). For the case $\varepsilon < 0$ the narrow pulses collapse in a similar way as displayed in Fig. 4 independently of the chosen parameter $\tau > 0$.

This behavior in the case of antisymmetric perturbations is expected since for $\tau < \tau_{\mathrm{As}}$ the only impact from the 'antisymmetric' part is the translation invariance of the bumps. For the cases $\tau > \tau_S$, $(\tilde{U}_e, \tilde{U}_i)$, and in the case of the narrow bump perturbation with negative ε the pulses collapse before ξ_a and ξ_b approach the same value. The evolution is very much similar to the symmetric case and we do not display it here. Thus, after a transient phase the evolution in the antisymmetric case is qualitatively the same as in the symmetric case, with the only exception that the symmetry axis is different.

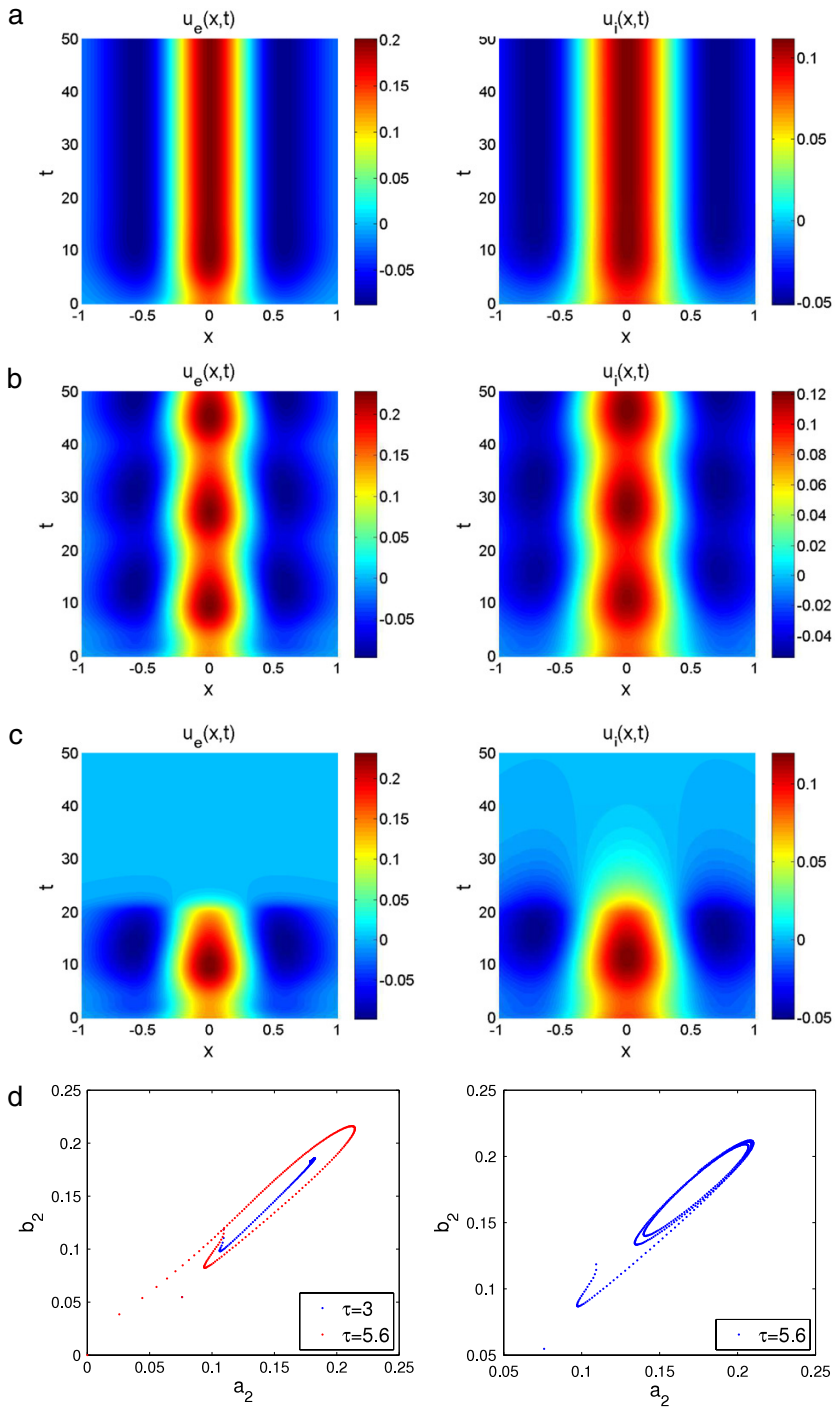

Fig. 3. The evolution of the symmetric perturbation of the narrow bump pair (U_e, U_i) (Fig. 1(b)). The perturbed pulses are given by (35) with (37), $\varepsilon = 0.01$. (a) Narrow excitatory (left) and inhibitory (right) unstable pulses convert to broad bump (Fig. 1(a)) when $\tau = 3$. (b) Narrow excitatory (left) and inhibitory (right) pulses convert to breathers when $\tau = 5.6$. (c) Narrow excitatory (left) and inhibitory (right) pulses collapse when $\tau = 6$. (d) The trajectory in the pulse width plane (a_2, b_2) for $\tau = 3$, $\tau = 6$ (left) and $\tau = 5.6$ (right).

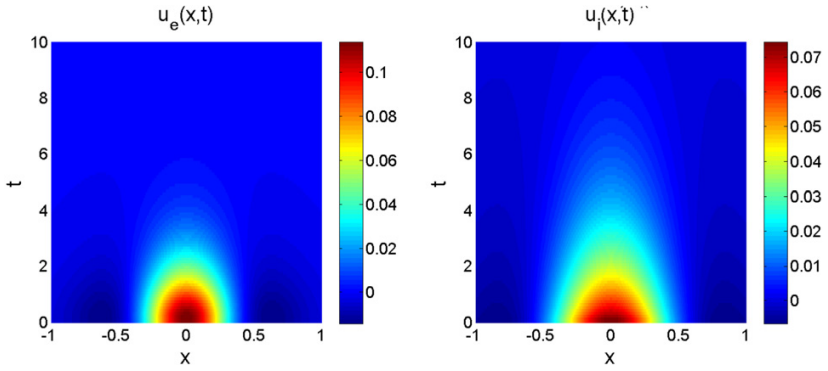

Fig. 4. The evolution of the symmetric perturbation of the narrow bump pair (U_e, U_i) (Fig. 1(b)). The perturbed pulses are given by (35) with (37), $\varepsilon = -0.01$. Narrow excitatory (left) and inhibitory (right) unstable pulses collapse for $\tau = 3$.

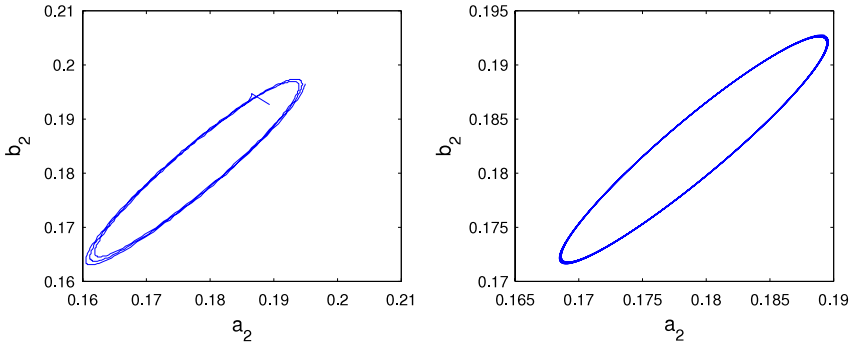

Fig. 5. The orbit in the pulse width plane (a_2, b_2) obtained (a) from the simulation of the rate-equation system (32) for $\tau = 5.6$, $T = 50$, and (b) from the Amari system (33) with $\tau = 5.69$, for $T = 300$. The initial conditions correspond to the symmetric perturbation of the broad bump, i.e., for (a) the condition is given as for Fig. 2, (35) with (37), $\bar{a}_0$ corresponds to the broad bump widths, $\varepsilon = 0.01$, and for (b) by (37) where $\bar{a}_0$ corresponds to the broad bump widths.

7. Conclusions

In the present paper, we have worked out a method for stability analysis for spatially symmetric bumps in a wide class of two-population neural-field models. The models are given by means of a Volterra system of equations. Our findings can be summarized as follows.

We derive the so-called Evans matrix for the problem and prove that it can be block-diagonalized into two blocks, with the upper block corresponding to spatially symmetric perturbations while the lower block takes care of the antisymmetric perturbations. The corresponding Evans function can be written as a product of determinants of the upper and lower blocks. The lower antisymmetric block contains as expected the translation invariance property of bumps. We emphasize that this is a general result and does not rely on any particular choice of the temporal kernels.

For the class of kernels which we call quasi-power functions (which contains both the exponentially decaying temporal kernels and the α-functions as special cases) it turns out that the Evans function approach is equivalent to the generalized Amari approach. One can check that the stability matrix obtained in [25] by the full linear stability analysis of the rate-equation system corresponds to the Evans matrix (see Section 4) with α_{mn} given as in (1) for $k_e = k_i = 0$. Then, it follows that the Jacobian of the Amari system only corresponds to the upper block of the Evans matrix, but not to the whole matrix as we prove here. This apparent paradox can be easily explained by the symmetry in the perturbation assumed for the Amari approach in [25]. As we relax on this assumption we get the antisymmetric part of the perturbations corresponding to the lower block of the Evans matrix; See Section 5.

The Evans function approach is more general and does not imply that the rate-equation formulation of (1) as the generalized Amari approach. However, the Evans function technique exclusively addresses the linear stability of bumps,

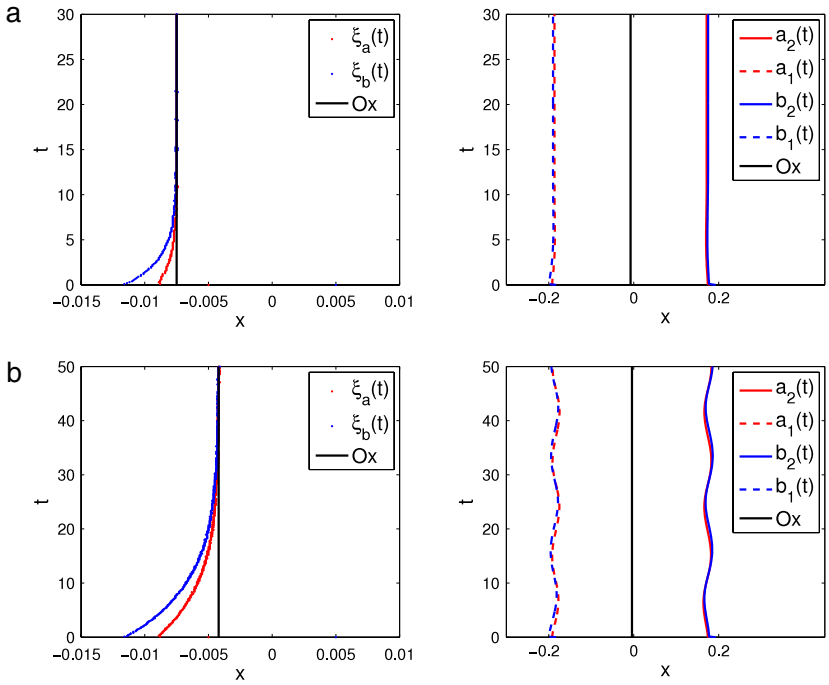

Fig. 6. The evolution of the antisymmetric perturbation of the broad bump pair (U_e, U_i) (Fig. 1(a)). The perturbed pulses are given by (35) with (38), $\varepsilon = 0.01$. On the left, we have plotted $\xi_a(t)$, $\xi_b(t)$, and the asymptotical symmetry axes Ox. On the right, the crossing coordinates $a_1(t)$, $a_2(t)$, $b_1(t)$, $b_2(t)$ are shown. (a) $\tau = 3$, $Ox : x = -0.0075$, (b) $\tau = 5.4$, $Ox : x = -0.0041$.

while the Amari system may be used to investigate nonlinear effects such as the stability of the breathers excited at the Hopf-bifurcation point by means of normal form expansions [25].

For the actual class of temporal kernels we can convert the two-population Volterra system into a system of rate equations. We prove that the solutions of the initial value problem of this system are uniformly bounded. The implication of this result is that any instability detected in the system will be saturated. We also prove that the narrow bump pair which is unstable within the framework of the Wilson–Cowan type of model (2) is unstable for all types of quasi-power temporal kernels.

Finally, we have illuminated these results by carrying out numerical simulations based on a fourth-order Runge–Kutta numerical scheme in time for the special mixed case modeled by α-functions and exponentially decaying functions; see Section 6. Excellent agreement between analytical predictions from the stability analysis and numerical simulations is obtained. We get an unstable narrow bump pair and a broad bump pair which is stable for small and moderate values of the relative inhibition time τ, is converted to a stable breather at a critical time τ_{cr} (which is identified as a Hopf-bifurcation point), and becomes unstable as this time scale exceeds τ_{cr}.

Notice that rate-equation representation of (1) allows us to develop a relatively simple numerical scheme in a vicinity of a spatially localized solution, [25]. This representation is also possible for more general class temporal kernels than the quasi-power kernels (1), e.g., quasi-polynomials [29].

A possible extension of the present work is to consider bump solutions and their stability for a system of Volterra equation (4) defined on two spatial dimensions. We conjecture that one can construct bump and ring solutions of this system and analyze their stability properties by means of the Evans function technique in a way similar to what has been done in Owen et al. [40]. Another possible extension consists of investigating more complex patterns by applying a level set description (interface dynamics) in two spatial dimensions. In this context one can make use of the rate-equation system (7) which is valid for any spatial dimensions. Here we suggest that one follows the ideas worked out by Goldstein et al. [65] for reaction–diffusion equations.

We are still at early times in computational neuroscience and at present it is unclear (i) under what situations neural-field models of the type discussed here are accurate representation of real neural dynamics and, more specifically, (ii) what choice of temporal kernels best mimics the dynamics of biological neural networks. The present work opens up for thorough the analysis of the bump dynamics for a large class of a priori biologically plausible neural-network models, not restricted to exponentially decaying temporal kernels only.

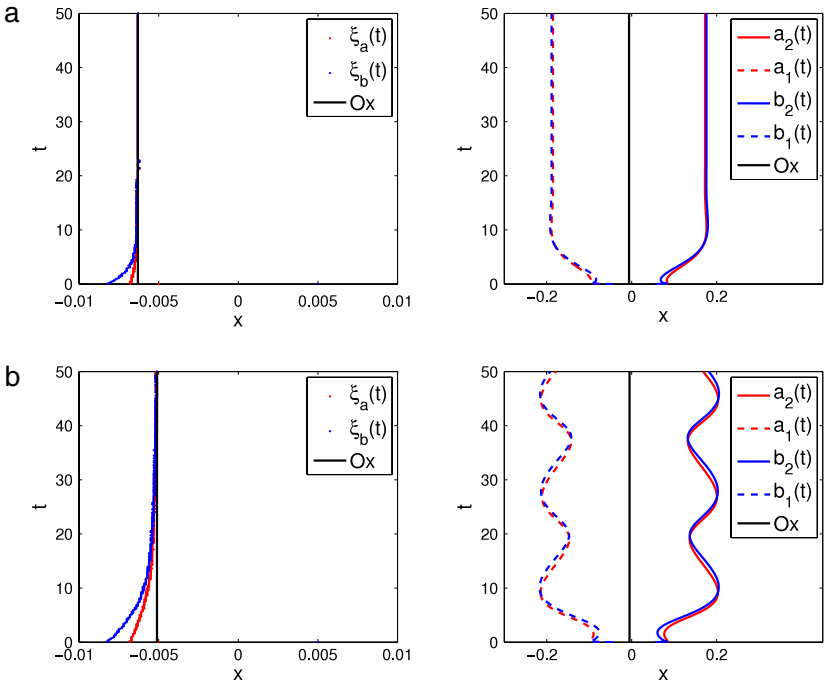

Fig. 7. The evolution of the antisymmetric perturbation of the narrow bump pair (U_e, U_i). The perturbed pulses are given by (35) with (38), $\varepsilon = 0.01$. On the left, we have plotted $\xi_a(t)$, $\xi_b(t)$, and the asymptotical symmetry axes Ox. On the right, the crossing coordinates $a_1(t)$, $a_2(t)$, $b_1(t)$, $b_2(t)$ are shown. (a) $\tau = 3$, $Ox : x = -0.0063$, (b) $\tau = 5.6$, $Ox : x = -0.0051$.

Acknowledgments

The authors would like to thank Professor Arkadi Ponossov (Norwegian University of Life Sciences), Professor Stephen Coombes (School of Mathematical Sciences, University of Nottingham, United Kingdom), and Professor Vadim Kostrykin (Johannes Gutenberg University, Mainz, Germany) for many fruitful and stimulating discussions during the preparation of this paper. John Wyller and Anna Oleynik also wish to thank the School of Mathematical Sciences, University of Nottingham for the kind hospitality during the stay. This research was supported by the Norwegian University of Life Sciences. The work has also been supported by The Research Council of Norway under grant no. 178892 (eNEURO-multilevel modeling and simulation of the nervous system) and grant no. 178901 (Bridging the gap: disclosure, understanding and exploitation of the genotype–phenotype map).

Appendix A. The boundedness property of the solutions of the Wilson–Cowan type of system

Here we derive the estimate for the solution of (9). This derivation is based on the Jordan block form (8) of the linear operator matrix $\mathbf{L}$. Indeed, the operator $R(t) = \mathrm{e}^{tL}$ is given by the block matrix

$$\mathbf{R}(t) = \begin{pmatrix} \mathrm{e}^{(t\mathbf{J}_e)} & \mathbf{O}_e \\ \mathbf{O}_i & \mathrm{e}^{(\frac{t}{\tau}\mathbf{J}_i)} \end{pmatrix}.$$

Exploiting the form of $\mathbf{J}_m$ we get the upper triangular matrix

$$\exp(s\mathbf{J}_m) = \mathrm{e}^{-s} \begin{pmatrix} 1 & s & \frac{s^2}{2!} & \cdots & \frac{s^{k_m}}{k_m!} \\ 0 & 1 & s & \cdots & \frac{s^{k_m-1}}{(k_m-1)!} \\ \vdots & & \ddots & \ddots & \vdots \\ 0 & 0 & & 1 & s \\ 0 & 0 & \cdots & 0 & 1 \end{pmatrix}, \quad m = e, i$$

with $s = t$ or $s = t/\tau$, for $m = e$ and $m = i$, respectively. Let $\bar{1} = (1, 1, \ldots, 1)^T$. We make two main observations:

(i) $\mathrm{e}^{(s\mathbf{J}_m)}\bar{1} < \bar{1}$, and
(ii) $\int_0^t \mathrm{e}^{(s\mathbf{J}_m)}\bar{1}\mathrm{d}s \le \int_0^\infty \mathrm{e}^{(s\mathbf{J}_m)}\bar{1}\mathrm{d}s = (k_m, k_m - 1, \ldots, 1)^T$.

Using (i) one readily obtains

$$|R\bar{V}| \le \|\bar{V}\|_\infty \bar{1}$$

for an arbitrary $\bar{V} \in (C_b(R))^N$, $N = k_e + k_i + 2$ with the norm $\|\cdot\|_\infty$ defined as (11).

From (ii) we find

$$\int_0^t |R(t-s)\bar{1}|\mathrm{d}t \le (k_e, k_e - 1, \ldots, 1, \tau k_i, \tau(k_i - 1), \ldots, \tau)^T.$$

From the properties of P_m and w_{mn} we notice that $|F\bar{U}| \le \bar{1}$. Then it follows

$$|\bar{U}(x,t)| \le |R\bar{U}^0| + \int_0^t |R(t-s)\bar{1}|\mathrm{d}t \le (\|\bar{U}^0\|_\infty + \max\{k_e, k_i\tau\})\bar{1}.$$

Hence we end up with the estimate

$$|U_i(x,t)| \le \|\bar{U}^0\|_\infty + \max\{k_e, k_i\tau\}.$$

Appendix B. The equivalence between the Evans function approach and the Amari approach

Here we give a detailed proof of the equivalence Theorem 1. The proof is carried out in several steps, which we conveniently divide into the two Appendices B.1 and B.2.

B.1. Similarity operations on the matrix $\mathbf{J}_A - \lambda\mathbf{E}$

The first step consists of performing similarity operations on the matrix $\mathbf{J}_A - \lambda\mathbf{E}$. We proceed as follows: let $\mathbf{E}$ denote the $(k_e + k_i + 2) \times (k_e + k_i + 2)$ identity matrix and $\mathbf{J}_A$ the Jacobian matrix of the RHS of the generalized Amari system (30) evaluated at the equilibrium (31). The matrix $\mathbf{J}_A - \lambda\mathbf{E}$ can be expressed as

$$\mathbf{J}_A - \lambda\mathbf{E} = \begin{pmatrix} \mathbf{A}^{(1)} & \mathbf{B}^{(1)} \\ \mathbf{B}^{(2)} & \mathbf{A}^{(2)} \end{pmatrix}$$

where the blocks $\mathbf{A}^{(j)}, j = 1, 2$, can be represented as

$$\mathbf{A}^{(j)} = \begin{pmatrix} \mathbf{A}_{11}^{(j)} & \mathbf{A}_{12}^{(j)} \\ \mathbf{A}_{21}^{(j)} & \mathbf{A}_{22}^{(j)} \end{pmatrix}, \tag{B.1}$$

with

$$\mathbf{A}_{11}^{(j)} = \begin{pmatrix} -\lambda & (-1)^j/p_1 & 0 & 0 & \cdots & 0 \\ 0 & -(2+\lambda) & 1 & 0 & \cdots & 0 \\ 0 & -1 & -(1+\lambda) & 1 & & 0 \\ \vdots & \vdots & & \ddots & \ddots & \\ 0 & -1 & & & -(1+\lambda) & 1 \\ \partial f_e^{(j)}/\partial a_j & -1 & & & & -(1+\lambda) \end{pmatrix},$$

$$\mathbf{A}_{22}^{(j)} = \begin{pmatrix} -\lambda & (-1)^j/(p_2\tau) & 0 & 0 & \cdots & 0 \\ 0 & -(2/\tau+\lambda) & 1/\tau & 0 & \cdots & 0 \\ 0 & -1/\tau & -(1/\tau+\lambda) & 1/\tau & & \\ \vdots & \vdots & & \ddots & \ddots & \\ 0 & -1/\tau & & & -(1/\tau+\lambda) & 1/\tau \\ \partial f_e^{(j)}/\partial b_j/\tau & -1/\tau & & & & -(1/\tau+\lambda) \end{pmatrix}.$$

The matrix $\mathbf{A}_{12}^{(j)}$ is a $(k_e+1)\times(k_i+1)$ sparse matrix, while the matrix $\mathbf{A}_{21}^{(j)}$ is a sparse $(k_i+1)\times(k_e+1)$ matrix which have only one non-zero element $\partial f_e^{(j)}/\partial b_j$ and $\partial f_i^{(j)}/\partial a_j$ evaluated at $(-a_0, -b_0, a_0, b_0)$, respectively, located in the right-low corner of the block. For notational convenience, we now assume that the partial derivatives of $f_m^{(j)}, j = 1, 2, m = e, i$, is evaluated at $(a_1, b_1, a_2, b_2) = (-a_0, -b_0, a_0, b_0,)$.

The matrix $\mathbf{B}^{(j)}$, $j = 1, 2$, is a sparse matrix of the form

$$\begin{array}{c} \\ m+1 \\ \\ n+1 \end{array} \overbrace{\phantom{\begin{pmatrix} a & b \\ c & d \end{pmatrix}}}^{m+1} \overbrace{\phantom{\begin{pmatrix} a & b \\ c & d \end{pmatrix}}}^{n+1} \left\{ \begin{array}{c} \\ \\ \\ \\ \end{array} \right. \left(\begin{array}{c|c} \beta_{11}^{(j)} & \beta_{12}^{(j)} \\ \hline \beta_{21}^{(j)} & \beta_{22}^{(j)} \end{array} \right) \tag{B.2}$$

where

$$\beta_{11}^{(1)} = \partial f_e^{(1)}/\partial a_2,\ \beta_{12}^{(1)} = \partial f_e^{(1)}/\partial b_2 \qquad \beta_{21}^{(1)} = \partial f_i^{(1)}/\partial a_2,\ \beta_{22}^{(1)} = \partial f_i^{(1)}/\partial b_2,$$
$$\beta_{11}^{(2)} = \partial f_e^{(2)}/\partial a_1,\ \beta_{12}^{(2)} = \partial f_e^{(2)}/\partial b_1 \qquad \beta_{21}^{(2)} = \partial f_i^{(1)}/\partial a_1,\ \beta_{22}^{(2)} = \partial f_i^{(2)}/\partial b_1.$$

Simple calculations yield

$$\frac{\partial f_e^{(1)}}{\partial a_1} = -\frac{\partial f_e^{(2)}}{\partial a_2} = -(B + C - D), \qquad \frac{\partial f_i^{(1)}}{\partial a_1} = -\frac{\partial f_i^{(2)}}{\partial a_2} = -E,$$
$$\frac{\partial f_e^{(1)}}{\partial a_2} = -\frac{\partial f_e^{(2)}}{\partial a_1} = B, \qquad \frac{\partial f_i^{(1)}}{\partial a_2} = -\frac{\partial f_i^{(2)}}{\partial a_1} = F,$$
$$\frac{\partial f_e^{(1)}}{\partial b_1} = -\frac{\partial f_e^{(2)}}{\partial b_2} = C, \qquad \frac{\partial f_i^{(1)}}{\partial b_1} = -\frac{\partial f_i^{(2)}}{\partial b_2} = H + E - F,$$
$$\frac{\partial f_e^{(1)}}{\partial b_2} = -\frac{\partial f_e^{(2)}}{\partial b_1} = -D, \qquad \frac{\partial f_i^{(1)}}{\partial b_2} = -\frac{\partial f_i^{(2)}}{\partial b_1} = -H.$$

From these relations we have that $\mathbf{B}^{(1)} = -\mathbf{B}^{(2)}$ and the left-low corners of the blocks $\mathbf{A}_{pq}^{(1)}$ and $\mathbf{A}_{pq}^{(2)}$, $p, q = 1, 2$, have opposite sign. The similarity of the matrix $\mathbf{J}_A - \lambda\mathbf{E}$ with

$$\begin{pmatrix} \mathbf{A}^{(2)} & \mathbf{B}^{(1)} \\ \mathbf{B}^{(1)} & \mathbf{A}^{(2)} \end{pmatrix}$$

now follows by multiplying the first and the $(m + 2)$th row; and the first and the $(m + 2)$ th column by -1.

The similarity

$$\begin{pmatrix} \mathbf{A}^{(2)} & \mathbf{B}^{(1)} \\ \mathbf{B}^{(1)} & \mathbf{A}^{(2)} \end{pmatrix} \sim \begin{pmatrix} \mathbf{A}^{(2)} + \mathbf{B}^{(1)} & \mathbf{B}^{(1)} \\ \mathbf{B}^{(1)} + \mathbf{A}^{(2)} & \mathbf{A}^{(2)} \end{pmatrix}$$

is obvious. Thus, we get

$$\begin{pmatrix} \mathbf{A}^{(1)} & \mathbf{B}^{(1)} \\ \mathbf{A}^{(2)} & \mathbf{B}^{(2)} \end{pmatrix} \sim \begin{pmatrix} \mathbf{A}^{(2)} & \mathbf{B}^{(1)} \\ \mathbf{B}^{(1)} & \mathbf{A}^{(2)} \end{pmatrix} \sim \begin{pmatrix} \mathbf{A}^{(2)} + \mathbf{B}^{(1)} & \mathbf{B}^{(1)} \\ \mathbf{B}^{(1)} + \mathbf{A}^{(2)} & \mathbf{A}^{(2)} \end{pmatrix}.$$

B.2. Computation of the determinant $\det(\mathbf{J}_A - \lambda\mathbf{E})$

The second step consists of computing the determinant of the matrix $\mathbf{J}_A - \lambda\mathbf{E}$. This computation is based on the similarity property shown in Appendix B.1. We first observe that

$$\begin{aligned} \det(\mathbf{J}_A - \lambda\mathbf{E}) &= \det((\mathbf{A}^{(2)} + \mathbf{B}^{(1)})\mathbf{A}^{(2)} - (\mathbf{A}^{(2)} + \mathbf{B}^{(1)})\mathbf{B}^{(1)}) \\ &= \det(\mathbf{A}^{(2)} + \mathbf{B}^{(1)}) \det(\mathbf{A}^{(2)} - \mathbf{B}^{(1)}) \end{aligned}$$

where we have exploited the fact that the determinant of

$$\begin{pmatrix} \mathbf{A}^{(2)} + \mathbf{B}^{(1)} & \mathbf{B}^{(1)} \\ \mathbf{B}^{(1)} + \mathbf{A}^{(2)} & \mathbf{A}^{(2)} \end{pmatrix}$$

can be computed as the determinant of a block matrix with commuting blocks [66]. We now show how to evaluate the determinants of $\mathbf{A}^{(2)} + \mathbf{B}^{(1)}$ and $\mathbf{A}^{(2)} - \mathbf{B}^{(1)}$. By the Laplace expansion using the first $(k_e + 1)$ rows of the matrix $\mathbf{A}^{(2)} \pm \mathbf{B}^{(1)}$ we get

$$\det(\mathbf{A}^{(2)} \pm \mathbf{B}^{(1)}) = M_1 M_1' + M_2 (-1)^{k_e+1} M_2', \tag{B.3}$$

where M_1 is the minor of the matrix based on first (k_e+1)th rows and the first (k_e+1)th columns, M_2 is the minor of the matrix based on the first $(k_e+1)'$ rows and on the second to (k_e+2)th columns; M_1' and M_2' are the complementary minors to the minor M_1 and M_2, respectively. All other possible products of minors of the matrix $\mathbf{A}^{(2)} \pm \mathbf{B}^{(1)}$, say $M_k M_k'$, are equal to zero. Therefore, they do not appear in the RHS of (B.3).

The minors M_2 and M_2' are easily obtained by the Laplace expansion based on the last and the first column, respectively, of the corresponding matrices, so we have

$$M_2 = d_2 p_2/p_1, \qquad M_2' = (-1)^{k_i} d_3 p_1/p_2 \tau^{-(k_i+1)}$$

for the matrix $\mathbf{A}^{(2)} + \mathbf{B}^{(1)}$, and

$$M_2 = -(C-D)/p_1, \qquad M_2' = (-1)^{k_i}(E-F)/p_2 \tau^{-(k_i+1)},$$

for $\mathbf{A}^{(2)} - \mathbf{B}^{(1)}$, in notations (21)–(23). To calculate the determinants M_1 and M_1' we first need to obtain the formula for the determinant of the auxiliary matrix

$$\mathbf{M} = \begin{pmatrix} \lambda_1 & a & & & \\ b & \lambda_2 & a & & \\ \vdots & & \ddots & \ddots & \\ b & & & \lambda_{n-1} & a \\ b & & & & \lambda_n \end{pmatrix}.$$

By Laplace expansion using the bottom row, we obtain the recursion formula $\det(\mathbf{M}) = D_n$ where

$$D_n = \lambda_n D_{n-1} + (-1)^{n-1} a^{n-1} b, \qquad D_1 = \lambda_1. \tag{B.4}$$

Using (B.4) we get in the case of the matrix $\mathbf{A}^{(2)} + \mathbf{B}^{(1)}$,

$$M_1 = (-\lambda) D_{k_e}^{(e)} + (-1)^{k_e} d_1, \qquad M_1' = (-\lambda) D_{k_i}^{(i)} + (-1)^{k_i} d_4 \tau^{-(k_i+1)},$$

and in the case of matrix $\mathbf{A}^{(2)} - \mathbf{B}^{(1)}$,

$$M_1 = (-\lambda) D_{k_e}^{(e)} + (-1)^{k_e}(C-D)/p_1, \qquad M_1' = (-\lambda) D_{k_i}^{(i)} + (-1)^{k_i}(F-E)/p_2 \tau^{-(k_i+1)},$$

where d_1 and d_2 is defined as (23) and

$$D_{k_e}^{(e)} = -(1+\lambda) D_{k_e-1}^{(e)} + (-1)^{k_i}, \qquad D_1^{(e)} = -(2+\lambda),$$
$$D_{k_i}^{(i)} = -(1/\tau + \lambda) D_{k_i-1}^{(i)} + (-1)^{k_i} \tau^{-n}, \quad D_1^{(i)} = -(2/\tau + \lambda).$$

Thus, we finally have

$$\begin{aligned} \det(\mathbf{A}^{(2)} + \mathbf{B}^{(1)}) = (-1)^{k_e+k} \left(\frac{1}{\tau}\right)^{(k_i+1)} & ((-1)^{k_e+k_i} \tau^{k_i+1} \lambda^2 D_{k_e}^{(e)} D_{k_i}^{(i)} \\ & + (-\tau)^{(k_i+1)} \lambda d_1 D_{k_i}^{(i)} + (-1)^{(k_e+1)} \lambda d_4 D_{k_e}^{(e)} + \gamma_S) \end{aligned} \tag{B.5}$$

and

$$\begin{aligned} \det(\mathbf{A}^{(2)} - \mathbf{B}^{(1)}) = (-1)^{k_e+k_i} \lambda \left(\frac{1}{\tau}\right)^{(k_i+1)} & \left((-1)^{k_e+k_i} \tau^{k_i+1} \lambda D_{k_e}^{(e)} D_{k_i}^{(i)} \right. \\ & \left. + (-\tau)^{(k_i+1)} \frac{C-D}{p_1} D_{k_i}^{(i)} + (-1)^{(k_e+1)} \frac{F-E}{p_2} D_{k_e}^{(e)} \right). \end{aligned} \tag{B.6}$$

We now prove that

$$\mathcal{P}_S(\lambda) = (-1)^{k_e+k_i} \tau^{k_i+1} \det(\mathbf{A}^{(2)} + \mathbf{B}^{(1)}) \tag{B.7}$$

and

$$\lambda \mathcal{P}_{As}(\lambda) = (-1)^{k_e+k_i} \tau^{k_i+1} \det(\mathbf{A}^{(2)} - \mathbf{B}^{(1)}). \tag{B.8}$$

We proceed as follows: comparing the components of the RHS and the LHS of the expressions (B.7) and (B.8), we notice that it is sufficient to prove that

$$P_{k_e} = (-1)^{k_e} D_{k_e}^{(e)}, \tag{B.9}$$

$$Q_{k_i} = (-1)^{k_i} \tau^{k_i} D_{k_i}^{(i)}, \tag{B.10}$$

where P_{k_e} and Q_{k_i} are given by (27). This can easily be done by mathematical induction. We show this proof in detail for (B.9) and omit it for (B.10) due to similarity. We proceed as follows.

1. Let $k_e = 1$. By (27), $P_1 = \lambda + 2$ while $D_1^{(e)} = -(2 + \lambda)$ by (B.2).
2. Assume that for $k_e = m$ we have $P_m = (-1)^m D_m^{(e)}$. By using (27) and (B.2) we now find that

$$\begin{aligned}(-1)^{m+1} D_{m+1}^{(e)} &= (-1)^{m+1}(-(\lambda+1)D_m^{(e)} + (-1)^m) = (1+\lambda)(-1)^m D_m^{(e)} - 1 \\ &= (1+\lambda)P_m(\lambda) - 1 = P_{m+1}.\end{aligned}$$

Notice that (B.7) and (B.8) make it possible to express the determinant of $\mathbf{J}_A - \lambda\mathbf{E}$ by means of the polynomials $\mathcal{P}_S(\lambda)$ and $\lambda\mathcal{P}_{\mathrm{As}}(\lambda)$ appearing in the factors $\mathcal{E}_S(\lambda)$ and $\mathcal{E}_{\mathrm{As}}(\lambda)$ in the Evans function $\mathcal{E}(\lambda)$. This completes the proof of the equivalence Theorem 1.

References

[1] H.R. Wilson, J.D. Cowan, Excitatory and inhibitory interactions in localized populations of model neurons, Biophys. J. 12 (1) (1972) 1–24.
[2] B.W. Knight, Dynamics of encoding in a population of neurons, J. Gen. Physiol. 59 (1972) 734–766.
[3] E. Nordlie, T. Tetzlaff, G.T. Einevoll, Rate dynamics of leaky integrate-and-fire neurons with strong synapses, Front. Comput. Neurosci. 4 (2010) 149.
[4] P.C. Bressloff, Spatially periodic modulation of cortical patterns by long-range horizontal connections, Physica D 185 (2003) 131–157.
[5] P.C. Bressloff, Traveling fronts and wave propagation failure in an inhomogeneous neural network, Physica D 155 (2001) 83–100.
[6] P.C. Bressloff, S.E. Folias, A. Pratt, Y.-X. Li, Oscillatory waves in inhomogeneous neural media, Phys. Rev. Lett. 91 (178101) (2003).
[7] Z.P. Kilpatrick, S.E. Folias, P.C. Bressloff, Traveling pulses and wave propagation failure in an inhomogeneous neural network, SIAM J. Appl. Dyn. Syst. 7 (2008) 161–185.
[8] X. Huang, W.C. Troy, Q. Yang, H. Ma, C.R. Laing, S.J. Schiff, J.-Y. Wu, Spiral waves in disinhibited mammalian neocortex, J. Neurosci. 24 (44) (2004) 9897–9902.
[9] S. Coombes, C.R. Laing, Pulsating fronts in periodically modulated neural field models, Phys. Rev. E 83 (2011) 011912.
[10] B.W. Knight, The relationship between the firing rate of a single neuron and the level of activity in a population of neurons, J. Gen. Physiol. 59 (1972) 767–778.
[11] G. Silberberg, M. Bethge, H. Markram, K. Pawelzik, M. Tsodyks, Dynamics of population codes in ensembles of neocortical neurons, J. Neurophysiol. 91 (2004) 704–709.
[12] H. Köndgen, C. Geisler, S. Fusi, Xiao-Jing Wang, H.-R. Lüscher, M. Giugliano, The dynamical response properties of neocortical neurons to temporally modulated noisy inputs in vitro, Cereb. Cortex 18 (2008) 2086–2097.
[13] P. Blomquist, A. Devor, U.G. Indahl, I. Ulbert, G.T. Einevoll, A.M. Dale, Estimation of thalamocortical and intracortical network models from joint thalamic single-electrode and cortical laminar-electrode recordings in the rat barrel system, PLoS Comput. Biol. 5 (2009) e1000328.
[14] C. Boucsein, T. Tetzlaff, R. Meier, A. Aertsen, B. Naundorf, Dynamical response properties of neocortical neuron ensembles: multiplicative versus additive noise, J. Neurosci. 29 (2009) 1006–1010.
[15] W. Gerstner, Population dynamics of spiking neurons: fast transients, asynchronous states, and locking, Neural Comput. 12 (1) (2000) 43–89.
[16] N. Brunel, F.S. Chance, N. Fourcaud, L.F. Abbott, Effects of synaptic noise and filtering on the frequency response of spiking neurons, Phys. Rev. Lett. 86 (2001) 2186–2189.
[17] B. Lindner, L. Schimansky-Geier, Transmission of noise coded versus additive signals through a neuronal ensemble, Phys. Rev. Lett. 86 (2001) 2934–2937.
[18] M. Mattia, P.D. Guidice, Population dynamics of interacting spiking neurons, Phys. Rev. E 66 (2002) 051917.
[19] N. Fourcaud, N. Brunel, Dynamics of the firing probability of noisy integrate-and-fire neurons, Neural Comput. 14 (2002) 2057–2110.
[20] N. Fourcaud-Trocmé, D. Hansel, C. van Vreeswijk, N. Brunel, How spike generation mechanisms determine the neuronal response to fluctuating inputs, J. Neurosci. 23 (2003) 11628–11640.
[21] B. Naundorf, T. Geisel, F. Wolf, Action potential onset dynamics and the response speed of neuronal populations, J. Comput. Neurosci. 18 (2005) 297–309.
[22] J. Pressley, T.W. Troyer, Complementary responses to mean and variance modulations in the perfect integrate-and-fire model, Biol. Cybernet. 101 (1) (2009) 63–70.
[23] M.J.E. Richardson, Firing-rate response of linear and nonlinear integrate-and-fire neurons to modulated current-based and conductance-based synaptic drive, Phys. Rev. Lett. 76 (2007) 021919.
[24] M.J.E. Richardson, R. Swarbrick, Firing-rate response of a neuron receiving excitatory and inhibitory synaptic shot noise, Phys. Rev. Lett. 105 (2010) 178102.
[25] P. Blomquist, J. Wyller, G.T. Einevoll, Localized activity patterns in two-population neuronal network, Physica D 206 (2005) 180–212.
[26] S. Amari, Dynamics of pattern formation in lateral-inhibition type neural fields, Biol. Cybernet. 27 (1977) 77–87.
[27] A. Destexhe, Z.F. Mainen, T.J. Sejnowski, Synthesis of models for excitable membranes, synaptic transmission and neuromodulation using a common kinetic formalism, J. Comput. Neurosci. 1 (3) (1994) 195–230.
[28] V.I. Arnol'd, Ordinary Differential Equations, Springer Verlag, New York, Berlin, Heidelberh, Tokyo, 1992.
[29] M. MacDonald, Time Lags in Biological Models, in: Lecture Note in Biomathematics, Springer Verlag, 1978.
[30] S. Coombes, Waves, bumps, and patterns in neural field theories, Biol. Cybernet. 93 (2005) 91–108.
[31] K. Kishimoto, S. Amari, Existence and stability of local excitations in homogeneous neural fields, J. Math. Biol. 7 (1979) 303–318.
[32] D.J. Pinto, G.B. Ermentrout, Spatially structured activity in synaptically coupled neuronal networks: II. Lateral inhibition and standing pulses, SIAM J. Appl. Math. 62 (2001) 226–243.
[33] C.R. Laing, W.C. Troy, B. Gutkin, G.B. Ermentrout, Multiple bumps in a neuronal network model of working memory, SIAM J. Appl. Math. 63 (2002) 62–97.
[34] C.R. Laing, W.C. Troy, Two-bump solutions af Amari- type models of neuronal pattern formation, Physica D 178 (2003) 90–218.
[35] S. Coombes, G.J. Lord, M.R. Owen, Waves and bumps in neuronal networks with axo-dendritic synaptic interactions, Physica D 178 (2003) 219–241.
[36] J.E. Rubin, W.C. Troy, Sustained spatial patterns of activity in neuronal populations without recurrent excitation, SIAM J. Appl. Math. 64 (2004) 1609–1635.
[37] S.E. Folias, P.C. Bressloff, Breathing pulses in an excitatory network, SIAM J. Appl. Dyn. Syst. 3 (2004) 378–407.
[38] S. Coombes, M.R. Owen, Bumps, breathers, and waves in a neural network with spike frequency adaptation, Phys. Rev. Lett. 148102 (2005).
[39] Y. Guo, C.C. Chow, Existence and stability of standing pulses in neural networks: I. Existence, SIAM J. Appl. Dyn. Syst. 4 (2005) 217–248.
[40] M.R. Owen, C.R. Laing, S. Coombes, Bumps and rings in a two-dimensional neural field: splitting and rotational instabilities, New J. Phys. 9 (2007) 378.
[41] Y. Guo, C.C. Chow, Existence and stability of standing pulses in neural networks: II. Stability, SIAM J. Appl. Dyn. Syst. 4 (2005) 249–281.
[42] G.B. Ermentrout, J.D. Cowan, Large scale spatially organized activity in neural nets, SIAM J. Appl. Math. 38 (1980) 1–21.
[43] J. Wyller, P. Blomquist, G.T. Einevoll, Turing instability and pattern formation in a two-population neuronal network model, Physica D 225 (2007) 75–93.
[44] A. Hutt, F.M. Atay, Analysis of nonlocal neural fields for both general and gamma-distributed connectivities, Physica D 203 (2005) 30–54.
[45] T.P. Vogels, K. Rajan, L.F. Abbott, Neural network dynamics, Annu. Rev. Neurosci. 28 (2005) 357–376.
[46] A. Hutt, M. Bestehorn, T. Wennekers, Pattern formation in intracortical neuronal fields, Netw., Comput. Neural Syst. 14 (2003) 351–368.

[47] F.M. Atay, A. Hutt, Stability and bifurcations in neural fields with finite propagation speed and general connectivity, SIAM J. Appl. Math. 65 (2005) 644–666.
[48] G.B. Ermentrout, J.D. Cowan, Temporal oscillations in neuronal nets, J. Math. Biol. 7 (1979) 265–280.
[49] G.B. Ermentrout, J.D. Cowan, Secondary bifurcations in neuronal nets, SIAM J. Appl. Math. 39 (1980) 323–340.
[50] R. Curtu, B. Ermentrout, Pattern formation in a network of excitatory and inhibitory cells with adaptation, SIAM J. Appl. Dyn. Syst. 3 (2004) 191–231.
[51] C. Laing, S. Coombes, The importance of different timings of excitatory and inhibitory pathways in neural field models, Netw., Comput. Neural Syst. 17 (2006) 151–172.
[52] M.A.P. Idiart, L.F. Abbott, Propagation of excitation in neural networks, Network 4 (1993) 285–294.
[53] D.J. Pinto, G.B. Ermentrout, Spatially structured activity in synaptically coupled neuronal networks: I. Traveling fronts and pulses, SIAM J. Appl. Math. 62 (2001) 206–225.
[54] P.C. Bressloff, S.E. Folias, Front bifurcations in an excitatory neural network, SIAM J. Appl. Math. 65 (2004) 131–151.
[55] S. Coombes, M.R. Owen, Evans functions for integral neural field equations with Heaviside firing rate functions, SIAM J. Appl. Dyn. Syst. 3 (2004) 574–600.
[56] D.J. Pinto, R.K. Jackson, C.E. Wayne, Existence and stability of traveling pulses in a continuous neuronal network, SIAM J. Appl. Dyn. Syst. 4 (2005) 954–984.
[57] H.R. Wilson, J.D. Cowan, A mathematical theory of the functional dynamics of cortical and thalamic nervous tissue, Kybernetik 13 (1973) 55–80.
[58] Ø Nordbø, J. Wyller, G.T. Einevoll, Neural network firing-rate models on integral form: effects of temporal coupling kernels on equilibrium-state stability, Biol. Cybernet. 97 (2007) 195–209.
[59] J. Wyller, P. Blomquist, G.T. Einevoll, On the origin and properties of two-population neural field models—a tutorial introduction, Biophys. Rev. Lett. 2 (1) (2007) 79–98.
[60] R. Potthast, P.B. Graben, Existence and properties of solutions for neural field equations, Math. Methods Appl. Sci. 33 (8) (2010) 935–949.
[61] G. Faye, O. Faugeras, Some theoretical and numerical results for delayed neural field equations, Physica D 239 (2010) 561–578.
[62] A. Pazy, Semigroups of Linear Operators and Applications to Partial Differential Equations, in: Applied Mathematical Sciences, vol. 44, Springer Verlag, New York Berlin, Heidelberg Tokyo, 1983.
[63] N.A. Venkov, Dynamics of Neural Field Models, Ph.D. Thesis, School of Mathematical Sciences, University of Nottingham, 2009. http://www.umnaglava.org/pdfs.html.
[64] B. Ermentrout, Neural networks as spatio-temporal pattern-forming systems, Rep. Progr. Phys. 61 (1998) 353–430.
[65] R.E. Goldstein, D.J. Muraki, D.M. Petrich, Interface proliferation and the growth of labyrinths in a system of reaction—diffusion system, Phys. Rev. E 53 (4) (1996).
[66] J.R. Silvester, Determinants of block matrices, Math. Gaz. 84 (501) (2000) 460–467.

Paper IV

ON THE PROPERTIES OF NONLINEAR NONLOCAL OPERATORS ARISING IN NEURAL FIELD MODELS

ANNA OLEYNIK, ARCADY PONOSOV, AND JOHN WYLLER

Abstract. We study existence and continuous dependence of stationary solutions of the one-population Wilson-Cowan model on the steepness of the firing rate functions. We investigate the properties of the nonlinear nonlocal operators which arise when formulating the stationary one-population Wilson-Cowan model as a fixed point problem. The theory is used to study existence and continuous dependence of localized stationary solutions of this model on the steepness of the firing rate functions. The present work generalizes and complements previously obtained results as we relax on the assumptions that the firing rate functions are given by smoothed Heaviside functions.

1. Introduction

Neural field models typically assume the form of integro-differential equations. Here we consider a one-population neural field model of the Wilson-Cowan type [1, 2, 3, 4, 5]

$$\frac{\partial}{\partial t}u(x,t) = -u(x,t) + \int_{\mathbb{R}} \omega(x,y)P(u(y,t))dy, \quad x \in \mathbb{R},\ t > 0. \tag{1.1}$$

This model describes the dynamics of the spatio-temporal electrical activity levels in neural tissue in one spatial dimension. Here $u(x,t)$ is interpreted as a local activity of a neural population at the position $x \in \mathbb{R}$ and time $t > 0$. The second term on the right hand side of (1.1) represents the synaptic input with P interpreted as a *firing rate function* which typically has sigmoidal shape. The function ω is called a *connectivity function* and models the spatial strength of the connectivity between the neurons. See [1, 2, 3, 4, 5] for more details regarding the relevance of the equation (1.1) in neural-field theory.

The most common simplification of the model consists of replacing the sigmoidal firing rate function by the unit step function. In the latter case it is possible to obtain closed form expressions for solutions describing coherent structures like stationary localized solutions (*bumps*) and traveling fronts [5] as well as to assess the stability of these structures using the Evans function approach [6]. It is conjectured that the model with unit step function reproduces the essential features in

Key words and phrases. Neural-field models, bumps, nonlinear operators, continuous dependence.

the steep firing-rate regime. This conjecture is supported by numerical simulations (see for example [7]) but there are far in between works addressing this problem in a rigorous mathematical way [8, 9, 10, 11].

This serves as a motivation for the present paper. In the present paper we relax on the assumptions that the firing rate function is given as a unit step function [4] and as a smoothed Heaviside function [8, 9], and allow for more general firing rate functions. We consider a one-parameter family of firing rate functions where the parameter measures the steepness of these functions. They approach the unit step function as the steepness parameter goes to infinity. Moreover, we do not restrict ω to be homogeneous functions, i.e., $\omega = \omega(|x - y|)$ of a 'Mexican-hat' type, [5]. We study the continuous dependence of the stationary localized solutions of (1.1) on the steepness of the firing rate functions. Then, by imposing some extra conditions on the firing rate functions P and the connectivity kernels ω we are able to prove the existence of bumps solutions.

The stationary solutions of (1.1) are solutions of a fixed point problem. This fixed point problem is described in terms of a Hammerstein operator which is the superposition of a Nemytskii operator and a linear integral operator. We study the properties of these operators. Due to discontinuity of the unit step function many properties of the Hammerstein operator will break down. Therefore one of the main challenges here is to choose function spaces and a suitable topology of the operators convergence that allow the continuous dependence properties of solutions to be fulfilled.

The paper is organized as follows: In Section 2 we explain our notations, prove some useful theorems, and state lemmas from functional analysis, to which we refer in the subsequent sections. In Section 3 we give a detailed description of the model. Next, we study continuity and compactness of the associated operators in Sobolev spaces. We define special regions where the Nemytskii operator associated with the unit step firing rate function is continuous. It is shown that the property of the Nemytskii operator to be continuous is very sensitive to the choice of the topology. One of the main results of the section is summarized in Theorem 3.14, which we will refer to as the continuous dependence theorem. Moreover, we formulate an existence theorem (Theorem 3.15) which enables us to prove the existence of solutions of the fixed point problem in steep firing-rate regime under the assumption that there exists an isolated solution of the limiting fixed problem (when the steepness parameter is equal to infinity). From this theorem it also follows that solutions will have the same number of intersections with a constant value θ as the solution of the limiting problem. In Section 4 we apply the results of Section 3 to prove continuous dependence of

spatially localized stationary solutions of (1.1) on the steepness of the firing rate function for both inhomogeneous and homogeneous connectivity functions. In particular, in the latter case we prove the existence of bumps in a steep firing-rate regime where the firing rate function takes values zero on a ray $(-\infty, h)$, $h > 0$. We emphasize that this result is more general than results on existence of bumps obtained in [8] and [11]. Section 5 contains conclusions and outlook.

2. Preliminaries

Let B be a open set of a real Banach space $\mathcal{B}$, then $\overline{B}$ denotes the closure of B in $\mathcal{B}$. We use the notation $\deg(A, B, p)$ for the degree defined for an operator $A : \overline{B} \to \mathcal{B}$, and $p \in \mathcal{B}$. We use $\mathrm{ind}(A, B)$ for the topological index of A, [12].

Let $W^{1,q}(\mathbb{R}, \mu)$, $1 \le q \le \infty$, denote a Sobolev space which consists of all functions $w \in L^q(\mathbb{R}, \mu)$ such that their generalized derivatives (with respect to the given measure μ) $dw/d\mu = \tilde{w} \in L^q(\mathbb{R}, \mu)$.

The element $w \in W^{1,q}(\mathbb{R}, \mu)$ then can be represented as

$$w(x) = w(0) + \int_0^x \widetilde{w}(\xi) d\mu(\xi). \tag{2.1}$$

We consider the following two norms in $W^{1,q}(\mathbb{R}, \mu)$

$$||w||_1 = ||w||_{L^q} + ||\widetilde{w}||_{L^q} \tag{2.2}$$

and

$$||w||_2 = |w(0)| + ||\widetilde{w}||_{L^q} \tag{2.3}$$

where $||\cdot||_{L^q}$ is the norm in $L^q(\mathbb{R}, \mu)$, i.e.,

$$||w||_{L^q} = \left(\int_{\mathbb{R}} |w(x)|^q d\mu(x) \right)^{1/q}, \quad 1 \le q < \infty$$

and

$$||w||_{L^\infty} = \sup_{x \in \mathbb{R}} |w(x)|.$$

Theorem 2.1. *The norms $||\cdot||_1$ and $||\cdot||_2$ are equivalent if μ is finite.*

Proof. From the representation (2.1) we have

$$||w||_{L^q} = \|w(0) + \int_0^x \tilde{w}(y) d\mu(y)\|_{L^q} \le \||w(0)| + \int_0^x |\tilde{w}(y)| d\mu(y)\|_{L^q} \le$$

$$\le \||w(0)| + \int_{\mathbb{R}} |\tilde{w}(y)| d\mu(y)\|_{L^q} = [\mu(\mathbb{R})]^{1/q} (|w(0)| + \|\tilde{w}\|_{L^1})$$

Using Hölder inequality we get $||\tilde{w}||_{L^1} \leq [\mu(\mathbb{R})]^{1/q'}||\tilde{w}||_{L^q}$ where q' is defined by the equality $1/q + 1/q' = 1$. Thus,

$$||w||_{L^q} \leq [\mu(\mathbb{R})]^{1/q}|w(0)| + \mu(\mathbb{R})||\tilde{w}||_{L^q}. \tag{2.4}$$

From (2.2) and (2.4) we get

$$||w||_1 \leq [\mu(\mathbb{R})]^{1/q}|w(0)| + \mu(\mathbb{R})||\tilde{w}||_{L^q} + \|\tilde{w}\|_{L^q}.$$

Therefore we get

$$\|w\|_1 \leq C_2||w||_2, \quad C_2 = \max\left\{[\mu(\mathbb{R})]^{1/q}, 1 + \mu(\mathbb{R})\right\}.$$

In a similar way we estimate $|w(0)|$, i.e.,

$$|w(0)| = [\mu(\mathbb{R})]^{-1/q}\|w(0)\|_{L^q} = [\mu(\mathbb{R})]^{-1/q}\|w(x) - \int_0^x \tilde{w}(y)d\mu(y)\|_{L^q} \leq$$
$$\leq [\mu(\mathbb{R})]^{-1/q}\left(\|w\|_{L^q} + \|\tilde{w}\|_{L^q}\right).$$

We have

$$\|w\|_2 \leq c_1\|w\|_1, \quad c_1 = [\mu(\mathbb{R})]^{-1/q} + 1.$$

Hence, we get

$$C_1\|w\|_2 \leq \|w\|_1 \leq C_2\|w\|_2,$$

with

$$C_1 = c_1^{-1} = \frac{[\mu(\mathbb{R})]^{1/q}}{[\mu(\mathbb{R})]^{1/q} + 1},\ C_2 = \max\left\{[\mu(\mathbb{R})]^{1/q}, 1 + \mu(\mathbb{R})\right\}.$$

By definition the norms then are equivalent. □

We denote the norm in $W^{1,q}(\mathbb{R}, \mu)$ as $\|\cdot\|_{W^{1,q}}$.

Lemma 2.2. *Let A be the following operator*

$$(Au)(x) = \int_{\mathbb{R}} k(x, y)u(y)d\mu(y), \quad x \in \mathbb{R}, \tag{2.5}$$

where μ is a finite complete measure on $\mathbb{R}$ and $k(x, y)$ is measurable on $\mathbb{R}^2$. Let the following conditions be satisfied

(i) *for any $x \in \mathbb{R}$, $k(x, \cdot) \in L^p(\mathbb{R}, \mu)$,*

(ii) *for any $\varepsilon > 0$ there exist a finite partitioning of $\mathbb{R}$ into measurable sets, say D_1, $D_2, \ldots, D_n$, such that*

$$\sup_{x_1, x_2 \in D_j} \|k(x_1, y) - k(x_2, y)\|_{L^{p'}} < \varepsilon, \quad j = 1, 2, ..., n. \tag{2.6}$$

Then the integral operator A maps $L^p(\mathbb{R}, \mu)$ to $L^\infty(\mathbb{R}, \mu)$ and it is compact, see [14].

Theorem 2.3. *Let D be a closed bounded subset of a real Banach space $\mathcal{B}$, Λ be a closed subset of $\mathbb{R}$, and an operator $T(\lambda, u) : \Lambda \times D \to \mathcal{B}$ be continuous with respect to both variables and collectively compact (i.e., $T(\Lambda \times D)$ is a pre-compact set in $\mathcal{B}$). Assume that $\lambda_n \to \lambda^*$ and $T(\lambda_n, u_n) = u_n$. Then the equation $T(\lambda^*, u) = u$ has at least one solution. Moreover, any limiting point of the sequence $\{u_n\}$ is a solution of this equation, i.e., if $u_{n_k} \to u^*$ then u^* is a solution of $T(\lambda^*, u^*) = u^*$.*

Proof. The sequence $\{u_n\}$ define by $T(\lambda_n, u_n) = u_n$ is a pre-compact set due to T is a collectively compact. Thus, there exist convergent subsequence of $\{u_n\}$,i.e., $\{u_{n_k}\} \to u^* \in D$. the continuity of T yields $\lim_{n_k \to \infty} T(\lambda_{n_k}, u_{n_k}) = T(\lambda^*, u^*) = u^*$. □

Remark 2.4. *If u^* is unique in D then u_n has only one limit point, that is, $u_n \to u^*$.*

Lemma 2.5 (Homotopy invariance)**.** *Let D be an open bounded subset of a real Banach space $\mathcal{B}$. Suppose that $\{h_t\}$ is a homotopy of operators $h_t : \bar{D} \to \mathcal{B}$ for $t \in [0, 1]$, and assume that $h_t - I$ is compact for each t. If $h_t f \neq p$ for any $f \in \partial D$ and $t \in [0, 1]$, then $\deg(h_t, D, p)$ is independent of t, see* [13].

3. Main results

The stationary Wilson-Cowan model (1.1) is equivalent to the fixed point problem

$$u = \mathcal{H}u, \tag{3.1}$$

where $\mathcal{H}$ is the Hammerstein operator

$$(\mathcal{H}u)(x) = \int_{\mathbb{R}} \frac{\omega(x, y)}{\rho(y)} P(u(y)) d\mu(y). \tag{3.2}$$

and

$$\mu A = \int_A \rho(y) dy$$

is an arbitrary probabilistic measure which is absolutely continuous with respect to the Lebesgue measure (i.e., $\mu\mathbb{R} = 1$ and $\mu A \geq 0$ whenever the Lebesgue measurable set A has a positive Lebesgue measure). This can be achieved by putting some necessary properties on the function ρ.

The function $\omega(x, y)$ is a measurable function satisfying the following assumptions:

(i) for any $x \in \mathbb{R}$, $\omega(x, \cdot) \in L^1(\mathbb{R})$, i.e.,

$$\forall x \in \mathbb{R} \quad \int_{\mathbb{R}} |\omega(x, y)| dy < \infty,$$

(ii) ω is differentiable with respect to the first variable and

$$\omega'_x(x,\cdot) \in L^1_{loc}(\mathbb{R}) \quad \forall x \in \mathbb{R},$$

(iii) ω is bounded, i.e.,

$$\exists C > 0 \quad |\omega(x,y)| < C \quad \forall x, y \in \mathbb{R},$$

(iv) for any $y \in \mathbb{R}$ $\lim\limits_{x\to\infty} \omega(x,y) = 0$.

The function P can be interpreted as a probability function of firing. Thus, P is a map from $\mathbb{R}$ to $[0,1]$. We consider the special family of $P : P(u) = S(\beta, u)$ where β takes values from $(0,\infty]$. We assume that S satisfies the following properties:

(i) $S : (0,\infty) \times \mathbb{R} \to [0,1]$ is a continuous function,

(ii) $S(\beta,\cdot)$ is monotonically non-decreasing,

(iii) $S(\beta,\cdot) \to S(\beta_0,\cdot)$ uniformly on $\mathbb{R}$ as $\beta \to \beta_0 \in (0,\infty)$,

(iv) as $\beta \to \infty$ $S(\beta,u)$ approaches $S(\infty,u)$ uniformly on $(-\infty, \theta - \varepsilon] \cup [\theta + \varepsilon, \infty)$ for any $\varepsilon > 0$, where $S(\infty,u)$ is the unit step function

$$S(\infty,u) = \begin{cases} 0, & u < \theta \\ 1, & u \geq \theta \end{cases}$$

with some threshold value $\theta > 0$.

The Hammerstein operator (3.2) can be represented as the superposition

$$(\mathcal{H}u)(x) = (\Omega \circ \mathcal{N}u)(x)$$

of the linear operator

$$(\Omega u)(x) = \int_{\mathbb{R}} \frac{\omega(x,y)}{\rho_1(y)} u(y) d\mu(y), \tag{3.3}$$

and the Nemytskii operator

$$(\mathcal{N}u)(x) = \frac{\rho_1(x)}{\rho(x)} P(u(x)). \tag{3.4}$$

Here ρ_1 is an auxiliary function satisfying the following properties

(i) $0 \leq \rho_1(x) \leq C_{\rho_1}$, where $C_{\rho_1} > 0$,

(ii) $\mathrm{supp}(\rho_1) \supseteq \mathrm{supp}(\rho)$,

(iii) $|\omega(0,y)| \leq C_\omega \rho_1(y)$ $\forall y \in \mathbb{R}$ and $C_\omega > 0$.

We set $\rho_1(x)/\rho(x) = 0$ and $\rho(x)/\rho_1(x) = 0$ for all $x \in \{\mathbb{R} - \mathrm{supp}(\rho_1)\}$.

Remark 3.1. *In particular, one can assume $\rho_1 \equiv \rho$. However, in order to keep the theory as general as possible, we allow ρ_1 to differ from ρ. In Section 4 we make use of this difference. See Example 4.5.*

Moreover, when we want to emphasize that some particular property is valid only for operators corresponding to $S(\beta,\cdot)$, $\beta\in(0,\infty)$ or $S(\infty,\cdot)$ we use the subindexes β and ∞, respectively. That is, we denote the Hammerstein operator (3.2) and the Nemytskii operator (3.4) as $\mathcal{H}_\beta$, $\mathcal{H}_\infty$ and $\mathcal{N}_\beta$, $\mathcal{N}_\infty$. When a property is valid for an operator with any $P:\mathbb{R}\to[0,1]$ we do not use any subindex, e.g., $\mathcal{H}$, $\mathcal{N}$.

Lemma 3.2. *Let $\widetilde{\Omega}: L^p(\mathbb{R},\mu)\to L^q(\mathbb{R},\mu)$, $1\le p,q\le\infty$ be an operator defined as*

$$(\widetilde{\Omega}v)(x)=\int\limits_{\mathbb{R}}\frac{\omega'_x(x,y)}{\rho(x)\rho_1(y)}u(y)d\mu(y). \tag{3.5}$$

Then, the operator Ω is a map from $L^p(\mathbb{R},\mu)$ to $W^{1,q}(\mathbb{R},\mu)$ and (a) it is a continuous operator if and only if $\widetilde{\Omega}$ is continuous, (b) it is a compact operator if and only if $\widetilde{\Omega}$ is a compact operator.

Proof. We formally apply (2.1) to the element $(\Omega u)(x)$. We have

$$(\Omega u)(x)=(\Omega u)(0)+\int\limits_0^x\widetilde{\Omega}u(y)d\mu(y)$$

where

$$(\Omega u)(0)=\int\limits_{\mathbb{R}}\frac{\omega(0,y)}{\rho_1(y)}u(y)d\mu(y),$$

and

$$(\widetilde{\Omega}u)(x)=\frac{d(\Omega u)(x)}{d\mu}=\int\limits_{\mathbb{R}}\frac{\omega'_x(x,y)}{\rho(x)\rho_1(y)}u(y)d\mu(y).$$

Using properties of ρ_1 we get

$$|(\Omega u)(0)|=\left|\int\limits_{\mathbb{R}}\frac{\omega(0,y)}{\rho_1(y)}u(y)d\mu(y)\right|\le C_\omega\|u\|_{L^p}. \tag{3.6}$$

Further, $\widetilde{\Omega}$ is a map from $L^p(\mathbb{R},\mu)$ to $L^q(\mathbb{R},\mu)$, hence Ω maps $L^p(\mathbb{R},\mu)$ to $W^{1,q}(\mathbb{R},\mu)$.

To prove (a) continuity and (b) compactness of Ω we introduce a linear operator $\mathcal{J}: W^{1,p}(\mathbb{R},\mu)\to\mathbb{R}\times L^p(\mathbb{R},\mu)$ such that

$$\mathcal{J}=(\mathcal{J}_1,\mathcal{J}_2):\ \mathcal{J}_1w=w(0)\in\mathbb{R},\ \mathcal{J}_2w=\frac{d}{d\mu}w\equiv\tilde{w}\in L^p(\mu,\mathbb{R}),$$

The inverse operator $\mathcal{J}^{-1}:\mathbb{R}\times L^p(\mathbb{R},\mu)\to W^{1,p}(\mathbb{R},\mu)$ then is given as

$$\mathcal{J}^{-1}(a,u)=a+\int\limits_0^x u(y)d\mu(y),\ (a,u)\in\mathbb{R}\times L^p(\mathbb{R},\mu).$$

It is easy to check that $\mathcal{J}$ is a homeomorphism: Indeed $\mathcal{J}$ is an isomorphism [15] and linear continuous. Thus, $\mathcal{J}^{-1}$ is continuous by the Banach theorem [16]. We present the proof of (b). The operator $\Omega_0 : L^p(\mathbb{R},\mu) \to \mathbb{R}$ given by $(\Omega_0 u)(x) = (\Omega u)(0)$ is compact as soon as it is bounded, which is the case due to the estimate (3.6). Therefore, for any bounded subset $D \subset L^p(\mathbb{R},\mu)$ there is a corresponding pre-compact subset $(\Omega_0 D, \tilde{\Omega} D) \subset \mathbb{R} \times L^p(\mathbb{R},\mu)$ which is homeomorphic to ΩD. Hence, ΩD is a pre-compact set in $W^{1,p}(\mathbb{R},\mu)$ and Ω is a compact operator.
Let us assume now that Ω is a compact operator, while $\tilde{\Omega}$ is not compact. Then, for any bounded D we get a pre-compact set ΩD which is homeomorphic to the non pre-compact set $(\Omega_0 D, \tilde{\Omega} D)$. This contradiction completes the proof. To prove (a) one can proceed in a similar way assuming boundedness of a set D instead of pre-compactness. □

Lemma 3.3. *If $\rho_1(x)/\rho(x)$ belongs to $L^p(\mathbb{R},\mu)$ the Nemytskii operator $\mathcal{N}$ maps $W^{1,q}(\mathbb{R},\mu)$ to $L^p(\mathbb{R},\mu)$, $1 \le p,q \le \infty$. Moreover $\mathcal{N}_\beta$, $\beta < \infty$, is continues. The operator $\mathcal{N}_\infty$ is discontinuous on $W^{1,q}(\mathbb{R},\mu)$, $1 \le q \le \infty$.*

Proof. First of all, we notice that due to the boundedness of P, i.e., $|P(u)| \le 1$, we have

$$\left|\frac{\rho_1(x)}{\rho(x)} P(u)\right| \le \left|\frac{\rho_1(x)}{\rho(x)}\right| \in L^p(\mathbb{R},\mu).$$

Hence, the Nemytskii operator is a map from $W^{1,q}(\mathbb{R},\mu)$ to $L^p(\mathbb{R},\mu)$. Moreover, $S(\beta,\cdot)$ satisfies to the Caratheodory conditions [14, 13]. We conclude that the Nemytskii operator $\mathcal{N}_\beta$ is continuous [14, 13].

To show that N_∞ is not continuous on $W^{1,q}(\mathbb{R},\mu)$ it is enough to give an example. Consider $u_n(x) = \theta + 1/n$ and $u(x) = \theta$. We have $(\mathcal{N}_\infty u_n)(x) = \rho_1(x)/\rho(x)$ for all $n \in N$ and $\mathcal{N}_\infty u = 0$. When $n \to \infty$ we get

$$\|u_n - u\|_{W^{1,q}} \to 0, \quad \text{and} \quad \|\mathcal{N}_\infty u_n - \mathcal{N}_\infty u\|_{L^p} = \|\rho_1/\rho\|_{L^p} \not\to 0.$$

□

Definition 3.4. *Let $\theta > 0$ be fixed. We say that $u \in W^{1,q}(\mathbb{R},\mu)$ satisfies the θ-condition if*

- *the function $u(x) - \theta$ has finitely many simple roots (i.e. $u(a) = \theta$ always implies $u'(a) \ne 0$);*
- *there exist $\sigma > 0$ and $A > 0$ such that $u(x) \le \theta - \sigma$ for all $|x| > A$.*

Remark 3.5. *Definition 3.4 implies that if $u \in W^{1,q}(\mathbb{R},\mu)$ satisfies the θ-condition then the number of intersections $u(x) = \theta$ is an even number.*

Lemma 3.6. *Let $\theta > 0$ be fixed and let $U \in W^{1,\infty}(\mathbb{R}, \mu)$ satisfies the θ-condition. Assume that the equation $U(x) = \theta$ has N solutions. Then there exists $\varepsilon > 0$ such that for any $u \in B(U, \varepsilon) = \{u : \ ||u - U||_{W^{1,\infty}} < \varepsilon\}$*

- *the function u satisfies the θ-condition;*
- *the equation $u(x) = \theta$ has exactly N solutions.*

Proof. Here we are going to use $\|\cdot\|_{W^{1,\infty}}$ given by (2.2). Let U satisfy the θ-condition, and $a^{(k)} : a^{(k)} < a^{(k+1)}$, $k = 1, ..., N$, be all solutions of the equation $U(x) = \theta$. Due to these assumptions there exist a positive ε and the points $b^{(k,1)}$, $b^{(k,2)}$, $k = 0, ..., N$, satisfying

$$a^{(k)} < b^{(k,1)} < b^{(k,2)} < a^{(k+1)}, \quad k = 1, ..., N-1,$$
$$b^{(0,1)} = -\infty, \ b^{(0,2)} < a^{(1)}, \ a^{(N)} < b^{(N,1)}, \ b^{(N,2)} = \infty,$$

such that

- $U(x) > \theta + 2\varepsilon$ if $x \in (b^{(k,1)}, b^{(k,2)})$, $k = 2m-1$, $0 \le k \le N$;
- $U(x) < \theta - 2\varepsilon$ if $x \in (b^{(k,1)}, b^{(k,2)})$, $k = 2m$, $0 \le k \le N$;
- $|U'(x)| > 2M\varepsilon$ if $x \in (b^{(k,2)}, b^{(k+1,1)})$, $0 \le k \le N-1$, where $M = \sup\limits_{x \in \mathbb{R}} \rho(x)$.

Let $u \in B(U, \varepsilon)$. Clearly,

$$|u(x) - U(x)| < \varepsilon, \qquad |u'(x) - U'(x)| < \varepsilon\rho(x) \text{ a.e. } x \in \mathbb{R}.$$

This implies the following estimates:

$$u(x) > \theta + \varepsilon \text{ if } x \in (b^{(k,1)}, b^{(k,2)}), \ k = 2m-1, \ 0 \le k \le N; \qquad (A1)$$

$$u(x) < \theta - \varepsilon \text{ if } x \in (b^{(k,1)}, b^{(k,2)}), \ k = 2m, \ 0 \le k \le N; \qquad (A2)$$

$$|u'(x)| > M\varepsilon \text{ if } x \in (b^{(k,2)}, b^{(k+1,1)}), \ 0 \le k \le N-1. \qquad (A3)$$

Therefore, the equation $u(x) = \theta$ has a unique solution in each interval $(b^{(k,2)}, b^{(k+1,1)})$, $0 \le k \le N-1$, while $|u'(x)| > M\varepsilon$ within any of these intervals. Remembering that $b^{(0,2)} = -\infty$ and that $u(x) < \theta$ for $x > b^{(N,1)}$ yield exactly N solutions of the equation $u(x) = \theta$, and all of these solutions must be simple. Fig.1 illustrates graphically Lemma 3.6 for $N = 4$. Here we have plotted schematically a function $u \in B(U, \varepsilon)$, where U has $N = 4$ intersections with $u = \theta$. □

Lemma 3.7. *Let $\theta > 0$ be fixed and let $U \in W^{1,q}(\mathbb{R}, \mu)$, $1 \le q < \infty$, satisfy the θ-condition. For any $\varepsilon > 0$ the ball $B(U, \varepsilon) = \{u : \ ||u - U||_{W^{1,q}} < \varepsilon\}$ contains functions which do not satisfy the θ-condition.*

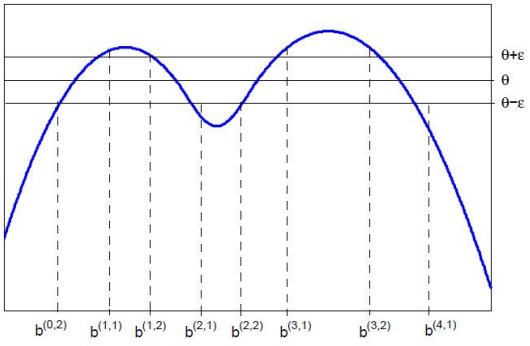

FIGURE 1. The θ-condition in $W^{1,\infty}(\mathbb{R},\mu)$ for $N=4$

Proof. For the proof we give the following example
(3.7)

$$u_n(x)=\begin{cases} U(x)-U(a^{(1)}-1/n)+\theta, & x\in(-\infty,-a^{(1)}-1/n) \\ \theta, & x\in\bigcup\limits_{j=1}^{2}[a^{(j)}-1/n,a^{(j)}+1/n] \\ U(x)-U(a^{(2)}+1/n)+\theta, & x\in[a^{(2)}+1/n,+\infty) \end{cases}$$

We consider the norm in $W^{1,q}(\mathbb{R},\mu)$ given by (2.3). It is easy to see that

$$\|u_n-U\|_{W^{1,q}}=\|\tilde{u}_n-\tilde{U}\|_{L^q}=\left(\bigcup_{j=1}^{2}\int\limits_{a^{(j)}-1/n}^{a^{(j)}+1/n}|\tilde{U}(x)|^q d\mu(x)\right)^{1/q}\leq$$

$$\leq A\left(\mu[a^{(1)}-1/n,a^{(1)}+1/n]+\mu[a^{(2)}-1/n,a^{(2)}+1/n]\right)^{1/q},$$

where $A=\sup\limits_{x}\{\tilde{U}(x)\}$, for $x\in[a^{(1)}-1/n,a^{(1)}+1/n]\bigcup[a^{(2)}-1/n,a^{(2)}+1/n]$. Thus, $\|u_n-U\|_{W^{1,q}}\to 0$ as $n\to\infty$, i.e., for any $\varepsilon>0$ there exist such n_ε that $\|u_n-U\|_{W^{1,q}}\leq\varepsilon$ for all $n\geq n_\varepsilon$. In Fig.2 we have plotted the graphs of $U(x)$ (red solid line) and $u^*(x)$ (blue solid line), where $u^*(x)$ is an example of (3.7) for some $n^*\leq n_\varepsilon$, together with the constant function θ. From the figure it is clear that $u^*(x)$ does not satisfy the θ-condition. □

Theorem 3.8. *Let $\theta>0$ be fixed, $U(x)\in W^{1,\infty}(\mathbb{R},\mu)$ satisfies the θ-condition and $U(x)=\theta$ has, say, N solutions $a^{(1)},a^{(2)},...,a^{(N)}$. Let $\rho_1(x)/\rho(x)$ belong to $L^p(\mathbb{R},\mu)$. (a) There exist $\varepsilon>0$ such that $\mathcal{N}_\infty: B(U,\varepsilon)=\{u:\|u-U\|_{W^{1,\infty}}<\varepsilon\}\to L^p(\mathbb{R},\mu)$ is continuous when $1\leq p<\infty$. (b) The operator $\mathcal{N}_\infty: B(U,\varepsilon)\to L^\infty(\mathbb{R},\mu)$ is continuous*

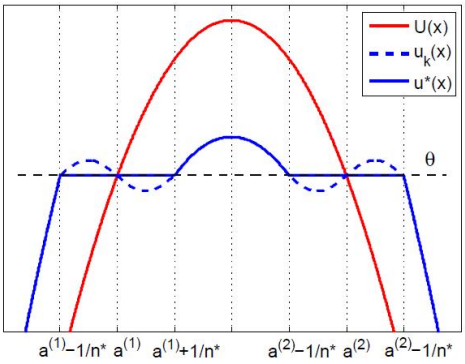

FIGURE 2. The violation of the θ-condition in $W^{1,q}(\mathbb{R},\mu)$ for $q<\infty$.

provided that there exist some $\delta>0$ *that* $\mathrm{supp}(\rho_1)\bigcap(a^{(k)}-\delta,a^{(k)}+\delta)=\emptyset$ *for any* $k=1,2,...,N$. *Otherwise, i.e., if for any* $\delta>0$ *there exist some* $\hat{k}$ *such that* $\mathrm{supp}(\rho_1)\bigcap(a^{(\hat{k})}-\delta,a^{(\hat{k})}+\delta)\neq\emptyset$, *we get discontinuity of* $\mathcal{N}_\infty: B(U,\varepsilon)\to L^\infty(\mathbb{R},\mu)$.

Proof. Let us consider $u_n,\ u\in B(U,\varepsilon)\subset W^{1,\infty}(\mathbb{R},\mu)$ such that $||u_n-u||_{W^{1,\infty}}\to 0$. By Lemma 3.6 it is always possible to choose ε in a such way that both u_n and u satisfy the θ-condition and the equations $u_n(x)=\theta$, $u(x)=\theta$ possess N simple roots each. We denote these roots as $a_n^{(k)}$ for the first equation, and $a_0^{(k)}$ for the second, $k=1,...,N$.

We derive the estimate

$$|(N_\infty u_n)(x)-(N_\infty u)(x)|=|\rho_1(x)/\rho(x)|\,\chi(x),$$

where

$$\chi(x)=\begin{cases}1, & x\in\bigcup\limits_{k=1}^{N}[a_n^{(k)},a_0^{(k)}],\\ \\ 0, & \text{otherwise.}\end{cases}$$

Here $[x_1,x_2]$ defines the interval $[x_1,x_2]$ when $x_2\geq x_1$ and $[x_2,x_1]$ if $x_2<x_1$.

First we consider $p<\infty$. Then, after the lemma (follows below), the case $p=\infty$ will be considered. When $1\leq p<\infty$ we have the following equality

$$\|(N_\infty u_n)(x)-(N_\infty u)(x)\|_{L^p}=\left(\int_{\mathbb{R}}\left|\frac{\rho_1(x)}{\rho(x)}\right|^p\chi(x)d\mu(x)\right)^{1/p}$$

Using now the Hölder inequality we get

$$\left(\int_{\mathbb{R}}\left|\frac{\rho_1(x)}{\rho(x)}\right|^p\chi(x)d\mu(x)\right)^{1/p}\leq\|\rho_1/\rho\|_{L^\infty}\left(\mu(\bigcup_{k=1}^{N}[a_n^k,a_0^k])\right)^{1/p}.$$

Since $|\rho_1(x)/\rho(x)|\in L^p(\mathbb{R},\mu)\subset L^\infty(\mathbb{R},\mu)$ then $\|\rho_1/\rho\|_{L^\infty}\leq C_\rho$, where $C_\rho>0$ is some constant. If now $\mu(\bigcup\limits_{k=1}^{N}[a_n^{(k)},a_0^{(k)}])\to 0$ as $n\to\infty$ we get the continuity of $N_\infty: B(U,\varepsilon)\to L^p(\mathbb{R},\mu)$. To prove that we use the following lemma.

Lemma 3.9. *For any $u_n,\ u\in B(U,\varepsilon)\subset W^{1,\infty}(\mathbb{R},\mu)$ such that $||u_n-u||_{W^{1,\infty}}\to 0$ we have $a_n^{(k)}\to a_0^{(k)}$.*

Proof. For our proof we use the norm (2.2) of $W^{1,\infty}(\mathbb{R},\mu)$. From $||u_n-u||_{W^{1,\infty}}\to 0$ follows that $\sup\limits_{x\in\mathbb{R}}|u_n(x)-u(x)|\to 0$.

Let us assume the contrary, i.e., there is $k=k^*$ such that $a_n^{(k^*)}\not\to a_0^{(k^*)}$. This means that

$$(\exists\sigma_0>0)\ (\forall N\in\mathbb{N})\ (\exists\tilde{n}\geq N):\ |a_{\tilde{n}}^{(k^*)}-a_0^{(k^*)}|\geq\sigma_0.$$

Then we have

$$\sup_{x\in\mathbb{R}}|u_{\tilde{n}}(x)-u(x)|\geq|u_{\tilde{n}}(a_{\tilde{n}}^{(k^*)})-u(a_{\tilde{n}}^{(k^*)})|=|\theta-u(a_{\tilde{n}}^{(k^*)})|=|u(a_0^{(k^*)})-u(a_{\tilde{n}}^{(k^*)})|.$$

Due to the transversality condition on the intersection of any $u(x)\in B(U,\varepsilon)$ and θ we have $|u(a)-u(b)|\geq\kappa$ if $|a-b|\geq\sigma_0$.

Thus

$$(\forall N\in\mathbb{N})\ (\exists\tilde{n}\geq N):\ \sup_{x\in\mathbb{R}}|u_{\tilde{n}}(x)-u(x)|>\kappa.$$

By definition $\sup\limits_{x\in\mathbb{R}}|u_n(x)-u(x)|$ diverges. Then $||u_n-u||_{W^{1,\infty}}$ diverges too. This contradiction completes the proof of the lemma. □

Next, we consider the case $p=\infty$. We get

$$\|N_\infty u_n-N_\infty u\|_{L^\infty}=\sup_{x\in\mathbb{R}}|(N_\infty u_n)(x)-(N_\infty u)(x)|=\alpha_n,$$

where α_n is a smallest value that $\mu\{x:\ |(N_\infty u_n)(x)-(N_\infty u)(x)|\geq\alpha_n\}=0$, i.e.,

$$\alpha_n=\sup_{x\in Q}|\rho_1(x)/\rho(x)|,\quad Q=\bigcup_{k=1}^{N}[a_n^{(k)},a_0^{(k)}].$$

Let us assume first that there is some $\delta>0$ such that $\mathrm{supp}(\rho_1)\bigcap(a^{(k)}-\delta,a^{(k)}+\delta)=\emptyset$ for any $k=1,2,...,N$. This means that $\mathrm{supp}(\rho_1)\bigcap Q=\emptyset$ which implies $\alpha_n=0$. Thus, $\mathcal{N}_\infty$ is continuous. Assume now that $\mathrm{supp}(\rho_1)\bigcap Q\neq\emptyset$. Due to $\rho_1(x)>0$ for all $x\in\mathrm{supp}(\rho_1)$ we have $\alpha_n=0$ if and only if $a_n^{(k)}=a_0^{(k)}$, for all $k=1,2,...,N$. That is not necessarily the case, thus, $\mathcal{N}_\infty$ discontinuous on $B(U,\varepsilon)$. □

Remark 3.10. *We notice here that the assumption* $\mathrm{supp}(\rho_1)\bigcap(a^{(k)}-\delta, a^{(k)}+\delta)=\emptyset$ *for all* $k=1,2,...,N$ *is not interesting here, as it breaks properties of the model. Thus, further we exclude these types of* ρ_1 *from consideration.*

Theorem 3.11. *Let* θ *be fixed,* $U(x)\in W^{1,q}(\mathbb{R},\mu)$, $1\le q<\infty$, *satisfies the* $\theta-$*condition. There exist no such* $\varepsilon>0$ *that* $\mathcal{N}_\infty : B(U,\varepsilon)\subset W^{1,q}(\mathbb{R},\mu)\to L^p(\mathbb{R},\mu)$, $1\le p\le\infty$ *is continuous operator.*

Proof. In Lemma 3.7 it has been shown that for any $\varepsilon>0$ there exists some n_ε that u_n, given by (3.7), for all $n\ge n_\varepsilon$ belongs to the ball $B(U,\varepsilon)$. We fix $n^*=n_{\varepsilon/2}$ and denote $u^*=u_{n_{\varepsilon/2}}$. Then we consider the sequence $u_k(x)$ given as

$$u_k(x)=\begin{cases}\theta-\dfrac{1}{\gamma k}\sin(\pi n^*(x-a_1)), & x\in[a_1-1/n^*,a_1+1/n^*]\\[2ex] \theta+\dfrac{1}{\gamma k}\sin(\pi n^*(x-a_2)), & x\in[a_2-1/n^*,a_2+1/n^*]\\[2ex] u^*(x), & \text{otherwise}\end{cases}$$

where γ is a positive constant. We have plotted the graphs of $U(x)$ (red solid line), $u^*(x)$ (blue solid line), and $u_k(x)$ (blue dashed line) in Fig.2 together with the constant θ. First, we prove that $u_k\to u^*$ and show that there exist $\gamma=\gamma^*$ such that $u^k\in B(U,\varepsilon)$. Next we prove that $\|\mathcal{N}_\infty u_k-\mathcal{N}_\infty u^*\|_{L^p}$ does not converges to zero.

We calculate the norm of $|u_k(x)-u^*(x)|$ using (2.3) and derive the following inequality

$$\|u_k-u^*\|_{W^{1,q}}=\|\tilde{u}_k-\tilde{u^*}\|_{L^q}=\|(u_k'-(u^*)')\rho^{-1}(x)\|_{L^q}=$$
$$=\left(\sum_{j=1}^{2}\int\limits_{a^{(j)}-1/n^*}^{a^{(j)}+1/n^*}\left|\frac{1}{\pi n^*\gamma k}\cos(\pi n^*(x-a^{(j)}))\right|^q dx\right)^{1/q}\le$$
$$\le\frac{1}{\pi n^*\gamma k}\left(\sum_{j=1}^{2}\left|(a^{(j)}+1/n^*)-(a^{(j)}-1/n^*)\right|\right)^{1/q}=\frac{1}{\pi n^*\gamma k}\left(\frac{2}{n^*}\right)^{1/q}.$$

From this inequality we see that $\|u_k-u^*\|_{W^{1,q}}\to 0$ as $k\to\infty$. Moreover, as we assign $\gamma^*=2/(\varepsilon\pi n^*)$ we get $\|u_k-u^*\|_{W^{1,q}}\le\varepsilon/2$. We have

$$\|u_k-U\|_{W^{1,q}}\le\|u_k-u^*\|_{W^{1,q}}+\|u^*-U\|_{W^{1,q}}\le\varepsilon/2+\varepsilon/2=\varepsilon,$$

for $k=1,2,...$, i.e., $u_k\in B(U,\varepsilon)$ for all $k\in\mathbb{N}$.

Using the definition of $\mathcal{N}_\infty$ we have

$$|(\mathcal{N}_\infty u_k)(x)-(\mathcal{N}u^*)(x)| = \begin{cases} \dfrac{\rho_1(x)}{\rho(x)}, & x \in \bigcup\limits_{j=1}^{2}[a^{(j)} - 1/n^*, a^{(j)} + /n^*], \\ 0, & \text{otherwise} \end{cases}.$$

Due to $\rho_1(x)/\rho(x) > 0$ we have $\|(\mathcal{N}_\infty u_k)(x) - (\mathcal{N}u^*)(x)\|_{L^p} = \delta > 0$ independently of k. Hence, we conclude that $(\mathcal{N}_\infty u_k)(x)$ does not converges to $(\mathcal{N}u^*)(x)$. It completes our proof.

□

Now we consider the Nemytskii operator $\mathcal{N}_\beta$ when β is not fixed, but belongs to $(0,\infty]$. Then, $\mathcal{N}_\beta$ is a map $(0,\infty]\times B(U,\varepsilon) \subset W^{1,\infty}(\mathbb{R},\mu) \to W^{1,\infty}(\mathbb{R},\mu)$. We have the following lemma.

Lemma 3.12. *Let $\theta > 0$ be fixed, $U \in W^{1,\infty}(\mathbb{R},\mu)$ satisfy the θ-condition, $\rho_1/\rho \in L^1(\mathbb{R},\mu)$ and $B(U,\varepsilon) = \{u : \|u - U\|_{W^{1,\infty}} < \varepsilon\}$. The operator $\mathcal{N}_\beta : (0,\infty]\times B(U,\varepsilon) \to L^1(\mathbb{R},\mu)$ is continuous at $\beta_0 \in (0,\infty]$ uniformly for all $u \in B(U,\varepsilon)$.*

Proof. From Lemma 3.3 and Theorem 3.8 $\mathcal{N}_\beta$ is a map from $(0,\infty]\times B(U,\varepsilon)$ to $L^1(\mathbb{R},\mu)$. Using properties of ρ_1 we have

$$||\mathcal{N}_\beta - \mathcal{N}_{\beta_0}||_{L^1} \le C_{\rho_1}\int\limits_{\mathbb{R}} |S(\beta,u(x)) - S(\infty,u(x))|dx.$$

For $\beta_0 < \infty$ from uniform convergence $S(\beta,z) \to S(\beta_0,z)$ we get pointwise convergence $S(\beta,u(x)) \to S(\beta_0,u(x))$. Boundedness of S allows us to applying Lebesque's dominated convergence theorem. Thus, we get

$$||\mathcal{N}_\beta - \mathcal{N}_{\beta_0}||_{L^1} \to 0, \quad \forall u \in B(U,\varepsilon). \tag{3.8}$$

When $\beta_0 = \infty$ the proof is not so straightforward. By Lemma 3.6 there is $\varepsilon > 0$ such that for given U there are defined $b^{(k,i)}$ ($k = 1,...,N$, $i = 1,2$) such that for any $u \in B(U,\varepsilon)$ the conditions (A1)-(A3) are satisfied. We have

$$\begin{aligned} ||\mathcal{N}_\beta - \mathcal{N}_\infty||_{L^1} &\le C_{\rho_1}\int\limits_{\mathbb{R}} |S(\beta,u(x)) - S(\infty,u(x))|dx = \\ &= \sum_{k=0}^{N}\int\limits_{b^{(k,1)}}^{b^{(k,2)}} |S(\beta,u(x)) - S(\infty,u(x))|dx = C_{\rho_1}(\Sigma_1 + \Sigma_2), \end{aligned} \tag{3.9}$$

where

$$\Sigma_1 = \sum_{k=0}^{N}\int\limits_{b^{(k,1)}}^{b^{(k,2)}} |S(\beta,u(x)) - S(\infty,u(x))|dx$$

and

$$\Sigma_2 = \sum_{k=0}^{N-1} \int\limits_{b^{(k,2)}}^{b^{(k+1,1)}} |S(\beta, u(x)) - S(\infty, u(x))| dx.$$

Notice, that Σ_1 contains only the integrals over such intervals that $S(\infty, u(x))$ does not have singularities, see for example Fig.1.

Let us consider first Σ_1 and then Σ_2. Using (A1)-(A2) we have

$$\Sigma_1 = \sum_{m=0}^{N/2} \int\limits_{b^{(2m,1)}}^{b^{(2m,2)}} |S(\beta, u(x)) - S(\infty, u(x))| dx +$$

$$+ \sum_{m=0}^{N/2-1} \int\limits_{b^{2m+1,1}}^{b^{(2m+1,2)}} |S(\beta, u(x)) - S(\infty, u(x))| dx \leq$$

$$\leq \sum_{m=0}^{N/2} \int\limits_{b^{(2m,1)}}^{b^{(2m,2)}} S(\beta, \theta - \varepsilon) dx + \sum_{m=0}^{N/2-1} \int\limits_{b^{(2m+1,1)}}^{b^{(2m+1,2)}} (1 - S(\beta, \theta + \varepsilon)) dx \leq$$

$$\leq S(\beta, \theta - \varepsilon) \sum_{m=0}^{N/2} (b^{(2m,2)} - b^{(2m,1)}) +$$

$$+ (1 - S(\beta, \theta + \varepsilon)) \sum_{m=0}^{N/2-1} (b^{(2m+1,2)} - b^{(2m+1,1)})$$

Using the property (iii) of $S(\beta, x)$ we have $\Sigma_1 \to 0$ as $\beta \to \infty$.

Consider now the second term in (3.9). On each interval $[b^{(k,2)}, b^{(k+1,1)}]$ the function $u(x)$ is monotone. Using the condition (A3) we get

$$\Sigma_2 \leq \int\limits_{U_{\min}}^{U_{\max}} |S(\beta, y) - S(\infty, y)| \frac{dy}{|u'(x)|} \leq \frac{1}{M\varepsilon} \int\limits_{U_{\min}}^{U_{\max}} |S(\beta, y) - S(\infty, y)| dy,$$

where $M = \sup\limits_{x \in \mathbb{R}} \rho(x)$, $U_{\min} = \inf\limits_{x \in \mathbb{R}} U(x)$, and $U_{\max} = \sup\limits_{x \in \mathbb{R}} U(x)$. Since $S(\beta, x) \to S(\infty, x)$ as $\beta \to \infty$ almost everywhere on $\mathbb{R}$ (see property (iii) of $S(\beta, x)$) and $|S(\beta, x)| \leq 1$ for all $\beta \in (0, \infty]$, then by Lebesque's dominance convergence theorem, the integral in the last inequality converges to 0 as $\beta \to \infty$. Combining the results for Σ_1 and Σ_2 we complete the proof. □

Theorem 3.13. *Let $\theta > 0$ be fixed and let $U \in W^{1,\infty}(\mathbb{R}, \mu)$ satisfy the θ-condition. We define a set Q as $Q = \operatorname{supp}(\rho)$ and a ball $B(U, \varepsilon) = \{u : \|u - U\|_{W^{1,\infty}} < \varepsilon\}$. If the following condition is fulfilled*

$$\sup_{x \in Q} \left(\sup_{y \in Q} \left| \frac{\omega'_x(x, y)}{\rho(x)\rho_1(y)} \right| \right) < \infty, \tag{3.10}$$

then there exists $\varepsilon > 0$ that the Hammerstein operator $\mathcal{H}_\beta : (0,\infty] \times B(U,\varepsilon)$ is continuous at $\beta_0 \in (0,\infty]$ uniformly for all $u \in B(U,\varepsilon)$.

Proof. We consider the norm of $|(\mathcal{H}_\beta u)(x) - (\mathcal{H}_{\beta_0} u)(x)|$ in $W^{1,\infty}(\mathbb{R},\mu)$ given by (2.3). Here u is an arbitrary function from the ball $B(U,\varepsilon)$. We have

$$\|\mathcal{H}_\beta u - \mathcal{H}_{\beta_0} u\|_{W^{1,\infty}} = |(\mathcal{H}_\beta u)(0) - (\mathcal{H}_{\beta_0} u)(0)| + \|(\tilde{\Omega}\circ\mathcal{N}_\beta)u - (\tilde{\Omega}\circ\mathcal{N}_{\beta_0})u\|_{L^\infty}.$$

Here $\tilde{\Omega}$ is given as in (3.5). We consider the first and the second term separately.

$$\begin{aligned} |(\mathcal{H}_\beta u)(0) - (\mathcal{H}_{\beta_0} u)(0)| = \\ = \Big| \int_{\mathbb{R}} \frac{\omega(0,y)}{\rho(y)} (S(\beta, u(y)) - S(\beta_0, u(y)))\, d\mu(y) \Big| \le \\ \le \int_{\mathbb{R}} \Big| \frac{\omega(0,y)}{\rho_1(y)} \Big| \Big| \frac{\rho_1(y)}{\rho(y)} \Big| |S(\beta, u(y)) - S(\beta_0, u(y))|\, d\mu(y)| \le \\ \le C_\omega \|\mathcal{N}_\beta u - \mathcal{N}_{\beta_0} u\|_{L^1} \end{aligned}$$

By Lemma 3.12 $|(\mathcal{H}_\beta u)(0) - (\mathcal{H}_{\beta_0} u)(0)|$ uniformly converges to zero.

Under the conditions of the theorem $\tilde{\Omega} : L^1(\mathbb{R},\mu) \to L^\infty(\mathbb{R},\mu)$ is bounded. Indeed, using the Hölder inequality we get

$$\|\tilde{\Omega} v\|_{L^\infty} \le C_{\tilde{\Omega}} \|u\|_{L^1}, \quad C_{\tilde{\Omega}} = \sup_{x\in Q} \left(\sup_{y \in Q} \left| \frac{\omega'_x(x,y)}{\rho(x)\rho_1(y)} \right| \right) < \infty.$$

Then it is easy to see that

$$\|(\tilde{\Omega}\circ\mathcal{N}_\beta)u - (\tilde{\Omega}\circ\mathcal{N}_{\beta_0})u\|_{L^\infty} \le C_{\tilde{\Omega}} \|\mathcal{N}_\beta u - \mathcal{N}_{\beta_0} u\|_{L^1}.$$

Applying Lemma 3.12 we complete our proof. □

We formulate our main theorem.

Theorem 3.14 (Continuous dependence)**.** *Let $\theta > 0$ be fixed and $U \in W^{1,\infty}(\mathbb{R},\mu)$ satisfy the θ-condition. Assume that $1 \le p < \infty$ and $\rho_1/\rho \in L^p(\mathbb{R},\mu)$, the operator Ω in (3.3) is a compact operator from $L^p(\mathbb{R},\mu)$ to $W^{1,\infty}(\mathbb{R},\mu)$, and (3.10) is satisfied. If there exist solutions of the equation $\mathcal{H}_\beta u_\beta = u_\beta$ which belong to $B(U,\varepsilon) = \{u : \|u - U\|_{W^{1,\infty}} < \varepsilon\}$ for any $\beta \in [C_\beta, \infty]$, $C_\beta > 0$, then there exist a solution of $\mathcal{H}_\infty u = u$ and it is any limiting point of the sequence $\{u_\beta\}$. Moreover, if the solution of $\mathcal{H}_\infty u = u$, say u^*, is unique then $\{u_\beta\} \to u^*$.*

Proof. We base our proof on Theorem 2.3. We choose D (in Theorem 2.3) to be a closure of $B(U,\varepsilon) = \{u : \|u - U\|_{W^{1,\infty}} < \varepsilon\}$, and $\lambda = 1/\beta$ and, thus, $\Lambda = [0, 1/C_\beta]$. The operator $\mathcal{H}_\beta \equiv \mathcal{H}_{1/\lambda} : \Lambda \times \overline{B(U,\varepsilon)} \to W^{1,\infty}(\mathbb{R},\mu)$ is continuous as a superposition of continuous operators, Ω and $N_{1/\lambda}$, for each $\lambda \in \Lambda$. The operator $\Omega : L^p(\mathbb{R},\mu) \to W^{1,\infty}(\mathbb{R},\mu)$ is

continuous by the conditions of the theorem, and continuity of $N_{1/\lambda}$: $\overline{B(U,\varepsilon)} \to L^p(\mathbb{R},\mu)$ follows from Lemma 3.3 (for $\lambda > 0$) and Theorem 3.8 (for $\lambda = 0$). Moreover, from Theorem 3.13 we conclude that $\mathcal{H}_{1/\lambda} : \Lambda \times \overline{B(U,\varepsilon)} \to W^{1,\infty}(\mathbb{R},\mu)$ is continuous with respect to both variables.

The observation that the operators $\mathcal{H}_{1/\lambda}$ are collectively compact as a superposition of a compact operator Ω and collectively bounded operators $\mathcal{N}_{1/\lambda}$ completes the proof. □

It is usually much easier to study the existence of solutions (which satisfy the θ-condition) of the fixed point problem $\mathcal{H}_\infty u = u$ than $\mathcal{H}_\beta u = u$, $\beta < \infty$. Next theorem allows us to prove existence of the fixed points of $\mathcal{H}_\beta$ using some knowledge about the fixed point of the limiting problem. We give more details on existence of fixed points of $\mathcal{H}_\infty$ in the next section.

Theorem 3.15 (Existence)**.** *Let the conditions of Theorem 3.14 be satisfied, i.e., $\theta > 0$ be fixed, $U \in W^{1,\infty}(\mathbb{R},\mu)$ satisfy the θ-condition, $\rho_1/\rho \in L^p(\mathbb{R},\mu)$, $1 \le p < \infty$, the operator $\Omega : L^p(\mathbb{R},\mu) \to W^{1,\infty}(\mathbb{R},\mu)$ is compact, and* (3.10) *is fulfilled. Let B_0 define an open subset of $B(U,\varepsilon) = \{u : \|u - U\|_{W^{1,\infty}} < \varepsilon\}$. If U is a unique fixed point of the operator $\mathcal{H}_\infty$ on $\overline{B_0}$ such that $\deg(\mathcal{H}_\infty - I, B_0, 0) \neq 0$, then $\mathcal{H}_\beta$ possesses a fixed point $u_\beta \in B_0$ for any $\beta >> 1$.*

Proof. We define $h_t(u) = (\mathcal{H}_{k/t} - I)(u)$, where I is an identity operator, $t \in [0,1]$, and $k \ge 1$. We show that h_t is a homotopy, i.e., (a) continuous with respect to t and u for all $t \in [0,1]$ and $u \in \overline{B_0}$, (b) $h_t(u) \neq 0$ for any $t \in [0,1]$ and $u \in \partial B_0$. The property (a) is satisfied. Indeed $\mathcal{H}_{k/t}$ is continuous (for details see proof of Theorem (3.14)) and thus, $\mathcal{H}_{k/t} - I$ is continuous as well.

In the proof of (b) we first observe that $\mathcal{H}_\infty u \neq u$ for all $u \in \partial B_0$ since U is a unique solution on $\bar{B}_0$ and $U \in B_0$. Assume that $\mathcal{H}_\beta u \neq u$ for all $u \in \partial B_0$ does not hold true, i.e., there exist $\{u_n\} \in \partial B_0$ such that $\mathcal{H}_{\beta_n} u_n = u_n$. From Theorem 3.14 it follows that $u_n \to u_0 \in \partial B_0$ where $u_0 = \mathcal{H}_\infty u_0$. This contradiction competes the proof of (b). It is easy to see that h_t satisfies the conditions of Theorem 2.5 and thus, $\deg(h_t, B_0, 0) = \deg(\mathcal{H}_\infty - I, B_0, 0) \neq 0$ for any $t \in [0,1]$. This implies existence of solutions of $\mathcal{H}_{k/t} u = u$ belonging to $B_0 \in B(U,\varepsilon)$. □

4. Bumps in neural field model

Definition 4.1. *Let $\theta > 0$ be fixed, and U be a stationary solution of* (1.1) *where $P(u) = S(\infty, u)$. A set $R[U] = \{x : U(x) \ge \theta\}$ is called an excited region of U,* [4].

Definition 4.2. *Let $\theta > 0$ be fixed, and U be a stationary solution of* (1.1) *where $P(u) = S(\infty, u)$. If the excited region of U is such that*

$R[U] = \bigcup_{k=1}^{N} [a^{(2k-1)}, a^{(2k)}]$ *and* $U'(a^{(k)}) \neq 0$, $k = 1, ..., 2N$ *then* $U(x)$ *is called a bump, or more specificity,* N*-bump.*

The existence of 1-bump solutions was studied in [4]. Later, 2-bumps and multibumps were considered in [17, 18]. In all these cases the connectivity function was assumed to be translation homogeneous, i.e., $\omega(x, y) = \varpi(x - y)$ where $\varpi(z)$ is an even function. These type of solutions were linked to the mechanisms of the working memory, representations in the head-direction system, and feature selectivity in the visual cortex, see [5] and references therein.

Remark 4.3. *Although the condition* $U'(a^{(k)}) \neq 0$, $k = 1, ..., 2N$ *was not postulated in* [4]*, it was used for studying stability of these bumps.*

Theorem 4.4. *A bump solution of* (1.1) *with* $P(u) = S(\infty, u)$ *belongs to* $W^{1,\infty}(\mathbb{R}, \mu)$ *and satisfy the* θ*-condition.*

Proof. By Definition 4.2 and (3.1) a bump is given as

$$U(x) = \int\limits_{R[U]} \omega(x, y)dy. \tag{4.1}$$

We use the norm (2.3) and get the following estimate

$$\|U\|_{W^{1,\infty}} = |\int\limits_{R[U]} \omega(0, y)dy| + \sup_{x\in\mathbb{R}} |\rho(x) \int\limits_{R[U]} \omega'_x(x, y)dy| \leq$$

$$\leq \int\limits_{R[U]} |\omega(0, y)|dy + M \sup_{x\in\mathbb{R}} \int\limits_{R[U]} |\omega'_x(x, y)|dy, \quad M = \sup_{x\in\mathbb{R}} \rho(x).$$

Applying the property (i) of ω to the first term of the sum, and the property (ii) to the second, we get $\|U\|_{W^{1,\infty}} < \infty$, i.e., $u \in W^{1,\infty}(\mathbb{R}, \mu)$.

Next, we show that U satisfies the θ-condition. By the definition of bumps the first condition of Definition 3.4 is fulfilled. To show that the second one is fulfilled as well we consider the limit

$$\lim_{|x|\to\infty} U(x) = \lim_{|x|\to\infty} \int\limits_{R[U]} w(x, y)dy.$$

The properties (iii) and (iv) of ω allows us to apply Lebesque's dominated convergence theorem, i.e., we get $\lim\limits_{|x|\to\infty} U(x) = 0$. This observations complete the proof. □

Below we give two examples where quite simple requirements on $\omega(x, y)$ allow us to choose ρ, ρ_1 in a such way that all conditions of Theorem 3.14 are satisfied.

Example 4.5. *For any ω such that*

$$|\frac{\partial^m \omega(x,y)}{\partial x^n}| \le Ce^{-a|x|}e^{-b|y|}, \quad m = 1, 2,\ a, b > 0, \tag{4.2}$$

the conditions of Theorem 3.14 are satisfied.

Proof. We set

$$\rho_1(x) = e^{-\alpha|x|}, \quad \rho(x) = \frac{\beta}{2}e^{-\beta|x|}, \tag{4.3}$$

for some positive α and β. To satisfy the first condition of Theorem 3.14 ($\rho_1/\rho \in L^p(\mathbb{R}, \mu)$, $1 \le p < \infty$), it is sufficient to fulfill the following inequality $p(\alpha - \beta) + \beta > 0$ or, equivalently,

$$\begin{array}{ll} \alpha > 0 & \text{if } p = 1, \\ \beta > \alpha p' & \text{if } p > 1. \end{array}$$

Let us now focus on the second condition of Theorem 3.14 (Ω is compact). By Lemma 3.2 it is sufficient to prove compactness of $\tilde{\Omega}$ given by (3.5). We use Lemma 2.2. We denote the kernel of the operator $\tilde{\Omega}$ as $k(x, y)$. Using the estimates (4.2) and (4.3) we have

$$|k(x,y)| \le 2\frac{C}{\beta}e^{-(a-\alpha)|x|}e^{-(b-\beta)|y|}, \tag{4.4}$$

and

$$|k'_x(x,y)| \le \frac{|\omega''_{xx}(x,y)| + |\rho'(x)/\rho(x)||\omega'_x(x,y)|}{\rho_1(y)\rho(x)} \le$$
$$\le \frac{|\omega''_{xx}(x,y)| + \alpha|\omega'_x(x,y)|}{\rho_1(y)\rho(x)} \le 2C'\frac{1+\alpha}{\alpha}e^{-(a-\alpha)|x|}e^{-(b-\beta)|y|}.$$

Moreover, the requirement

$$a > \alpha, \quad b > \beta, \tag{4.5}$$

implies that both conditions of Lemma 2.2 are satisfied. While it is obvious that $k(x, \cdot) \in L^{p'}(\mathbb{R}, \mu)$ for almost all $x \in \mathbb{R}$, (2.6) is needed to be explained. We notice that

$$|k(x,y)| \le C_1e^{-c|x|}, \quad |k'_x(x,y)| \le C_2e^{-c|x|}, \tag{4.6}$$

where $c = a - \alpha > 0$, and $C_1, C_2 > 0$. First, we assign A to be some constant larger than $c^{-1}\ln(2C_1/\varepsilon)$. Then, for $|x| > A$ we have $C_1e^{-c|x|} < \varepsilon/2$ and for any $x_1, x_2 :\ |x_1| > A,\ |x_2| > A$ we get

$$|k(x_1,y) - k(x_2,y)| \le C_1(e^{-c|x_1|} + e^{-c|x_2|}) < \varepsilon/2 + \varepsilon/2 = \varepsilon. \tag{4.7}$$

Next, using the mean value theorem we have

$$\begin{aligned} |k(x_1,y) - k(x_2,y)| &\le |k'_x(\tilde{x},y)(x_2 - x_1)| \le \\ &\le C_2e^{-c|\tilde{x}|}|x_2 - x_1| \le C_2|x_2 - x_1|, \end{aligned} \tag{4.8}$$

where $\tilde{x} = \lambda x_1 + (1-\lambda x_2)$, $\lambda \in [0,1]$. We define some $\Delta:\ 0 < \Delta < \varepsilon/C_2$ and set

$$D_1 = (\infty, -A),\ D_2 = (-A, -A+\Delta),$$
$$D_3 = (-A+\Delta, -A+2\Delta),\ \dots D_n = (-A+n\Delta, +\infty),$$

where n is defined in a such way that $-A+n\Delta > A$, e.g., $n = [2A/\Delta]+1$. Therefore, (2.6) is fulfilled for $j = 1, n$ due to (4.7), and for $j = 2, 3, ..., n-1$ due to (4.8). Thus, under assumptions (4.5) the operator $\tilde{\Omega}$ maps $L^p(\mathbb{R}, \mu)$ to $L^\infty(\mathbb{R}, \mu)$ and is compact.

Combining all the restrictions on α, β we have

$$\begin{array}{ll} 0 < \alpha < a,\ 0 < \beta < b & \text{if } p = 1, \\ 0 < \alpha < a,\ \alpha p' < \beta < b & \text{if } p > 1. \end{array} \tag{4.9}$$

It is clear that for any given $a, b > 0$, and $1 \le p < \infty$ it is always possible to choose α and β satisfying (4.9).

Finally, using (4.4) it is easy to see that (3.10) is valid. □

The case when $\omega(x,y) = \varpi(x-y)$ seems to be more complicated. The main difficulty here is that the kernel of the operator Ω becomes unbounded along the line $y = x$. We have not found a general approach how to deal with this problem. However, the theory developed in previous section works very well for the family of firing rate functions, $S(\beta, u)$, which possesses the following property:

$$S(\beta, u) = 0 \ \text{ for all } \ u \le \theta - \tau, \ \text{ and } \ \beta > 0. \tag{4.10}$$

Example 4.6. *Let ω be given as $\omega(x,y) = \varpi(x-y)$ with $\varpi(z)$ such that*

$$\varpi^{(m)}(z) \le Ce^{-c|z|}, \quad m = 1, 2. \tag{4.11}$$

In addition to the properties of S, we assume (4.10)*. Then there exist such $\tau > 0$ that the conditions of Theorem 3.14 are satisfied.*

Proof. Let $\theta > 0$ be fixed and $U \in W^{1,\infty}(\mathbb{R}, \mu)$ satisfy the θ-condition. Moreover, assume that $U(x) = \theta$ has N solutions. Then, by Lemma 3.6 there exist such $\varepsilon > 0$, and $b^{(0,2)},\ b^{(N,1)}$ that for any $u \in B(U, \varepsilon) = \{u : \|u - U\|_{W^{1,\infty}} < \varepsilon\}$ the following inequality $U(x) < \theta - \varepsilon$ for all $x \in (-\infty, b^{(0,2)}) \cup (b^{(N,1)}, \infty)$ is valid.

We introduce a set $D = [b^{(0,2)}, b^{(N,1)}]$. Next, we set $\tau < \varepsilon$ and define

$$\rho(x) \equiv \rho_1(x) = \begin{cases} 1/(b^{(N,1)} - b^{(0,2)}), & x \in D, \\ 0, & x \notin D. \end{cases}$$

This definition of ρ implies that $L^s(\mathbb{R}, \mu) \equiv L^s(D)$ and $W^{1,s}(\mathbb{R}, \mu) \equiv W^{1,s}(D)$ for any $1 \le s \le \infty$.

By Theorem 3.3 and Theorem 3.8 $\mathcal{N}$ is a continuous map from $B(U, \varepsilon)$ to $L^p(D)$.

Using Lemma 3.2 and Lemma 2.2 we next show that the operator Ω is compact operator from $L^p(D)$ to $W^{1,\infty}(D)$. The operator $\tilde{\Omega}$ is given by

$$(\tilde{\Omega}u)(x) = \int_D \varpi'(y-x)u(y)dy, \quad x \in D.$$

Due to the estimate (4.11) the first condition of Lemma 2.2 is satisfied. It remains to check the second condition of Lemma 2.2. Making use of the mean value theorem and (4.11) for $m = 2$, we get

$$\|\varpi'(x_1 - y) - \varpi'(x_2 - y)\|_{L^{p'}} \leq \|\varpi''(\tilde{x} - y)\|_{L^{p'}}|x_2 - x_1| \leq C|x_2 - x_1|.$$

Here we assume $\tilde{x} = \lambda x_1 + (1 - \lambda x_2)$, $\lambda \in [0, 1]$.

Similarly to Example 4.5 we choose some $\Delta :\ \Delta < \varepsilon/C$ and set

$$D_1 = (b^{(0,2)}, b^{(0,2)} + \Delta), \quad D_2 = (b^{(0,2)} + \Delta, b^{(0,2)} + 2\Delta),$$

$$\ldots, \quad D_n = (b^{(0,2)} + n\Delta, b^{(N,1)}),$$

where n is defined in a such way that $b^{(0,2)} + n\Delta < b^{(N,1)}$ and $b^{(0,2)} + (n+1)\Delta \geq b^{(N,1)}$, e.g., $n = \left[(b^{(N,1)} - b^{(0,2)})/\Delta\right]$. Thus, by Lemma 2.2 $\tilde{\Omega} : L^p(\mathbb{R}, \mu) \to L^\infty(\mathbb{R}, \mu)$ is compact. This implies $\Omega : L^p(\mathbb{R}, \mu) \to W^\infty(\mathbb{R}, \mu)$ be a compact operator, see Lemma 3.2.

Finally, we remark that (3.10) is fulfilled. Hence, all the conditions of Theorem 3.14 are verified. □

In neural field theory one often assumes that $\omega(x, y)$ is given as a homogeneous and distant dependent function, i.e., $\omega(x, y) = \varpi(x - y)$, where ϖ is an even function. In this case any stationary solution of (1.1) is translation invariant.[1] A typical example of a homogeneous connectivity function ϖ is

$$\varpi(x) = M_1 e^{-m_1|x|} - M_2 e^{-m_2|x|},\ M_1 > M_2,\ m_1 > m_2. \tag{4.12}$$

This function is called a 'Mexican-hat' function and models a neural network with local excitation and distal inhibition. This function satisfies (4.11) and thus it is a particular case of Example 4.6. Existence of 1- and 2-bumps for the model (1.1) with $P(\cdot) = S(\infty, \cdot)$ and this type of connection was shown in [4] and [17], respectively.

Next, we formulate our second theorem which rigorously shows that the bumps solutions in the steep firing rate regime approach the bumps solutions of the stationary Wilson-Cowan model in the unit step function approximation of the firing rate function.

Theorem 4.7. *Assume that $\omega(x, y) = \varpi(x - y)$ with ϖ be an even function satisfying* (4.11)*. Let $\theta > 0$ be fixed and U be a symmetric* 1*-bump solution of* (1.1) *where $P(\cdot) = S(\infty, \cdot)$. Moreover, we let $S(\beta, \cdot)$ satisfy the condition* (4.10)*. Then, there exists $\varepsilon > 0$ such that for any $\tau < \varepsilon$ and all $\beta >> 1$ the operator $\mathcal{H}_\beta$ has a fixed point $u_\beta \in$*

[1] i.e., if $U(x)$ is a solution so is $U(x + c)$ for any $c \in \mathbb{R}$.

$B_e(U,\varepsilon) = \{u - \textit{even function:} \|u-U\|_{W^{1,\infty}} < \varepsilon\}$. *Moreover,* u_β *depends continuously on* β, *i.e.,* $u_\beta \to U$ *as* $\beta \to \infty$.

The proof of the theorem involves some knowledge of degree theory and topological fixed point index theory. We do not recall any definitions and properties here but refer a reader to [12].

Proof. We notice that all conditions of Theorem 3.14 are fulfilled, see Example 4.6. This means that if $u = \mathcal{H}_\beta u$ possesses a solution $u_\beta \in B(U,\varepsilon)$ for for all $C_\beta < \beta < \infty$ then $u_\beta \to U$. It remains to show that such u_β exist. For that we are going to use Theorem 3.15 where we choose $B_0 = B_e(U,\varepsilon)$. To be able to apply Theorem 3.15 we need to show that (a) U is a unique fixed point of $\mathcal{H}_\infty$ in $B_e(U,\varepsilon)$ and (b) $\deg(\mathcal{H}_\infty - I, B_e(U,\varepsilon,0)) \neq 0$.

By Theorem 4.4, U satisfies the θ-condition and $U \in W^{1,\infty}(\mathbb{R},\mu)$. By Lemma 3.6 there exists $\varepsilon > 0$ such that any $u \in B(U,\varepsilon) = \{u : \|u - U\|_{W^{1,\infty}} < \varepsilon\}$ satisfies the θ-condition and possesses exactly two intersections with the straight line θ. Obviously, the same properties are valid for $u \in B_e(U,\varepsilon)$, i.e., for any $u \in B_e(U,\varepsilon)$ there is $c_u > 0$ such that $u(\pm c_u) = \theta$, $u'(\pm c_u) \neq 0$. For $u = U$ we denote the intersections as $\pm a$.

We define an auxiliary function

$$W(x) = \int_0^x \varpi(y)dy.$$

Then, for any $u \in B_e(U,\varepsilon)$ there is defined $v(x) = (H_\infty u)(x) = W(x + c_u) - W(x - c_u)$. In particular, we have

$$U(x) = W(x+a) - W(x-a), \tag{4.13}$$

where

$$W(2a) = \theta,\ \varpi(2a) < 0. \tag{4.14}$$

Lemma 4.8. *A symmetric* 1*-bump,* U, *is a unique fixed point of* $\mathcal{H}_\infty$ *on* $B_e(U,\varepsilon)$.

Proof. Let us assume the contrary. Then there exist a sequence $\{u_n\} \in B_e(U,\varepsilon)$ such that $u_n \to U$ and $\mathcal{H}_\infty u_n = u_n$. Similarly to (4.13) and (4.14) we have

$$u_n(x) = W(x + a_n) - W(x - a_n) \tag{4.15}$$

with

$$W(2a_n) = \theta,\ \varpi(2a_n) < 0 \tag{4.16}$$

where we set $a_n = c_{u_n}$.

From Lemma 3.9 we have $a_n \to a$. The condition $\varpi(2a) < 0$ implies that any vicinity of a contains such a_n that $W(2a_n) \neq \theta$. This contradicts with (4.16) and thus, with u_n being a fixed point of $\mathcal{H}_\infty$.

We conclude that U is an isolated fixed point of the operator $\mathcal{H}_\infty$ on $B_e(U,\varepsilon)$. Therefore, without loss of generality we assume that $B_e(U,\varepsilon)$ does not contain any other fixed points than U. We emphasize here, that U is not an isolated fixed point of $\mathcal{H}_\infty$ on $W^{1,\infty}(\mathbb{R},\mu)$ due to the translation invariance translation invariance of bumps in a homogeneous neural field. □

Due to Lemma 4.8 and definition of the topological fixed point index we have

$$\deg(\mathcal{H}_\infty - I, B_e(U,\varepsilon), 0) = \operatorname{ind}(\mathcal{H}_\infty, B_e(U,\varepsilon)).$$

We notice that $\mathcal{H}_\infty$ maps $\overline{B_e(U,\varepsilon)}$ into a manifold $E_M \subset W^{1,\infty}(\mathbb{R},\mu)$, where $E_M = \{v : v = W(\cdot + c) - W(\cdot - c),\ c \in [m, M]\}$. The interval $[m, M]$ is chosen in a such way that it contains c_u for all $u \in \overline{B_e(U,\varepsilon)}$. By Lemma 3.6 this is possible to achieve if one chooses, for example, $m = 0$, and $M = b^{(N,1)}$.
We define $\phi : [m, M] \to E_M$ where $\phi(c) = v(x) \equiv W(x+c) - W(x-c)$, $x \in \mathbb{R}$. Next, we show that ϕ is a homeomorphism.

Lemma 4.9. *The map ϕ is a homeomorphism from $[m, M]$ to E_M, and E_M is ANR*[2].

Proof. First we show that ϕ is bijection. It is a surjection since E_M is defined as an image of $[m, M]$. To prove that ϕ is injection we assume the contrary: Let $c_1, c_2 \in [m, M]$ and $c_1 \neq c_2$ imply $v_1 = v_2$. From $v_1 = v_2$ and $v_1, v_2 \in W^{1,\infty}(\mathbb{R},\mu)$ it follows that $|v_1(x) - v_2(x)| = 0$ for almost all $x \in \mathbb{R}$. Applying the mean value theorem we get

$$\begin{aligned} |v_1(x) - v_2(x)| &= |W(x + c_1) - W(x - c_1) - \\ &\quad - W(x + c_2) + W(x - c_2)| = \\ &= |\varpi(x + \xi) + \varpi(x - \eta)||c_1 - c_2| = 0, \text{ a.e. on } \mathbb{R} \end{aligned} \tag{4.17}$$

where $\xi, \eta \in [c_1, c_2]$.

As $c_1 \neq c_2$ we have

$$\varpi(x + \xi) = -\varpi(x - \eta) \text{ a.e. on } \mathbb{R},$$

or, that is equivalent,

$$\varpi(x + 2(\xi + \eta)) = \varpi(x) \text{ a.e. on } \mathbb{R}.$$

The last equality contradicts with the property (iv) of ω. Thus, ϕ is a bijective map.
Next, we observe that ϕ is differentiable for all $c \in [m, M]$ and $\phi'(c) \neq 0$. Indeed, as we assume the contrary we get

$$\varpi(x + c) = -\varpi(x - c), \text{ a.e. on } \mathbb{R}$$

which implies $4c$ periodicity of ϖ. This contradicts with the property (iv) of ω. Hence, we conclude that ϕ defines a homeomorphism on

[2]Absolute Neighborhood Retract, see [12].

$[m, M]$. Moreover, since $[m, M]$ is a closed convex subset on $\mathbb{R}$ then it is ANR. By properties of homeomorphism $\phi([m, M]) = E_M$ is ANR too.

□

Let $\mathcal{H}'_\infty$ be the excision of $\mathcal{H}_\infty$ on $E_M \cap \overline{B_e(U,\varepsilon)}$, i.e.,

$$\mathcal{H}'_\infty = \mathcal{H}_\infty|_{E_M \cap \overline{B_e(U,\varepsilon)}} : E_M \cap \overline{B_e(U,\varepsilon)} \to E_M. \tag{4.18}$$

The fixed point U belongs to $E_M \cap \overline{B_e(U,\varepsilon)}$ and thus, by the property of the topological fixed point index [12] $\mathcal{H}'_\infty$ is *admissible*[3] compact map and

$$\operatorname{ind}(\mathcal{H}_\infty, B_e(U,\varepsilon)) = \operatorname{ind}(\mathcal{H}'_\infty, E_M \cap B_e(U,\varepsilon)).$$

Next, we apply the topological invariance property of the index and get

$$\operatorname{ind}(\mathcal{H}'_\infty, E_M \cap B_e(U,\varepsilon)) = \operatorname{ind}(\phi^{-1} \circ \mathcal{H}'_\infty \circ \phi, \mathcal{D})$$

where $\mathcal{D}$ denotes the following set $\phi^{-1}(\mathcal{H}_\infty(E_M \cap B_e(U,\varepsilon)))$.
We prove the following lemma which enables us to compute $\operatorname{ind}(\phi^{-1} \circ \mathcal{H}'_\infty \circ \phi, \mathcal{D})$.

Lemma 4.10. *There exist such $\delta > 0$ that $\mathcal{D} = \phi^{-1}(\mathcal{H}_\infty(E_M \cap \overline{B_e(U,\varepsilon)})) \supset [a-\delta, a+\delta]$.*

Proof. The map $\bar{c} : u \mapsto c_u$ is defined for all $u \in \overline{B_e(U,\varepsilon)}$. Let $v(x) = W(x+c) - W(x-c)$, $c \in [m, M]$. Then using the norm (2.3) in $W^{1,\infty}(\mathbb{R}, \mu)$, the equality (4.13), and the mean value theorem we have

$$\|U - v\|_{W^{1,\infty}} = (\|\varpi(\xi_1) + \varpi(\eta_1)\|_{L^\infty} + \|\varpi(x+\xi_2) + \varpi(x-\eta_2)\|_{L^\infty})\,|c-a|,$$

$\xi_i, \eta_i \in [c, a]$, $i = 1, 2$.

Thus, using (4.11) we get

$$\|U - v\|_{W^{1,\infty}} \le 4C|c-a| < \varepsilon,$$

for all $c \in [a-\delta, a+\delta]$, where $\delta < \varepsilon/4C$. From this observation we conclude that

$$\bar{c}(B(U,\varepsilon) \cap E_M) \supset [a-\delta, a+\delta]$$

which implies

$$\mathcal{H}_\infty(\overline{B_e(U,\varepsilon)} \cap E_M) \supset E_\delta = \{v : v = W(\cdot+c) - W(\cdot-c), c \in [a-\delta, a+\delta]\}.$$

Furthermore, it follows that

$$\phi^{-1}(\mathcal{H}_\infty(B_e(U,\varepsilon) \cap E_M)) \supset \phi^{-1}(E_\delta) = [a-\delta, a+\delta].$$

□

[3]A continuous map $g : B \to \mathcal{B}$ is called admissible provided B is an open subset of $\mathcal{B}$ and the fixed point set of g is compact, see [12].

Finally, we have all the ingredients to calculate $\mathrm{ind}(\phi^{-1}\circ\mathcal{H}'_\infty\circ\phi,\mathcal{D})$. We define the finite dimension operator $T=\phi^{-1}\circ\mathcal{H}'_\infty\circ\phi$ which, as we have shown above, maps $[a-\delta,a+\delta]\to[m,M]$. It is easy to check that a is a fixed point of T, i.e., $T(a)=a$. Moreover a is an isolated fixed point of T. The latter statement follows from U being the isolated fixed point of $\mathcal{H}_\infty$ and topological invariance property of the index. The topological index of a finite dimensional map can be calculated as

$$\mathrm{ind}(T,\mathcal{D})=\mathrm{sgn}(T'(a)-1),$$

see [19].

The following equality holds true fore all $c\in[a-\delta,a+\delta]$

$$W(T(c)+c)-W(T(c)-c)=\theta.$$

Using the implicit function theorem and the chain rule for differentiation we find

$$T'(a)=\frac{\varpi(0)+\varpi(2a)}{\varpi(0)+\varpi(2a)}.$$

Thus, we have

$$\deg(\mathcal{H}_\infty,B_e(U,\varepsilon),0)=\mathrm{ind}(T,\mathcal{D})=\mathrm{sgn}(\varpi(2a))=1.$$

Combining all the results, we get that there exists $C_\beta>>1$ that $u=\mathcal{H}_\beta u$ possesses a solution $u_\beta\in B_e(U,\varepsilon)$ for all $\beta>C_\beta$ and $u_\beta\to U$. We also notice here that u_β is a symmetric function which satisfy the θ-condition and has two intersection points with straight line θ. □

5. Conclusions and outlook

In the present paper we have studied the properties of the one-parameter family of Hammerstein operators $\mathcal{H}_\beta$, $0<\beta\le\infty$ given by (3.2). Fixed points of an operator belonging to this family are stationary solutions of (1.1). For functions in $W^{1,q}(\mathbb{R},\mu)$, $1\le q\le\infty$ we have introduced the definition of the $\theta-$condition, which means that we consider functions with a finite number of intersection points with the line $u=\theta$. We have shown that the continuous dependence theorem (Theorem 3.14) holds in a vicinity of a function $U\in W^{1,\infty}$ satisfying the $\theta-$condition, while for the case $U\in W^{1,q}(\mathbb{R},\mu)$, $1\le q<\infty$ the conditions of the theorem are not satisfied. Next, with Theorem 3.15 we show that if $\mathcal{H}_\infty$ possess an unique fixed point with some additional assumptions, then the solutions of the fixed point problem $\mathcal{H}_\beta u=u$ exist for $\beta>C_\beta$. This theorem allows us to prove existence of multi-bump solutions of (1.1) with sigmoidal firing rate functions.

We believe that these results can be very useful in neural-field theory. We have given two examples of restrictions on the connectivity functions (one with inhomogeneous connectivity and the second one for homogeneous connectivity) where all the conditions of the continuous dependence theorem are satisfied. Moreover, for a homogeneous

type of connectivity we have proved existence of 1−bump solutions for (1.1) with steep gradient continuous firing rate function, $S(\beta, \cdot)$, satisfying the condition (4.10). Although the latter condition imposes restrictions on the choice of $S(\beta, \cdot)$, we would like to emphasize that this result is more general than one obtained in [8, 11]. Here we would like to point out that the results of this paper can be useful for studying not only continuous dependence and existence of bumps but also stability of these solutions. The methods for studying stability of bumps, Evans function technique and Amari approach, assume that small perturbation of a bump solution possess the same number of intersection with a straight line θ as a bump itself. As we have shown, this is the case only if we work in the Sobolev space $W^{1,\infty}(\mathbb{R}, \mu)$. However, if one studies stability of bump in $W^{1,q}(\mathbb{R}, \mu)$, $1 \leq q < \infty$, then any vicinity of a bump contains functions which do not satisfy the $\theta-$condition, and thus, these stability approaches do not work.

6. Acknowledgements

The authors would like to thank Professor Stephen Coombes (School of Mathematical Sciences, University of Nottingham, United Kingdom), and Professor Yury Nepomnyashchikh (Dept. of mathematics and Informatics, Eduardo Mondlane University, Mozambique) for fruitful and stimulating discussions during the preparation of this paper. John Wyller also wishes to thank the School of Mathematical Sciences, University of Nottingham for the kind hospitality during the stay. This research was supported by the Norwegian University of Life Sciences. The work has also been supported by The Research Council of Norway under the grant No. 178892 (eNEURO-multilevel modeling and simulation of the nervous system) and the grant No. 178901 (Bridging the gap: disclosure, understanding and exploitation of the genotype-phenotype map).

References

[1] H. R. Wilson and J. D. Cowan, Excitatory and inhibitory interactions in localized populations of model neurons, Biophysical Journal 12 (1972) pp. 1-24.

[2] H. R. Wilson and J. D. Cowan, A mathematical theory of the functional dynamics of cortical and thalamic nervous tissue, Kybernetik 13 (1973) pp. 55-80.

[3] S. Amari, Homogeneous nets of neuron-like elements, Biological Cybernetics 17 (1975) pp. 211-220.

[4] S. Amari, Dynamics of Pattern Formation in Literal-Inhibition Type Neural Fields, Biol. Cybernetics, 27 (1977) pp.77-87.

[5] S. Coombes, Waves, bumps, and patterns in neural field theories, Biological Cybernetics 93 (2005).

[6] S.Coombes and M.R.Owen, Evans functios for integral field equations with Heavisite firing rate function, SIAM Journal on Applied Dynamical Systems 34 (2004) pp. 574-600.

[7] J. Wyller, P. Blomquist and G.T. Einevoll, Turing instability and pattern formation in a two-population neuronal network model, Physica D 225 (2007) pp. 7593.

[8] K. Kishimoto, S. Amari, Existence and Stability of Local Excitations in Homogeneous Neural Fields, J.Math. Biology 7 (1979) pp. 303-318.

[9] S. Coombes and H. Schmidt, Neural fields with sigmoidal firing rates: Approximate solutions,Discrete and Continuous Dynamical Systems 28 (2010) pp. 1369-1379.

[10] O. Faugeras, F.Grimbert, and J.-J. Slotine, Absolute stability and complete synchronization in a class of neural field models, SIAM J. Appl. Math. 63 (2008) pp.205-250.

[11] A. Oleynik, A. Ponosov and J. Wyller, Iterative schemes for bump solutions in a neural field model, Submitted to SIAM Journal on Applied Mathematics, April 2011.

[12] A. Granas, The Leray-Schuder index and the fixed point theorey for arbitrary ANRs, Bull.Soc.math.France 100 (1972) pp. 209-228.

[13] V.Hutson, J.S.Pym, and M.J. Cloud, Applications of functional analysis and operator theory, 2nd Edition, Volume 200, Elsevier, 2005.

[14] M.A. Krasnosel'skii, A.I. Koshelev, S.G. Mikhlin, L.S. Rakovshchik, V.Ya. Stet'senko, P.P. Zabreiko, Integral Equations, Leyden: Noordhoff International Publishing (1975) 443p.

[15] 9. N. Azbelev, V. Maksimov, L. Rakhmatullina, Introduction to the theory of functional differential equations: methods and applications, Hindawi Publishing Corporation, New York, Cairo (2007) 314p.

[16] A.N. Kolmogorov and S.V. Fomin, Introductory Real Analasis, Dover publications Inc. (1975) 403p.

[17] C.R. Laing and W.C. Troy, Two-bump solutions of Amari-type models pf neuronal patter formation, Physica D 178 (2003) pp. 190-218.

[18] C. Laing, W.C. Troy, B.Gutkin, and G.B. Ermentrout, Multiple bumps in a neural model of working memory, SIAM J. Appl. Math 63:1 (2005) pp.62-97.

[19] M.A. Krasnosel'skii, P.P. Zabreiko, Geometrical methods of nonlinear analysis, Berlin-Heidelberg-New York-Tokyo: Springer Verlag , Grundlehren Der Mathematischen Wissenschaften, A Series of Comprehensive Studies in Mathematics 263 (1984) 409p.

List of changes (made after submission)

1) Paper I, Section 3, Theorem 3.1. The typos in the formulation of the theorem have been corrected.

2) Paper I, Section 2. There was a misprint in the sentence after Assumption 2. "ge" was corrected to "get".

3) Paper III became published. Thus we have changed "In Press" to the citation details, and have provided the author's personal copy of the publication, see pp. 53-74.